NASA Contractor Report 177571

Fully Automatic Guidance and Control for Rotorcraft Nap-of-the-Earth Flight Following Planned Profiles Volume I – Real-Time Piloted Simulation

Warren F. Clement, Peter J. Gorder, and Wayne F. Jewell

Contract Number NAS2-12640
January 1991

National Aeronautics and
Space Administration

NASA Contractor Report 177571

Fully Automatic Guidance and Control for Rotorcraft Nap-of-the-Earth Flight Following Planned Profiles Volume I – Real-Time Piloted Simulation

Warren F. Clement, Peter J. Gorder, and Wayne F. Jewell
Systems Technology, Inc., Mountain View, California

Prepared for
Ames Research Center
Contract Number NAS2-12640
January 1991

National Aeronautics and
Space Administration

Ames Research Center
Moffett Field, California 94035-1000

FOREWORD AND ACKNOWLEDGEMENTS

The work described herein was performed under NASA Contract NAS2-12640 (SBIR Phase II) for the NASA Ames Research Center (ARC), under the technical direction of the Flight Guidance and Navigation Branch (Code FSN) as part of its automatic nap-of-the-earth flight program in cooperation with the Army Research and Technology Activity of the U.S. Army Aviation Systems Command. The NASA ARC Code FSN contract technical monitor was Harry N. Swenson. The project engineer for Systems Technology, Inc., (STI) was Warren F. Clement, and the STI technical director was Duane T. McRuer. This work was performed during the period from September 1987 through September 1990. Mrs. Sharon A. Duerksen of STI published the report. This research required the subcontracted services of McDonnell-Douglas Helicopter Company (MDHC) for whom Donald G. Caldwell served as project engineer. MDHC's report, prepared by E. Christopher Nehls, III, and Kevin D. Sokol, has been incorporated in Appendices A through F herein.

The authors wish to acknowledge the assistance, in scheduling and operating the Vertical Motion Simulator at NASA ARC, of Thomas Alderete and David Astill of the NASA ARC Simulation Experiments Branch; Richard Bray of the NASA ARC Flight Dynamics and Controls Branch; and Ernest Inn, Mary Shirin Sheppard, Frederic G. Kull, Jr., and their colleagues at SYRE. We also wish to express our gratitude to the very patient, cooperative, and well-qualified test pilot subjects who participated in this simulation and without whom it could not have succeeded: Chan Morse and Larry Proper of MDHC; Munro Dearing, Gordon Hardy, Mike Stortz, and George Tucker of NASA; and Ron Gerdes of SYRE. A special note of thanks goes to Richard A. Coppenbarger of the NASA ARC Flight Guidance and Navigation Branch for his diligent assistance and encouragement during the NASA ARC simulation and data analysis.

ABSTRACT

Developing a single-pilot, all-weather nap-of-the-earth (NOE) capability requires fully automatic NOE (ANOE) navigation and flight control. Innovative guidance and control concepts are investigated in a four-fold research effort that: (1) organizes the on-board computer-based storage and real-time updating of NOE terrain profiles and obstacles in course-oriented coordinates indexed to the mission flight plan; (2) defines a class of automatic anticipative pursuit guidance algorithms and necessary data preview requirements to follow the vertical, lateral, and longitudinal guidance commands dictated by the updated flight profiles; (3) automates a decision-making process for unexpected obstacle avoidance; and (4) provides several rapid response maneuvers. Acquired knowledge from the sensed environment is correlated with the forehand knowledge of the recorded environment (terrain, cultural features, threats, and targets), which is then used to determine an appropriate evasive maneuver if a non-conformity of the sensed and recorded environments is observed. This four-fold research effort has been evaluated in both fixed-base and moving-base real-time piloted simulations, thereby providing a practical demonstration for evaluating pilot acceptance of the automated concepts, supervisory override, manual operation, and re-engagement of the automatic system. Volume I describes the major components of the guidance and control laws as well as the results of the piloted simulations. Volume II describes the complete mathematical model of the fully automatic guidance system for rotorcraft NOE flight following planned flight profiles.

TABLE OF CONTENTS

TABLE OF CONTENTS (CONTINUED)

TABLE OF CONTENTS (CONTINUED)

TABLE OF CONTENTS (CONTINUED)

TABLE OF CONTENTS (CONCLUDED)

LIST OF FIGURES

LIST OF FIGURES (CONTINUED)

LIST OF FIGURES (CONCLUDED)

LIST OF TABLES

LIST OF ABBREVIATIONS

ADFCS	Advanced digital flight control system
AFPG	Automatic flight path guidance
AGL	Above ground level
ANOE	Automatic nap of the earth
ARC	Ames Research Center
CGI	Computer-generated image
Cn	Pilot rating for confidence in the automatic guidance system
CRT	Cathode-ray tube
dm	Decameter(s)
dmls	Dimensionless
Dn	Pilot rating for attentional workload
FCS	Flight control system
FFT	Finite Fourier transform
ft	Foot, feet
GE	General Electric
HUD	Head-up display
IHADSS	Integrated helmet and display sight system
Kn	Pilot rating for display clutter
kt	Knot(s)
LHX	Light helicopter, experimental
MDHC	McDonnell-Douglas Helicopter Company
MFD	Multifunction display
MMD	Moving map display
msl	Mean sea level
MUF	Maneuver urgency factor
m	Meter(s)
NASA	National Aeronautics and Space Administration
NOE	Nap of the earth
ODAMS	Obstacle detection and avoidance maneuver selection

LIST OF ABBREVIATIONS (CONCLUDED)

rad	Radian(s)
RMS	Root mean square
RT	Reaction time
RVR	Runway visual range
SCAS	Stability and control augmentation system
SCTT	Sub-critical tracking task
SD	Standard deviation
sec	Second(s)
Sn	Pilot rating for utility of displayed status information
STI	Systems Technology, Inc.
TVC	Translational velocity command
VMC	Visual meteorological conditions
VMS	Vertical Motion Simulator

LIST OF SYMBOLS

a_1	Break frequency for trim control (rad/sec)
A_i	i^{th} element of the MX sine terms in a sum of sinusoids approximating a given terrain elevation profile
B_i	i^{th} element of the MX cosine terms in a sum of sinusoids approximating a given terrain elevation profile
C_0	Constant added to the sum of sinusoids approximating a given terrain elevation profile
C_1	Trend added to the sum of sinusoids approximating a given terrain elevation profile
dt	Frame time of digital computer (sec)
$\bar{e}(s)$	Error vector
E_{CTE}	Eastward error between the aircraft and the $(i+1)^{th}$ waypoint in the MDHC simulation
$\bar{G}_1(s)$	Compensatory control matrix
h	Altitude (m) above mean sea level (msl)
h_c	Commanded altitude (m)
$h_E(x,y)$	Terrain elevation function (m)
h_{min}	Minimum navigable height above the terrain (m)
$\dot{h}$	Vertical velocity (m/sec)
$\dot{h}_{max}$	Maximum vertical velocity limit (m/sec)
$\dot{h}_{min}$	Minimum vertical velocity limit (m/sec)
$\dot{h}_{ref}$	Vertical velocity command signal (m/sec)
$\ddot{h}$	Vertical acceleration (m/sec)
$\ddot{h}_c$	Vertical acceleration command signal (m/sec)
$\ddot{h}_{max}$	Maximum vertical acceleration limit (m/sec^2)
$\ddot{h}_{min}$	Minimum vertical acceleration limit (m/sec^2)
$\dddot{h}_c$	Vertical jerk command (m/sec^3)
$\dddot{h}_{max}$	Maximum vertical jerk limit (m/sec^3)

LIST OF SYMBOLS (CONTINUED)

$\dddot{h}_{min}$	Minimum vertical jerk limit (m/sec^3)
H	Vertical axis height coordinate of centroid (ft) of safety margin envelope surrounding the rotorcraft with respect to msl
H_{min}	Desired terrain following altitude (ft) in the MDHC simulation
H_{RADAR}	Aircraft radar altitude (ft) in the MDHC simulation
H_c	Commanded vertical speed (ft/sec) in the MDHC simulation
i_x	Along-course terrain data index
I	Identity matrix or row index integer in the along-course anticipative array of sensed obstacles
j_y	Across-course terrain data index
J	Column index integer in the along-course anticipative array of sensed obstacles
J_{com}	Column index integer determined by the lateral destination command
k_1	Velocity command gain (1/sec) for compensatory guidance
K_c	High frequency gain (1/sec) of controlled element response to a velocity command
K_H	Altitude error gain (ft/sec/ft) in the MDHC simulation
K_Y	Lateral tracking error gain (deg/ft) in the MDHC simulation
$K_{\dot{Y}}$	Lateral tracking rate gain (deg/ft/sec) in the MDHC simulation
M	Maximum value of integer I
MX	Number of approximating complex coefficients used for along-course approximation of terrain
MY	Number of approximating complex coefficients used for across-course approximation of terrain
N_{CTE}	Northward error between the aircraft and the $(i+1)^{th}$ waypoint in the MDHC simulation
NX	Number of terrain data points along the course
NY	Number of terrain data points across the course
R	Maximum value of integer J

LIST OF SYMBOLS (CONTINUED)

R2	Integer representing the number of along-course cells between the present position and the anticipative array reference point in the array of sensed obstacles ($R2 = V_x T_{p_x}$)
R_x	Cell length along course in the anticipative array (ft or dm) of sensed obstacles
R_y	Cell width across course in the anticipative array (ft or dm) of sensed obstacles
$\bar{r}(s)$	Position command vector
$\underline{R}_n$	Stored terrain, obstacle, threat, flight profile vector
$\hat{\underline{R}}_n$	Sensed terrain, obstacle, threat, flight profile vector
RH	Half the minimum vertical separation of the upper and lower surfaces of the anticipative array of sensed obstacles (ft or m)
RX	Cell length along course in the anticipative array (ft or dm) of sensed obstacles
RY	Cell width across course in the anticipative array (ft or dm) of sensed obstacles
s	Laplace operator; also sample standard deviation
T_{p_x}	ODAMS reference preview interval (sec) along course
u_{R_p}	Nonlinear longitudinal cyclic gain
U_{EST}	Easterly component of ground speed (ft/sec or m/s) in the MDHC simulation
U_{NTH}	Northerly component of ground speed (ft/sec or m/s) in the MDHC simulation
v_{R_p}	Nonlinear lateral cyclic gain
V_x	Waypoint course resolved velocity component (ft/sec or m/s) or Component of the velocity vector (HUD)
VY	Across-course component of ground velocity (ft/sec or m/s)
VLSW	Maximum vertical velocity hold switch
x	Longitudinal (along-course) position of centroid of safety margin envelope surrounding rotorcraft (ft)
x_c	Distance along course leg (earth coordinates) (m)

LIST OF SYMBOLS (CONTINUED)

X_{CRS}	Along course position (m)
$\dot{X}_{CRS}$	Along course velocity (m/sec)
X_e	Latitude coordinate (m)
X	Along-course axis of coordinates of centroid of safety margin envelope surrounding rotorcraft
$X_{a/c}$	Northerly coordinate of aircraft's current position (ft or m) in the MDHC simulation
X_{fp}	Along-course coordinate of the reference point of the along-course anticipative array (ft or m)
X_{CTE}	Along-track distance on the $(i+1)^{th}$ waypoint in the MDHC simulation
$X_{(i+1)}$	Northerly coordinate of next waypoint (ft or m) in the MDHC simulation
$\dot{X}_{CTE}$	Closing rate on the $(i+1)^{th}$ waypoint in the MDHC simulation
$\underline{X}$	Vehicle state vector
y	Lateral (across-course) position of centroid of safety margin envelope surrounding rotorcraft (ft)
y_c	Across-course position
y_{com}	Lateral offset command
y_{CRS}	Across-course position
y_e	Longitude coordinate (m)
$\dot{y}_{CRS}$	Across-course velocity (m/sec)
$\dot{y}_{max}$	Lateral velocity command limit (ft/sec or kt)
Y	Across-course axis of coordinates of centroid of safety margin envelope surrounding rotorcraft
$Y_{a/c}$	Easterly coordinate of aircraft's current position (ft or m) in the MDHC simulation
Y_c	Controlled element matrix
Y_{ef}	Across-course coordinate of the reference point of the along-course anticipative array of sensed obstacles
Y_{CTE}	Lateral ground track error in the MDHC simulation

LIST OF SYMBOLS (CONCLUDED)

$Y_{(i+1)}$	Easterly coordinate of next waypoint (ft or m) in the MDHC simulation
Y_{CTE}	Lateral ground track rate error in the MDHC simulation
$\overline{y}(s)$	Position vector
$\overline{Y}_c(s)$	Velocity command controlled element matrix
$\overline{Y}_{pp}(s)$	Feedforward pursuit guidance control matrix
Z	Axis of coordinates in the earth-vertical direction
α_2, α_3	One-half of the change in course at waypoints 2 and 3, respectively
Δ	Incremental operator
θ_{max}	Pitch attitude limit (deg)
$\dot{\theta}_{max}$	Pitch rate limit (deg/sec)
$\ddot{\theta}_{max}$	Pitch angular acceleration limit (deg/sec^2)
λ_n	Direction of course leg relative to North (rad or deg)
σ	Standard deviation
τ_c	Velocity command time lag (sec) in the controlled element
ϕ	Roll attitude (rad)
ϕ_{max}	Bank angle limit (deg)
$\dot{\phi}_{max}$	Roll rate limit (deg/sec)
$\ddot{\phi}_{max}$	Roll angular acceleration limit
Φ_c	Roll angle command (deg) in the MDHC simulation
ψ	Heading (deg)
ψ_c	Commanded heading
$\dot{\psi}$	Yaw rate (deg/sec)
$\dot{\psi}_{max}$	Yaw rate limit (rad/sec)
ψ_{R_p}	Nonlinear pedal gain
$\ddot{\psi}_{max}$	Yaw angular acceleration limit (rad/sec^2)
Ψ_m	(i)th leg bearing in the MDHC simulation

METRIC CONVERSION FACTORS

Approximate Conversions to Metric Measures

Symbol	When You Know	Multiply by	To Find	Symbol
	LENGTH			
in	inches	*2.5	centimeters	cm
ft	feet	30	centimeters	cm
yd	yards	0.9	meters	m
mi	miles	1.6	kilometers	km
	AREA			
in^2	square inches	6.5	square centimeters	cm^2
ft^2	square feet	0.09	square meters	m^2
yd^2	square yards	0.8	square meters	m^2
mi^2	square miles	2.6	square kilometers	km^2
	acres	0.4	hectares	ha
	MASS (weight)			
oz	ounces	28	grams	g
lb	pounds	0.45	kilograms	kg
	short tons (2000 lb)	0.9	tonnes	t
	VOLUME			
tsp	teaspoons	5	milliliters	ml
Tbsp	tablespoons	15	milliliters	ml
fl oz	fluid ounces	30	milliliters	ml
c	cups	0.24	liters	l
pt	pints	0.47	liters	l
qt	quarts	0.95	liters	l
gal	gallons	3.8	liters	l
ft^3	cubic feet	0.03	cubic meters	m^3
yd^3	cubic yards	0.76	cubic meters	m^3
	TEMPERATURE (exact)			
°F	Fahrenheit temperature	5/9 (after subtracting 32)	Celsius temperature	°C

*1 in = 2.54 (exactly). For other exact conversions and more detailed tables, see NBS Misc. Publ. 286, Units of Weights and Measures, Price $2.25, SD Catalog No. C13.10:286.

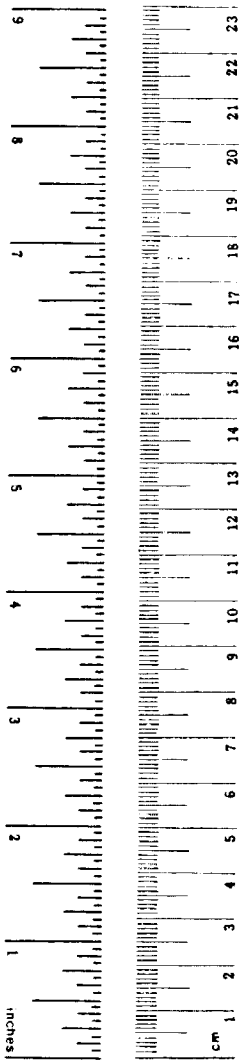

Approximate Conversions from Metric Measures

Symbol	When You Know	Multiply by	To Find	Symbol
	LENGTH			
mm	millimeters	0.04	inches	in
cm	centimeters	0.4	inches	in
m	meters	3.3	feet	ft
m	meters	1.1	yards	yd
km	kilometers	0.6	miles	mi
	AREA			
cm^2	square centimeters	0.16	square inches	in^2
m^2	square meters	1.2	square yards	yd^2
km^2	square kilometers	0.4	square miles	mi^2
ha	hectares (10,000 m^2)	2.5	acres	
	MASS (weight)			
g	grams	0.035	ounces	oz
kg	kilograms	2.2	pounds	lb
t	tonnes (1000 kg)	1.1	short tons	
	VOLUME			
ml	milliliters	0.03	fluid ounces	fl oz
l	liters	2.1	pints	pt
l	liters	1.06	quarts	qt
l	liters	0.26	gallons	gal
m^3	cubic meters	35	cubic feet	ft^3
m^3	cubic meters	1.3	cubic yards	yd^3
	TEMPERATURE (exact)			
°C	Celsius temperature	9/5 (then add 32)	Fahrenheit temperature	°F

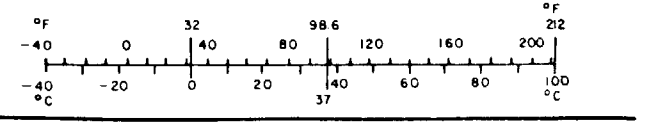

EXECUTIVE SUMMARY

The automatic nap-of-the-Earth (ANOE) flight program is a cooperative National Aeronautics and Space Administration (NASA)/U.S. Army effort to develop technology that will lead to enhanced low-altitude and NOE flight path management, guidance, and control through computer aiding. Nap-of-the-Earth flight typically involves covert operations in areas where topography and vegetation provide concealment. The rotorcraft is usually flown below tree-top level wherever possible. Typical ground clearance is less than 3 meters, and typical ground speeds range from walking speeds to about 20 knots, with an occasional dash up to 40 knots. The main application for automated guidance and control is during flight in a single-pilot rotorcraft in which the mission tasks require an attention level that could compromise manual guidance and control. However, the issue of pilot acceptance of ANOE flight is a major obstacle to progress toward automation of various mission phases. The main objective of the research reported herein was to evaluate pilot acceptance of the ANOE flight system described herein using real-time flight simulators.

Recent research at NASA Ames Research Center identified the necessary guidance considerations for automated flight in terms of three loops depicted in Fig. ES-1.

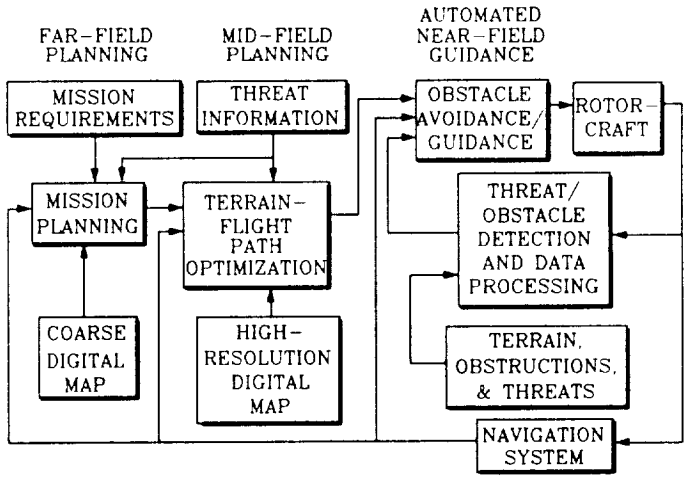

Figure ES-1. Nap-of-the-Earth Guidance

The outermost guidance loop consists of the far-field mission planning. A digital map, along with mission requirements and threat information, is used to

generate an overall mission plan. In the research reported here, this was a pre-flight function. Other researchers are investigating in-flight replanning capabilities that respond to changes in threat conditions and vehicle resources.

The intermediate guidance loop consists of mid-field mission planning. This consists of terrain and flight path optimization. This is done using a high resolution digital map, along with detailed threat information. Optimality is achieved through a specified terrain following and avoidance performance index discussed elsewhere. Here, this loop was also executed as a pre-flight function to generate a complete planned flight path.

The main emphasis of the research reported here was on the innermost automated near-field guidance loop. This loop provides the necessary guidance commands for following the flight path defined in the intermediate loop. In addition, planned flight path modifications required by sensed terrain, obstacles, and threats are determined in this loop. All functions of this inner-most loop are performed by an on-board computer. The evaluation of pilot acceptance of this innermost guidance loop is the main objective of this research.

Figure ES-2 will clarify several key features of the innermost guidance loop.

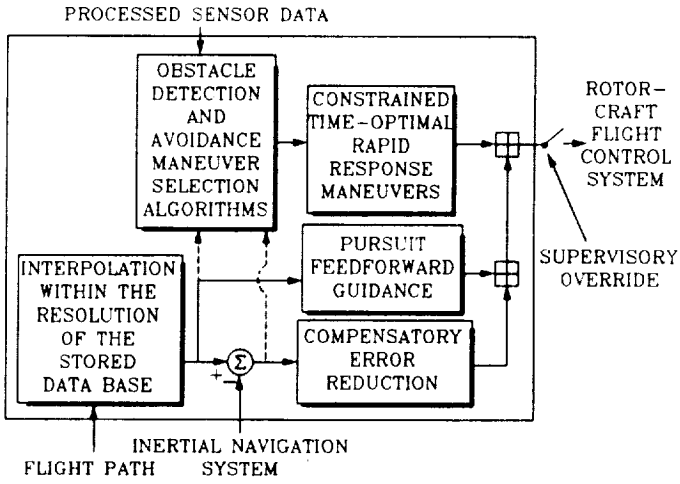

Figure ES-2. Near-Field Obstacle Avoidance and Guidance

Terrain contour and threat data along and across the planned flight path are compressed and stored in a data base for subsequent interpolation. Likewise, planned velocity and position along the nominal and alternate routes defined by sequences of waypoints are also stored as part of the flight path data base. Interpolation within the resolution of the stored data base provides near-field

guidance commands, which are compared with the velocity and position along the route sensed by the inertial navigation system to provide compensatory guidance error reduction through the rotorcraft flight control system.

Extraordinary precision in following guidance commands is required in nap-of-the-Earth flight operations, dictated primarily by the risk of damaging rotors, fuselage, empennage, and undercarriage. In order to attain this level of precision, pursuit feedforward guidance commands are included in the automatic guidance system. Pursuit guidance refers here in a generic sense to the direct operation on the course command and its higher derivatives for the purpose of control. That part of the guidance error associated with course and profile commands may be reduced by the ideal pursuit guidance adjustment, which is proportional to the inverse controlled element describing function. Experiments with human operators have examined various preview distances in the external visual field. These were in the context of vehicle guidance along curved courses to discern conditions promoting pursuit guidance. These experiments show that an experienced human operator will adopt a pursuit feedforward guidance control input when sufficient preview of the course curvature is available. The result is a reduction in the curved course following error.

In the piloted simulation, the pursuit guidance algorithm guided the rotorcraft along the planned course and vertical profile with extremely small errors, even in the presence of turbulence and wind shears. This method of guidance met with universal acceptance from the evaluation pilots.

In an automatically piloted vehicle flying in nap-of-the-Earth conditions along a planned course and vertical profile, provisions must be made for unexpected obstacle avoidance. The next two features of the Automated Near-Field Guidance in Fig. ES-2 account for this stipulation. First, the obstacle detection and avoidance maneuver selection logic processes sensor data to determine necessary evasive action. The obstacle algorithm compares the expected terrain profile from the stored digital data base with the sensed terrain, cultural features and threats to determine if conflicts exist with the primary stored course and profile. If a conflict does exist, the obstacle algorithm attempts to identify which combination of stored evasive maneuvers will resolve the conflict. If no combination of evasive maneuvers will resolve the conflict, the rotorcraft is commanded to halt and await pilot input.

The obstacle algorithm proved trustworthy and acceptable to the pilots in the piloted simulation.

The stored evasive maneuvers mentioned earlier were four rapid-response obstacle-avoidance movements programmed into the flight computer for selection by the obstacle algorithm. Each maneuver involved one of the four independent axes of the rotorcraft, namely, bob-up and -down, hover turn, lateral side step,

and longitudinal acceleration/deceleration. These maneuvers are fundamental in completing most nap-of-the-Earth flight operations and were designed to ensure pilot acceptance by mimicking human piloting strategies measured in flight.

The programmed evasive maneuvers performed accurate, smooth, repeatable, aggressive movements. The evaluation pilots were initially skeptical about these maneuvers, especially the aggressive bob-down at low altitudes. However, the pilots gained confidence in the automatic system after experiencing the maneuvers several times.

The last feature of the innermost guidance loop, also shown in Fig. ES-2, is the supervisory override. The history of automating vehicle flight path control during critical situations indicates that pilots are reluctant to accept automation unless the pilot can participate in the control process. In the automatic control system designed for this project, this participation was in the form of a supervisory override. The pilot had the option to take control of the rotorcraft at any time. Beyond a certain threshold level, pilot inputs through the controllers disengage the automatic guidance system. The pilot's control inputs then modulate the reference velocity vector

As previously stated, the main application for automated nap-of-the-Earth flight is during times when the mission tasks require an attention level sufficient to compromise the single pilot's guidance and control of the rotorcraft. Since pilot acceptance of automated nap-of-the-Earth flight has been a major obstacle to automating many mission phases, piloted simulations were conducted at the McDonnell-Douglas Helicopter Company in Mesa, Arizona, and on the Vertical Motion Simulator at the NASA Ames Research Center. These simulations were designed to evaluate pilot acceptance by emulating the various conditions listed below that would require automated guidance and control and to compare manual and automated guidance and control techniques.

- Workload-intensive side tasks
- Pilot's visibility, 500 ft and 1,000 ft RVR
- Multiple courses
- Manual versus automatic guidance and control.

The evaluation pilots were asked to perform three side tasks having variable workload intensity during simulated automated flights to imitate the divided attention required by various mission tasks other than guidance and control of the rotorcraft. These side tasks were performed in addition to the primary pilot task of monitoring the rotorcraft's operational performance. Two densities of fog were simulated to decrease the pilot's visibility, giving less preview of

visual information on which to act. This, in turn, increases the workload for monitoring the automatic guidance and control of the rotorcraft. Multiple courses were also included to inhibit the pilots from learning one course.

The pilots were also asked to fly the same courses manually as the automatic guidance system. No side tasks were used during this comparison of manual and automatic guidance. After each manual flight, the pilots were asked to rate the flying qualities of the task. During automatic flight, the pilots were asked to provide other types of ratings.

One of the subjective ratings solicited from the pilots was of confidence in the automatic guidance system. A five-level confidence scale (shown in Fig. ES-3) was devised, with a rating of C1 being the highest level of confidence in the automatic system, and a rating of C5 representing complete lack of confidence.

CRITERIA		DESCRIPTIVE PHRASE	RATING
AUTOGUIDANCE ACCEPTABLE	CONFIDENCE LEVEL		
YES	HIGH	VERY HIGH LEVEL OF CONFIDENCE, NO INSTANCES TEMPTING MANUAL INTERVENTION	C1
		HIGH LEVEL OF CONFIDENCE, FEW INSTANCES TEMPTING MANUAL INTERVENTION	C2
	LOW	LOW LEVEL OF CONFIDENCE, INSTANCES REQUIRING MANUAL INTERVENTION	C3
		MARGINALLY ACCEPTABLE LEVEL OF CONFIDENCE; SEVERAL INSTANCES REQUIRING MANUAL INTERVENTION	C4
NO		COMPLETE LACK OF CONFIDENCE IN AUTOMATIC GUIDANCE SYSTEM	C5

Figure ES-3. Pilot Opinion Rating Scale for Confidence in Automatic Guidance

The pilots were asked to consider six questions in assigning their confidence level from C1 to C5. First, did the automatic guidance system guide the rotorcraft with acceptable precision along the flight path? Second, did it execute obstacle avoidance maneuvers in a timely fashion? Third, were the avoidance maneuvers relatively benign in light of their timeliness? Fourth, did the automatic guidance system quickly and precisely re-acquire the planned flight path following the evasive action? Fifth, did the automatic guidance system emulate the pilot's own strategies and techniques? And last, did the automatic guidance system maintain acceptable levels of excursion in attitudes, attitude rates, accelerations, and control authority used?

The results of the simulation, shown in Fig. ES-4, are very promising. The confidence ratings of one and two indicate there were no or few instances in which the pilot was tempted to intervene and take control of the rotorcraft. It is true, however, that the confidence of a pilot in an automatic guidance system for nap-of-the-Earth flight operations would be affected by the real-world environment. In the simulation environment, no possible harm could come to the evaluation pilot. In the particular simulators used for this investigation, it was not possible to indicate instances, such as rotor strikes, where harm could have come to the rotorcraft and/or the pilot. Nevertheless, the high confidence of the evaluation pilots in the automatic guidance system reflects the adherence of the system to the precision and safety requirements necessary for automated nap-of-the-Earth flight operations.

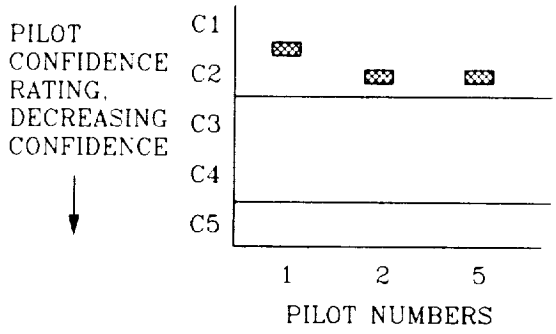

Figure ES-4. Evaluation Pilots' Confidence Ratings

SECTION I

INTRODUCTION

The automatic nap-of-the-earth (ANOE) flight program is a cooperative National Aeronautics and Space Administration (NASA)/U.S. Army effort to develop technology that will lead to enhanced low-altitude and NOE flight path management, guidance, and control through computer aiding. The main application of ANOE flight is in a single pilot rotorcraft in which the mission tasks require an attention level sufficient to compromise the manual guidance and control of the rotorcraft. However, the issue of pilot acceptance of ANOE flight is a major obstacle to progress toward automation of various mission phases. For example, the consensus of the pilots for a typical helicopter manufacturer reveals that they will currently accept automatic flight only when they are affected by a personal disability in returning to base. The main objective of the research reported herein was to evaluate pilot acceptance of the ANOE system described herein using real-time flight simulators.

The technology for fully-ANOE flight does not currently exist. The ultimate success in automating NOE operational functions will depend on major breakthroughs in real-time flight planning, confidence-inspiring methods for the pilot to monitor and interact with the automated functions, understanding of visual images, and sensor processing, fusion, and development. Reference 1 presents a description of the necessary considerations for ANOE rotorcraft flight. Included in the description is a hierarchical apportionment of the guidance structure into three vector feedback loops (Fig. 1 from Ref. 1). Research reported in Refs. 2 and 3 addresses the outermost of these loops, real-time automatic mission planning. Other research (Refs. 4 and 5) addresses the intermediate loop, the integration of the real-time route planning function with the guidance solution. The innermost feedback loop consists of the near-field obstacle avoidance and guidance of the rotorcraft and is the focus of this report. Research conducted at NASA Ames Research Center (ARC) has progressed in this area. Reference 6 treats the two-dimensional problem, and Refs. 7 and 8, the three-dimensional problem of obstacle avoidance using algorithms depending on heuristic arguments.

In contradistinction to the three loop structure in Fig. 1, the research reported here presumes separation of the (preflight) mission and route planning functions from the flight guidance and obstacle avoidance activities. The design of the near-field obstacle avoidance and guidance loop addressed three issues:

1. Interpolation within the resolution of the stored NOE terrain-and-flight plan data base using a stored model of an approximating continuous surface and forward- and side-looking sensors and combining the stored and sensed data for real-time display, guidance, and control purposes

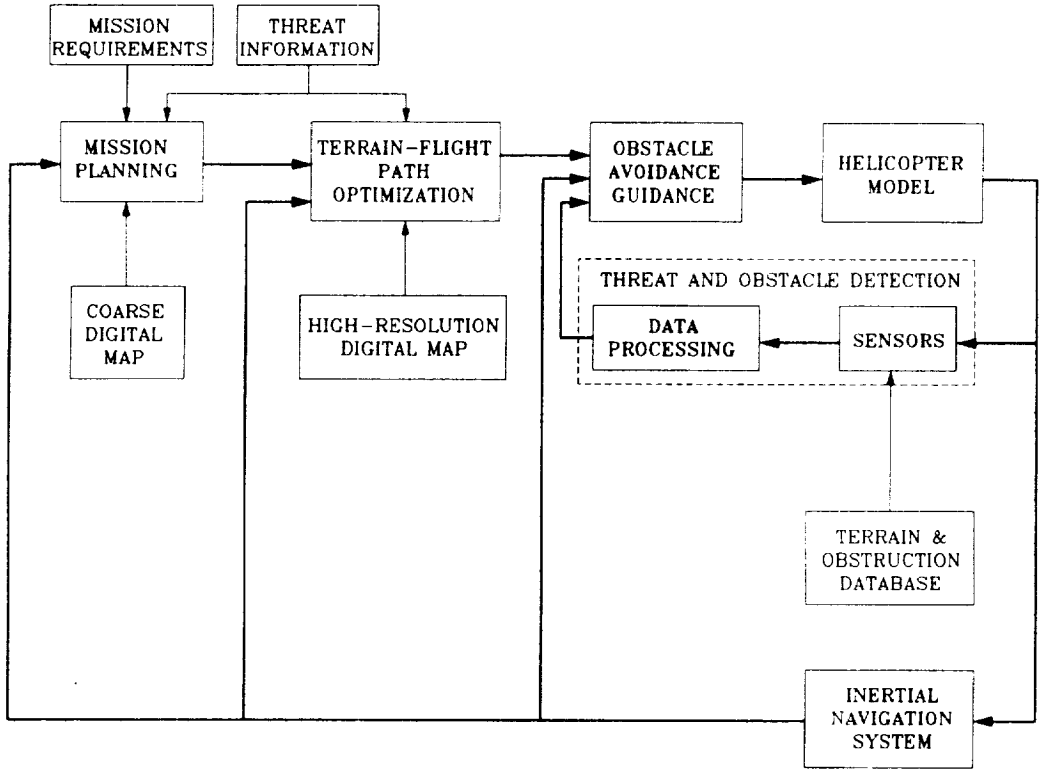

Figure 1. ANOE Guidance Structure (from Ref. 1)

2. Development of path and attitude command signals from this data array that are appropriate to command the safe NOE flight of a three-dimensional helicopter (in contrast to a point mass helicopter)

3. Pilot acceptance of ANOE flight.

The first and second issues were separated into the four research tasks depicted in Fig. 2, i.e., (1) Interpolation Within the Resolution of the Stored NOE Data Base, (2) Obstacle Detection and Avoidance Maneuver Selection Logic, (3) Pursuit Feedforward Guidance, and (4) Constrained Time-Optimal Rapid Response Maneuvers, the results of which are compatible for automatic control of a rotorcraft model with a translational velocity command stability and control augmentation system (TVC-SCAS) and are described respectively in Sections II through V of this report.

The third issue of pilot acceptance, the main objective of this research, was addressed as Task 5, Piloted Real-Time Simulation Evaluations. In order to accomplish this objective, two different real-time, piloted simulations were performed. The first simulation was performed at McDonnell-Douglas Helicopter

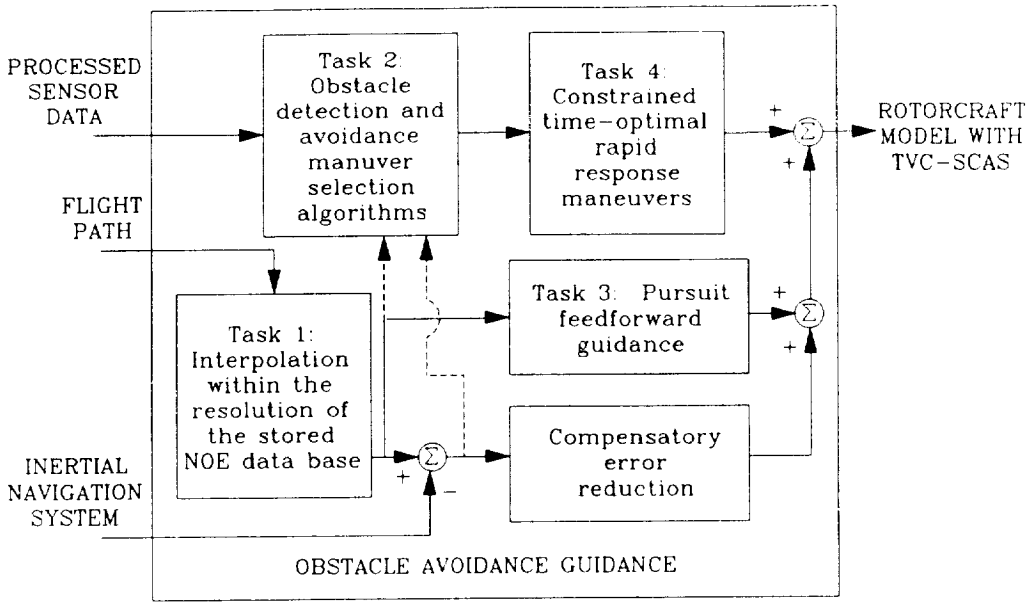

Figure 2. Vector Block Diagram for Multiloop Guidance and Control System Showing Research Tasks for Near-Field Obstacle Avoidance and Guidance

Company (MDHC) in Mesa, Arizona, during the summer of 1989. Two MDHC pilots evaluated the experiment on a fixed-base simulator equipped with a General Electric (GE) Compuscene IV computer-generated image (CGI) of the terrain . The main objective of this simulation was to debug algorithms of the various ANOE subsystems described herein and to obtain initial pilot reactions. Appendices A through G describe this simulation: Appendix A demonstrates compression of the stored data base representing terrain, Appendix B describes the gaming area course from the GE Compuscene IV CGI, Appendix C describes the MDHC control system, and Appendix D, the cockpit display; and Appendices E, F, and G present pilot comments, side-task results, and conclusions and recommendations, respectively.

The second simulation was performed in the fall of 1989 with five NASA pilots using the moving-base, six-degree-of-freedom Vertical Motion Simulator (VMS, Refs. 9 and 10) at the NASA ARC, Moffett Field, California. However, a scheduling conflict required substitution of the Evans & Sutherland CT-5A CGI with a new gaming area course in lieu of the Compuscene IV CGI and its gaming area course in Appendix B. The major components, test plan, and results of this second simulation are the topics of Sections VI, VII, and VIII, respectively, of this report. The ANOE test matrix and the side task data from the NASA ARC simulation are presented as Appendices H and I, respectively. Overall recommendations are presented in the final section, Section IX, which is followed by a list of references and the appendices described above.

SECTION II

INTERPOLATION WITHIN THE RESOLUTION OF THE STORED DATA BASE (TASK 1)

The first task addressed was the interpolation within the resolution of the stored data base to provide guidance for following flight plans. The method developed employs compressed data storage of terrain using preflight parameter identification of the planned gaming area course by modeling the digital terrain data base with an approximating continuous function. The storage and real-time updating of terrain profiles and obstacles have been organized in "gaming area course coordinates" that are indexed to the defined gaming area course. The terrain modeling function is represented by the "Task 1" block of Fig. 2.

A. GAMING AREA COURSE COORDINATE TRANSFORMATION

The gaming area course is a 100-decameter (dm) wide corridor specified prior to the NOE mission that defines the geographic bounds of the mission. The example of terrain selected for the work reported herein is that of the Fulda Gap (Germany) section of the General Electric Compuscene IV CGI data base used at the MDHC facility at Mesa, Arizona. More details of the example are presented in Appendix B.

The gaming area course is transformed from an earth-coordinate system to its own coordinate system for convenience in defining the approximate surface of the terrain; this will be described in the next section. In its own coordinate system, the entire gaming area course is straightened into a rectangular corridor 100 dm wide (Fig. 3). This corridor is divided into a number of rectangular sections based on the number of course points used to define changes in gaming area course direction, each of which defines a course leg in gaming area course coordinates.

The gaming area course coordinate system has a nonlinear relationship with the earth-fixed axis system because, although the lengths of the two sides of the course leg sections are of equal length in the course-oriented coordinate system, the actual distances these two sides represent in the earth-fixed axis system are, in general, different due to turns in the gaming area course. This is demonstrated in Fig. 4, where the third course leg of the defined gaming area course (Fig. 3) is isolated. A thorough description of the gaming area course coordinate transformation is presented in Ref. 11.

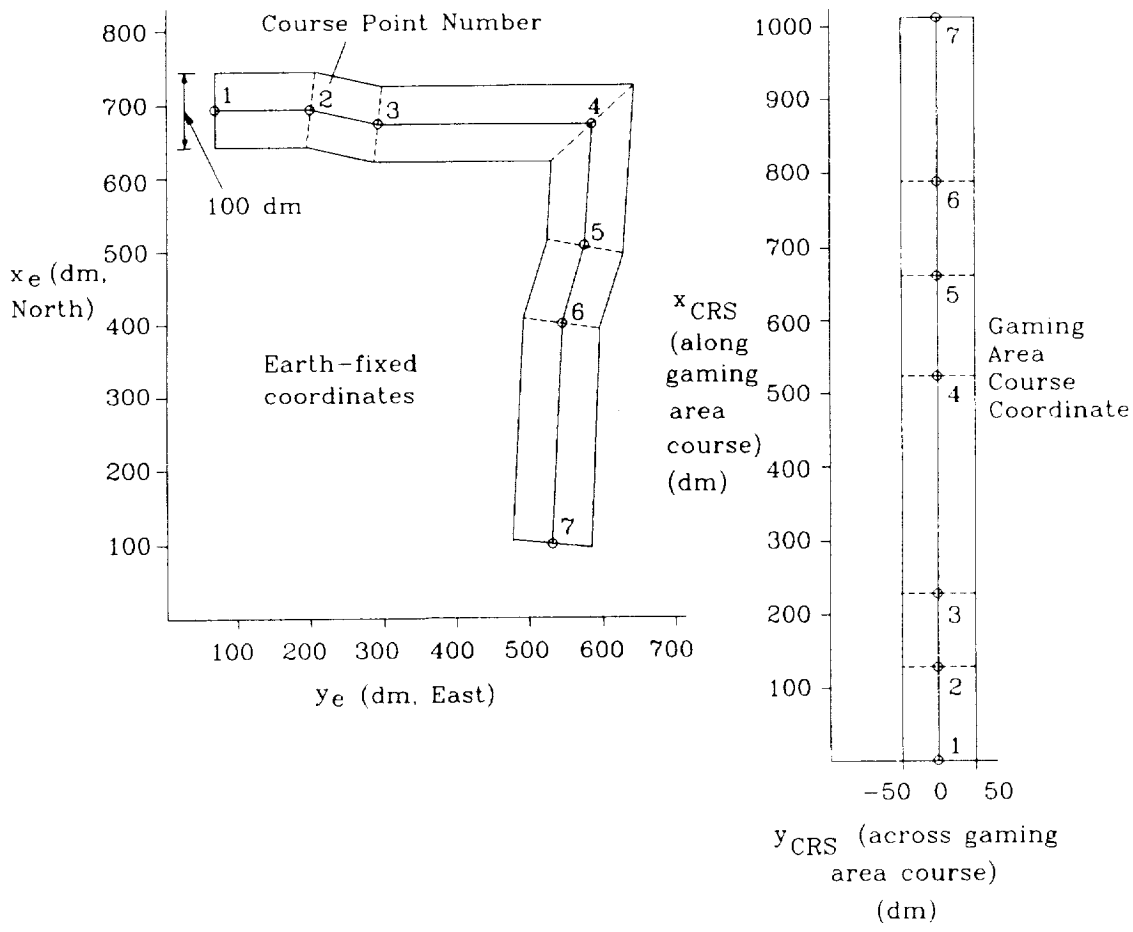

Figure 3. Transformation of Gaming Area Course from Earth-Fixed Coordinates to Gaming Area Course Coordinates

B. AN APPROXIMATING SURFACE FOR REPRESENTING THE TERRAIN PROFILE

In order to create a continuous representation of the terrain profile and threat exposure height, the rectangular gaming area course corridor is mapped with an approximate terrain surface and threat exposure height function to reduce the storage requirements and facilitate the interpolation within the resolution of the stored data base. To accomplish this, the steps in the following paragraphs were taken. Reference 11 elaborates on the accompanying mathematics.

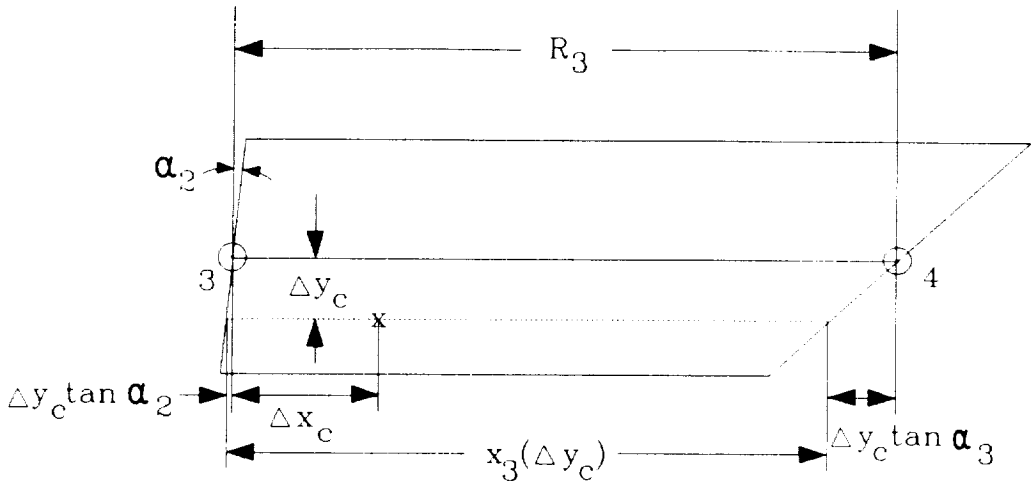

where $\alpha_2 = \frac{1}{2}(\lambda_2 - \lambda_3) = 5.8\,\text{deg}$ and $\alpha_3 = \frac{1}{2}(\lambda_3 - \lambda_4) = -46.5\,\text{deg}$

$$x_3(\Delta y_c) = R_3 + \Delta y_c \tan\alpha_2 + \Delta y_c \tan\alpha_3$$

and where λ_n is the direction angle of the nth course leg relative to North
Δx_c is incremental along course position
Δy_c is incremental across course position

Figure 4. Third Course Leg of the Gaming Area Course

1. Indexing the Course Coordinates

The corridor is indexed in an along- and across-course manner, with the i_x index incrementing from 1 to NX along the course and the j_y index incrementing from 1 to NY from left to right across the course. Each (i_x, j_y) point is then assigned the elevation of the closest data point in the terrain data base. The spacing of these indexed points is determined by the resolution of the terrain data base. (Note that a unit of length along the center line of the gaming area course is the same in the gaming area course and the earth-fixed coordinate systems.) Each set of NX points along the course for a given j_y will be referred to as a strip from the gaming area course.

2. Computing the Finite Fourier Transforms of All Strips

The finite Fourier transform (FFT) for each of the NY strips of NX terrain altitude data points is computed. The mean bias and trend of the strips are removed prior to computing the finite Fourier transforms (FFTs). The altitude profiles are then approximated by adding the mean biases and trends to truncated sums of sinusoids using the first MX complex coefficients from the NX/2 complex coefficients resulting from the computation of the FFTs of the strips.

3. Computing the Finite Fourier Transforms of the Approximating Coefficient Matrices

The finite Fourier transform (FFT) for each of the sets of coefficients generated in the first series of FFT calculations is computed. The means, $C_0(y_{CRS})$, and trends, $C_1(y_{CRS})$, are removed prior to the computation of the Fourier coefficients, $A_i(y_{CRS})$ and $B_i(y_{CRS})$. The coefficients are then approximated by adding the means and trends to truncated sums of sinusoids using the first MY complex coefficients of the NY/2 complex coefficients resulting from the FFTs of the coefficient matrices.

The final expression for the terrain elevation as a function of both along- and across-course position, $h(x_{CRS}, y_{CRS})$, is

$$h(x_{CRS}, y_{CRS}) = C_0(y_{CRS}) + C_1(y_{CRS}) \cdot (x_{CRS} + 1) + \sum_{i=1}^{MX} [A_i(y_{CRS}) \sin \omega_i x_{CRS} + B_i(y_{CRS}) \cos \omega_i x_{CRS}]$$

An example showing the ability of this approximating surface to represent the terrain profile accurately is presented in Fig. 5. The coordinates of longitude and latitude are congruous with the earth coordinates in Fig. 3. The corresponding altitude contour map is shown in Fig. 4 of Ref. 11. The course is 1098 dm long by 101 dm wide. The horizontal resolution of the data base is 1 square dm; and the vertical resolution is 0.01 dm. The overall stored terrain data compression factor is 110. (See Appendix A for details on the compression of the stored data base representing terrain.)

4. Calculating the First and Second Derivatives for the Pursuit Guidance Algorithm

Because the slope and curvature, in addition to the elevation, of the terrain are required for the pursuit guidance logic, the following expressions are used in the calculation of these quantities, based on the above approximation for the terrain elevation.

$$\dot{h}(x_{CRS}, y_{CRS}) = \frac{\partial}{\partial x_{CRS}}(h(x_{CRS}, y_{CRS})) \cdot \dot{x}_{CRS} + \frac{\partial}{\partial y_{CRS}}(h(x_{CRS}, y_{CRS})) \cdot \dot{y}_{CRS}$$

$$\ddot{h}(x_{CRS}, y_{CRS}) = \frac{\partial}{\partial x_{CRS}}(h(x_{CRS}, y_{CRS})) \cdot \ddot{x}_{CRS} + \frac{\partial^2}{\partial x_{CRS}^2}(h(x_{CRS}, y_{CRS})) \cdot \dot{x}_{CRS}^2 + 2\frac{\partial^2}{\partial x_{CRS} \partial y_{CRS}}(h(x_{CRS}, y_{CRS})) \cdot \dot{x}_{CRS}\dot{y}_{CRS} + \frac{\partial^2}{\partial y_{CRS}^2}(h(x_{CRS}, y_{CRS})) \cdot \dot{y}_{CRS}^2 + \frac{\partial}{\partial y_{CRS}}(h(x_{CRS}, y_{CRS})) \cdot \ddot{y}_{CRS}$$

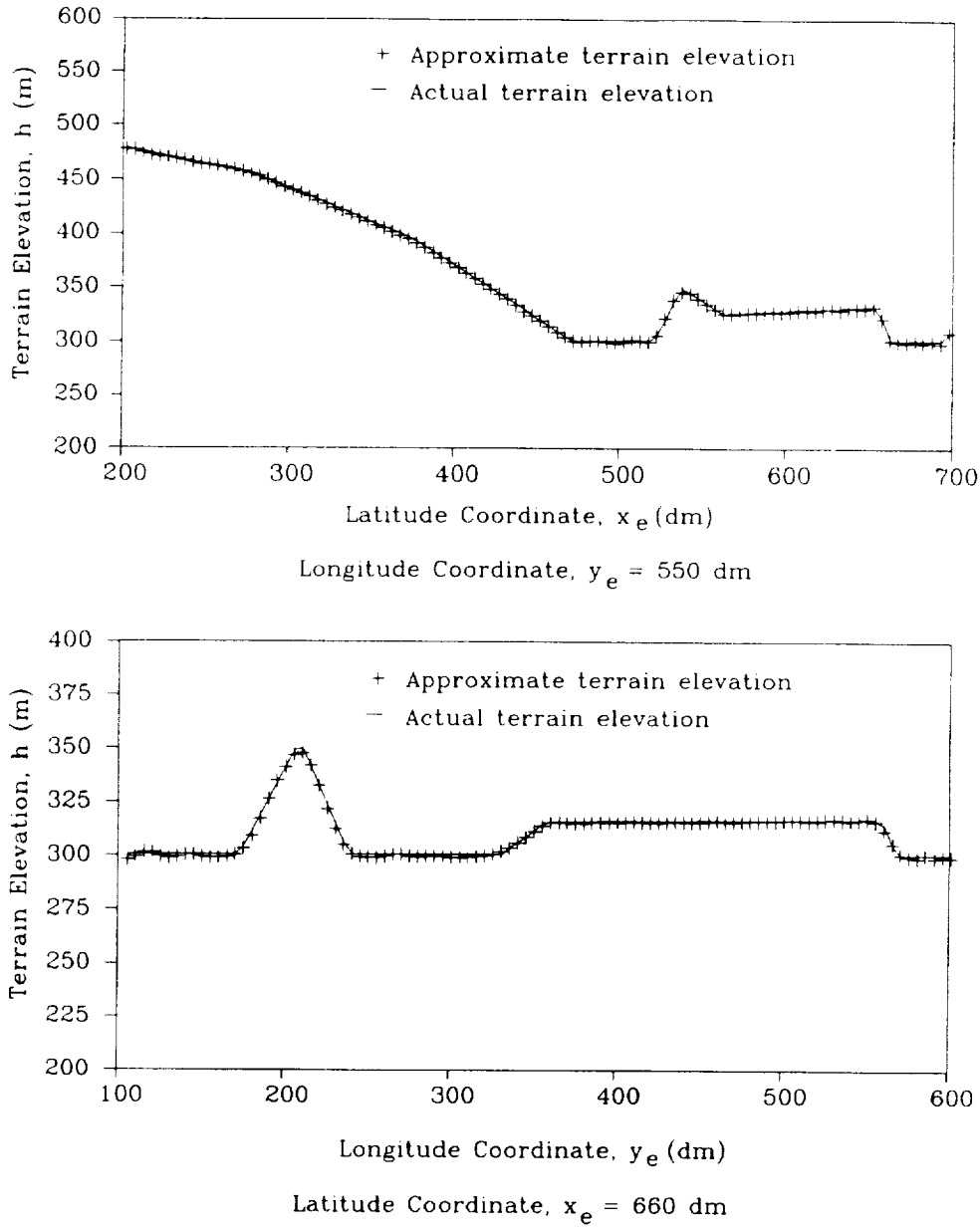

Figure 5. **Sample Fulda Gap Terrain Profiles, Approximate and Actual Elevation**

A more thorough description of the truncated two-dimensional sequential FFT technique for modeling digital terrain data bases is presented in Ref. 12.

SECTION III

OBSTACLE DETECTION AND AVOIDANCE MANEUVER SELECTION LOGIC (TASK 2)

In an automatically piloted vehicle flying in NOE conditions along a prescribed course, provisions must be made for unexpected obstacle avoidance. To this end, obstacle detection and avoidance maneuver selection (ODAMS) logic has been developed for the automatic guidance system and is represented by the "Task 2" block of Fig. 2. The correlation procedure demonstrated in Fig. 6 is performed in the along-course* coordinates; similar logic could be extended to across-course coordinates. The procedure uses a continuous approximation of the terrain between points from a Defense Mapping Agency (DMA) digital data base. Threats are represented in terms of an exposure height function of course coordinates. Obstacles are characterized by height increments either rising above the terrain height profile or descending below the threat exposure height profile. Obstacles that penetrate a volume surrounding the rotorcraft signify conflicts with the primary flight profile, which then invoke the avoidance logic shown in Fig. 6.

Two data bases with a common navigational reference system are identified at the top of Fig. 6: the stored flight profiles (vector $\underline{R}_n$), at the upper left; and the sensed profiles of terrain, obstacles, and threats, together with offset bias requirements for safety, at the upper right (vector $\hat{\underline{R}}_n$). For this project, it was assumed that the sensor(s) had perfect knowledge of all obstacles in the NOE gaming area [i.e., no attempt was made to simulate the sensor(s) or sensor fusion algorithms]. It is necessary to compare $\hat{\underline{R}}_n$ with $\underline{R}_n$ in real-time, resolve conflicts with the planned flight profile by automatically selecting a combination of lateral and vertical evasive maneuvers, and return to the planned flight profile where possible. If no combination of lateral and vertical evasive maneuvers will resolve a conflict between $\hat{\underline{R}}_n$ and $\underline{R}_n$, the rotorcraft is commanded to stop, and the pilot must select another flight plan.

A. DEFINITION OF SAFETY MARGIN ENVELOPES FOR DETECTING OBSTACLES

A three-dimensional safety margin envelope is defined mathematically in the form of a rectangular parallelepiped that encompasses the extremities of the rotorcraft with room to spare. This envelope, shown in Fig. 7, is centered on

*For the purposes of this discussion, the terms along-course and across-course refer to the rotorcraft total velocity direction relative to the pre-planned flight profile. In the nominal case, if the rotorcraft is following the pre-planned flight profile, the across-course velocity is zero.

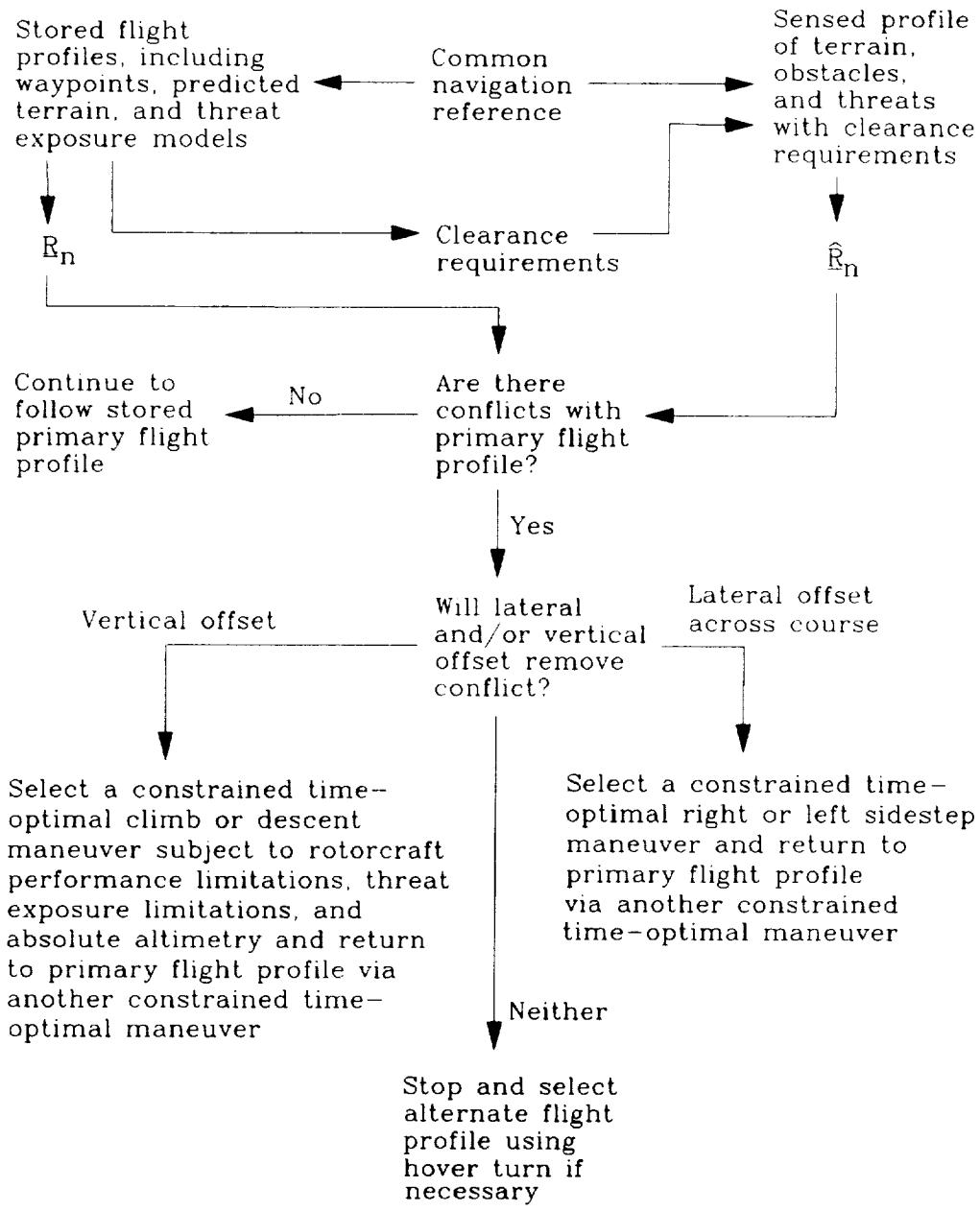

Figure 6. Procedural Flow Diagram for Avoidance of Unexpected Obstacles Encountered in the Along-Course Anticipative Array (Combined vertical and lateral maneuvers are possible)

the position of the rotorcraft at all times. Typical dimensions for encompassing the H-60 series rotorcraft or the XV-15 tilt-rotor aircraft would be: RX = RY = 10 meters (m) and RH = 7.5 m. The upper and lower surfaces of the safety margin envelope are partitioned into four squares each. If sensed obstacles penetrate one or more of these squares, from above or below, an appropriate action will be commanded to counteract the penetration(s). Testing for obstacle penetration constitutes the absolute altimetry portion of the obstacle avoidance logic. All vertical maneuvers commanded by this logic pre-empt vertical maneuvers commanded by the anticipative enveloping arrays described subsequently.

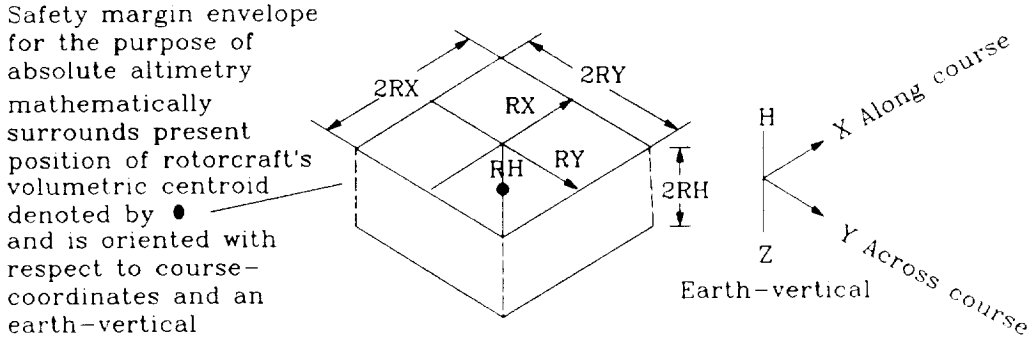

Figure 7. Safety Margin Envelope for Applying Absolute Altimetry to the Sensed Data Base to Avoid Obstacles

B. DEFINITION OF ALONG-COURSE ANTICIPATIVE ARRAY FOR SELECTION OF LATERAL EVASIVE MANEUVERS

When the rotorcraft is translating along the course, an anticipative array extends along and across the course (Fig. 8). This array consists of blocks measuring RX long by RY wide by at least 2×RH high and is referenced to a point ahead of the vehicle a distance R2×RX, called the "anticipative array reference point," equal to the along-course anticipative time, T_{p_x}, multiplied by the along-course velocity, V_x, and at a point above the terrain equal to the immediate radar altitude of the rotorcraft. The height of the blocks varies with commanded vertical deviations from the nominal radar altitude (discussed subsequently). Along the course, the blocks extend back from the anticipative array reference point a distance R2×RX to encompass the position of the rotorcraft and ahead of the anticipative array reference point 4×RX in Section 1 plus (R2+1)×RX in Section 2. The along-course anticipative array thus extends a total distance (R2+5)×RX forward of the anticipative array reference point. Across the course, the blocks extend ±4×RY. The sufficient field of coverage for the anticipative array is discussed in Ref. 13 from the viewpoint of maneuvering capability. The

anticipative array illustrated in Fig. 8 is divided into five sections (four contributing to the selection of the lateral evasive maneuvers and the fifth, to the vertical evasive maneuvers), each of which are described below.

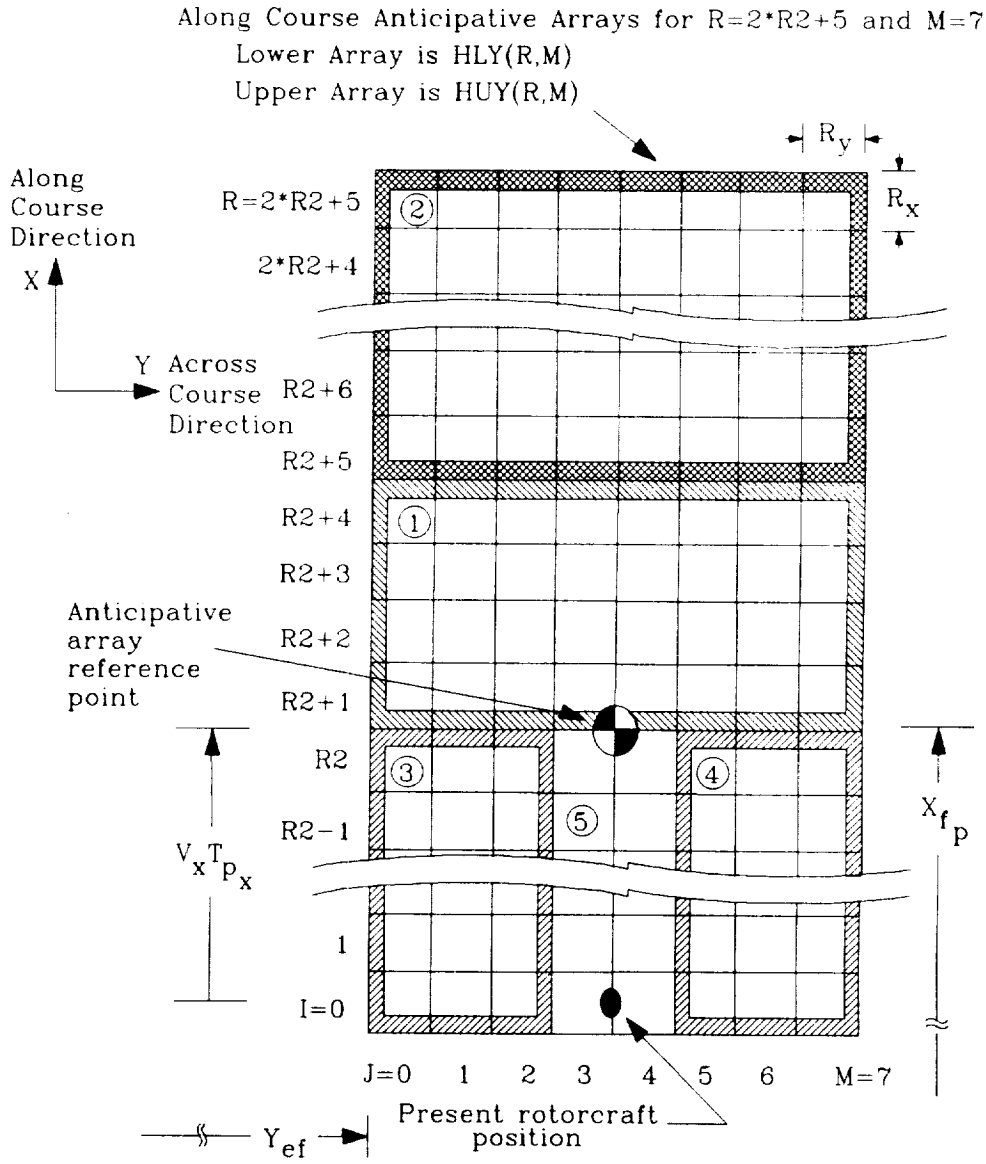

Figure 8. Plan View of Along-Course Anticipative Array of Sensed Terrain, Obstacle, and Threat Elevation Data for Safety Margin Envelopes

1) The first section (outlined with a leftward slanting border) consists of the four rows* of blocks beginning at the anticipative array reference point and extending away from the rotorcraft position. The section columns* are searched to detect obstructions in and around the planned flight path. An obstruction is defined as a point within a block that cannot be avoided using a vertical maneuver without exposing the rotorcraft to threats. This information is used to select an appropriate lateral evasive maneuver, if necessary. A more thorough description of the maneuver selection procedure is presented subsequently.

The obstacle detection and avoidance maneuver selection logic is disabled during a lateral evasive maneuver; therefore, it is essential that there be no obstruction between the rotorcraft and the along-course anticipative array reference point when the obstacle detection and avoidance maneuver selection logic is re-enabled at the conclusion of such a maneuver.

2) The second section in Fig. 8 (outlined with a crosshatched border) is used to search for unexpected obstructions just beyond Section 1 before the avoidance maneuver is initiated.

3) This section (outlined with a rightward slanting border) consists of the blocks before those of the first section and to the left of the middle two columns. These blocks represent obstacle data from the side-looking sensors. When a leftward lateral evasive maneuver is proposed, these blocks are interrogated for obstacles that would impede the maneuver. Only if the path is clear of obstacles is the proposed maneuver executed.

4) This is a mirror image of Section 3, and it governs rightward lateral evasive maneuvers.

5) The last section consists of the blocks of the middle two columns between the third and fourth sections and before the along-course anticipative array reference point. These blocks govern vertical evasive maneuver commands.

C. SELECTION OF APPROPRIATE LATERAL EVASIVE MANEUVERS

In every cycle of the rotorcraft's navigation computer, the updated columns of Section 1 are searched for obstructions, and a value of one or zero is associated with each column depending on whether obstructions are found in that column (1 = yes, 0 = no), and a lateral command is proposed (see Table 1 for interpretations).

*Rows and columns in the along-course anticipative array consist of blocks longitudinally and laterally equidistant from the reference point, respectively.

TABLE 1. PROCEDURAL DECISION LOGIC USING BLOCKS OF SECTION 1 OF THE ALONG-COURSE ANTICIPATIVE ARRAY DEPICTED IN FIG. 8

J = Left	0 1 2 3	4 5 6 7	Right	Decision regardless of unspecified elements	Destination Column	Command
	0	0		Continue to follow flight profile	$J_{com} = 3$	$y_{com} = y_{com}$
	0 0	1		Left-step RY	$J_{com} = 2$	$y_{com} = y_{com} - RY$
	1	0 0		Right-step RY	$J_{com} = 4$	$y_{com} = y_{com} + RY$
	0 0 1	1		Left-step 2*RY	$J_{com} = 1$	$y_{com} = y_{com} - 2RY$
	0 0 1	1 0 1		Left-step 2*RY	$J_{com} = 1$	$y_{com} = y_{com} - 2RY$
	1	1 0 0		Right-step 2*RY	$J_{com} = 5$	$y_{com} = y_{com} + 2RY$
	1 0 1	1 0 0		Right-step 2*RY	$J_{com} = 5$	$y_{com} = y_{com} + 2RY$
	0 0 1	1 0 0		Right-step 2*RY if VY $\geq$ 0, Left-step 2*RY if VY < 0	$J_{com} = 5$ or 1	$y_{com} = y_{com} \pm 2RY$
	0 0 1	1 1 1		Left-step 3*RY	$J_{com} = 0$	$y_{com} = y_{com} - 3RY$
	0 0 1	1 0 1		Left-step 3*RY	$J_{com} = 0$	$y_{com} = y_{com} - 3RY$
	0 0 1 1	0 1 1		Left-step 3*RY	$J_{com} = 0$	$y_{com} = y_{com} - 3RY$
	1 1 1	1 0 0		Right-step 3*RY	$J_{com} = 6$	$y_{com} = y_{com} + 3RY$
	1 0 1	1 0 0		Right-step 3*RY	$J_{com} = 6$	$y_{com} = y_{com} + 3RY$
	1 1 0	1 1 0 0		Right-step 3*RY	$J_{com} = 6$	$y_{com} = y_{com} + 3RY$
	0 0 1	1 1 0 0		Right-step 3*RY if VY $\geq$ 0, Left-step 3*RY if VY < 0	$J_{com} = 6$ or 0	$y_{com} = y_{com} \pm 3RY$
	0 0 1 1	0 1 0 0		Right-step 3*RY if VY $\geq$ 0, Left-step 3*RY if VY < 0	$J_{com} = 6$ or 0	$y_{com} = y_{com} \pm 3RY$
	0 0 1	1 1 0 1		Left-step 3*RY	$J_{com} = 6$	$y_{com} = y_{com} - 3RY$
	1 0 1 1	1 0 0		Right-step 3*RY	$J_{com} = 0$	$y_{com} = y_{com} + 3RY$

Legend: 0 = No obstruction present in Jth column of Section 1
1 = At least one element of the Jth column of Section 1 contains an obstruction

If a lateral position command is proposed as a result of the decision logic in Table 1, a maneuver urgency factor (MUF) is assigned by determining which block in Section 1 of Fig. 8 necessitates the maneuver. The least urgent maneuver (MUF = 1) would be necessitated by an obstruction in a block in the farthest row of Section 1, since the rotorcraft would then have the maximum distance in which to maneuver. Conversely, a maneuver necessitated by an obstruction in a block in the nearest row of Section 1 would be the most urgent (MUF = 4).

Following the MUF determination, all blocks to be passed through by the vehicle's safety margin envelope during the planned maneuver are selected from those of Sections 3 or 4 in Fig. 8. If penetration of any of these blocks, either from above or below, conflicts with current height commands, the maneuver is disallowed. If the nearest blocks of both the third and forth columns of the first section are clear of obstructions, the rotorcraft continues without lateral deviation. This phenomenon is exhibited in Fig. 9, where the initiation of the first lateral evasive maneuver was delayed until the maneuver path cleared the obstacle on the right side of the rotorcraft. If either of the nearest blocks of the third or fourth columns of Section 1 is obstructed, all columns of Section 1 to the side of the obstructed maneuver path are artificially assigned the value of 1, and the decision tree of Table 1 is re-evaluated, as demonstrated in Fig. 10. The flanking obstacle on the right side in Section 4 at X_{Crs} = 400 ft

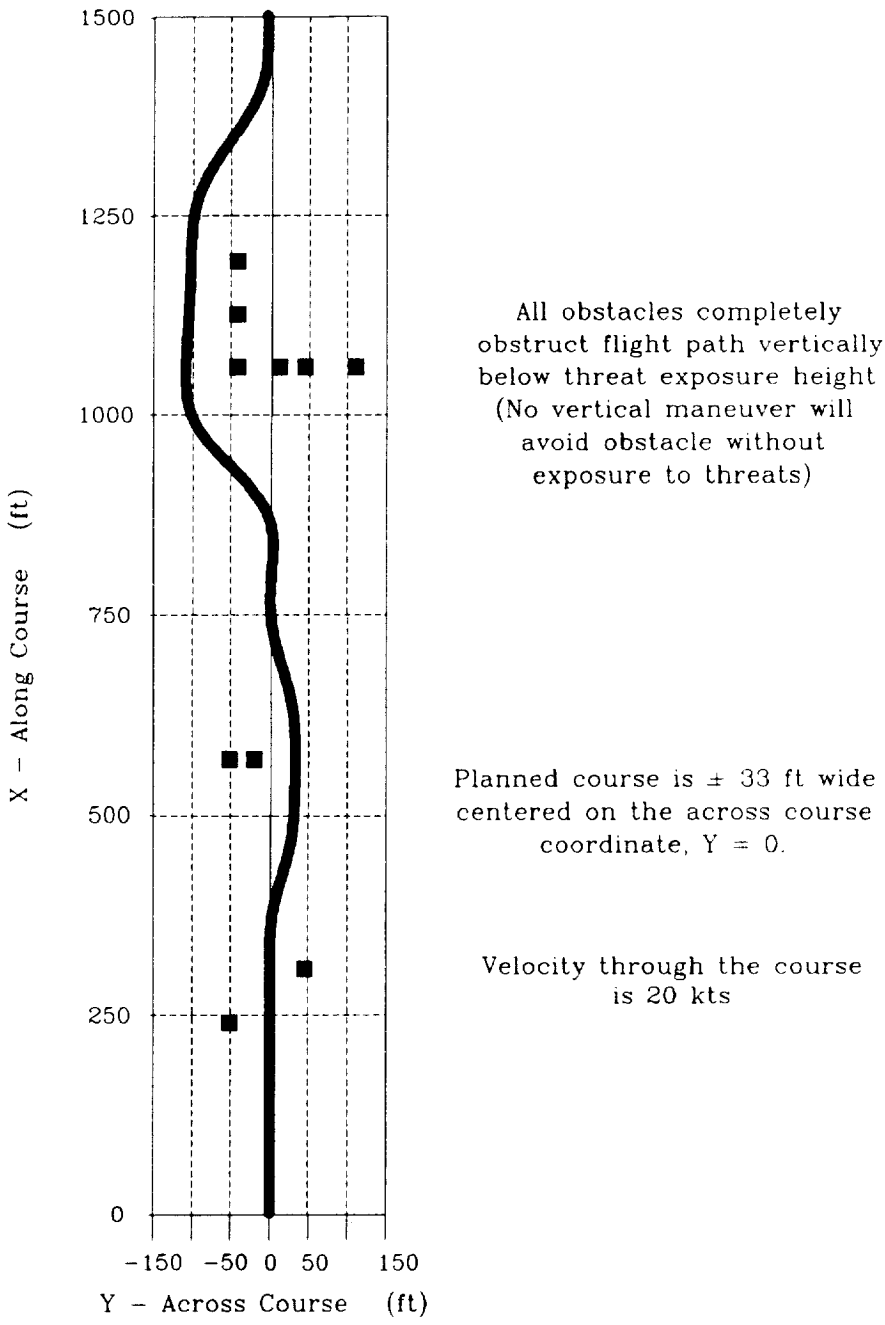

Figure 9. Unexpected Obstacle Avoidance Using Lateral Evasive Maneuvers Only

disallows a side step to the right. Because the originally proposed right step maneuver path did not clear the flanking obstacle before the obstructions necessitating the second maneuver entered the first row of Section 1, an alternate, more circuitous route via a 100-ft (30.5 m) left-step was chosen.

If all of the blocks of the path comply with the acceptance requirement stated above, the decision to continue the maneuver is governed by the post-maneuver blocks of Section 2. These first R2+1 blocks following the proposed maneuver are searched to expose obstructions. If no obstructions are detected, the proposed lateral evasive maneuver is initiated, and the obstacle detection and avoidance maneuver selection logic is disabled until its completion. If an obstruction is detected, however, the maneuver is disallowed, an obstruction is artificially placed in the last row of Section 1 in the column corresponding to the obstruction detected in Section 2, and the decision tree of Table 1 is re-evaluated. This is demonstrated in Fig. 11. Although the fifth and sixth obstacles on the course (counted from X = 0) were not in Section 1 of the along-course anticipative array when the decision was made to take evasive action, the interrogation of Section 2 caused a modification of the original commanded lateral displacement, and these obstacles were safely avoided.

D. RETURNING TO THE PRE-PLANNED FLIGHT PATH FOLLOWING A LATERAL EVASIVE MANEUVER

Upon completion of a lateral evasive maneuver, the automatic guidance routine attempts to return the rotorcraft to the pre-planned flight path via another constrained time-optimal lateral maneuver. To this end, a preliminary decision step is appended to the obstacle detection and avoidance maneuver selection logic when travelling with a steady offset from the pre-planned flight path. This preliminary step begins with a proposed lateral maneuver back toward the pre-planned flight path and determines the feasibility of such a maneuver based on the procedure outlined above. If possible, the return lateral maneuver is instigated. Otherwise, the obstacle detection and avoidance maneuver selection logic continues as previously described, interrogating the anticipative array for obstructions in the current flight path. Figure 9, for example, depicts a case in which two lateral evasive maneuvers were required to avoid unexpected obstructions in the pre-planned flight profile. Following the second maneuver, the return path was blocked for some distance; therefore, a clear return to the flight path could not be verified, and the return command was delayed until the obstacles were cleared.

Following this procedure, it is quite possible, through a series of lateral translations, for the rotorcraft to find itself more than $3 \times RY$ laterally displaced from the pre-planned flight path. Because the largest allowable lateral displacement command at present is $3 \times RY$, it is this command in the direction of the flight path that is sought by the return-to-path logic. Through a series of such commands, the vehicle can be brought back safely to the pre-planned flight path.

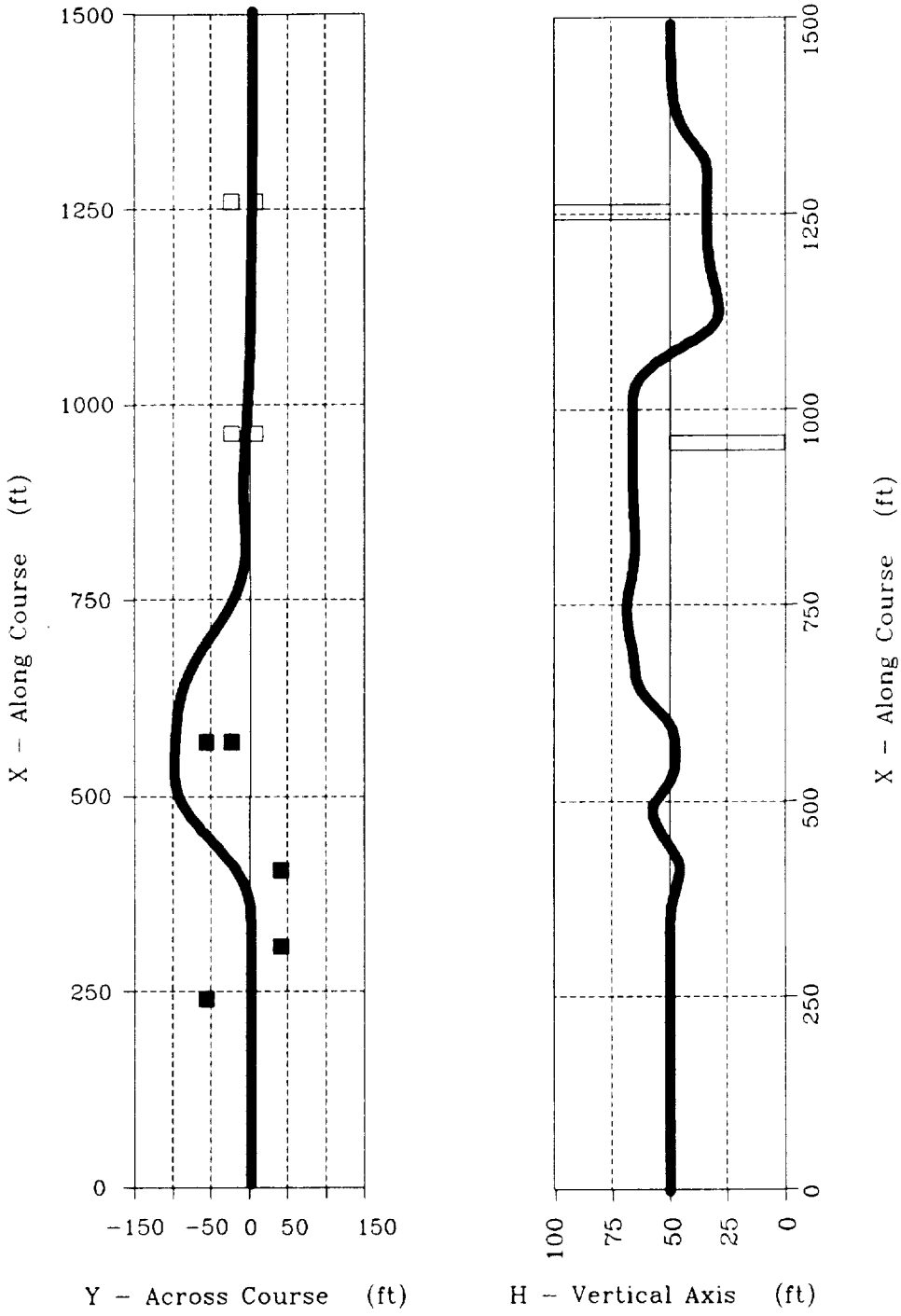

Figure 10. Unexpected Obstacle Avoidance Using Independent Lateral and Vertical Evasive Maneuvers

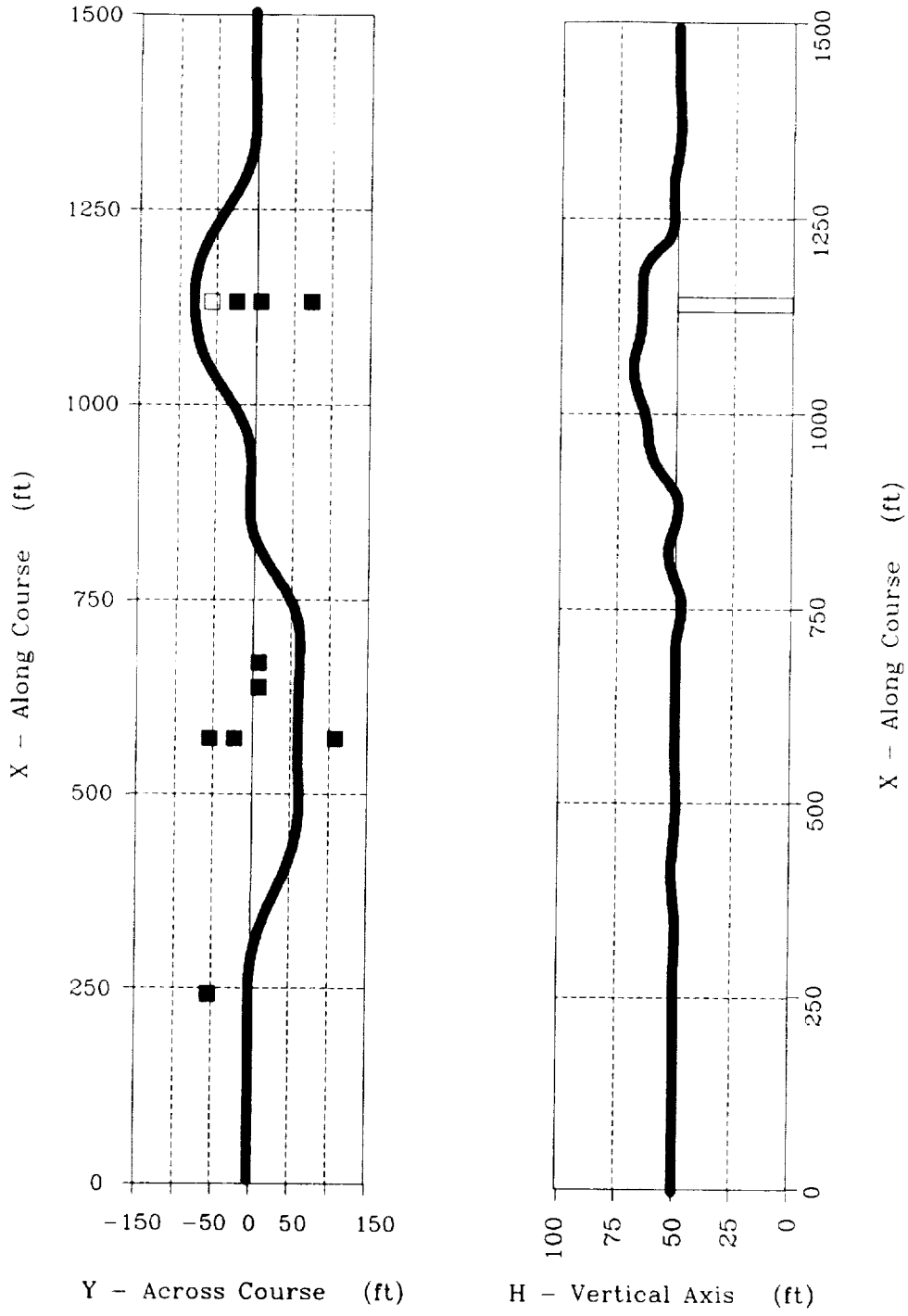

Figure 11. Unexpected Obstacle Avoidance Using Coupled Lateral and Vertical Evasive Maneuvers

E. SELECTION OF APPROPRIATE VERTICAL EVASIVE MANEUVERS

Because the rotorcraft will, in general, be traveling over uneven terrain, the altitude of the along-course anticipative array is based on the course altitude at the anticipative array reference point. The positions of the upper and lower surfaces of the anticipative array are depicted in Fig. 12, where V_{h_c} is the rate of change of course altitude at the reference point. The positions of the upper and lower surfaces are further modified by the current commanded height deviation from the pre-planned flight path altitude (Fig. 13).

If a lateral evasive maneuver is commanded, the search blocks for the commanded height deviation logic consist of those blocks in Sections 1 and 2 that define the proposed post-maneuver flight path. This height command is the destination height command. The absolute altimetry routine continues throughout the lateral evasive maneuver to modify this command appropriately. At the end of the lateral maneuver, the rotorcraft should be at the commanded destination height.

When no lateral evasive maneuver is required, the blocks of Section 5 determine the appropriate height deviation command. Each block is searched to identify penetrations from either above or below. For cases in which there is no current height deviation command, any penetration requires evasive action. If obstacles are discovered penetrating one or more of the blocks from below, the highest among them is determined, and the height required to clear it is commanded. Similarly, if obstacles are discovered penetrating one or more blocks from above, the lowest among them is determined, and the height required to clear it is commanded. If obstacles are discovered penetrating from both above and below, a stop command is issued, and the pilot must determine an appropriate course of action.

For cases in which there is a current height deviation command, the height of the anticipative array blocks is greater than required by the rotorcraft for safe navigation. It is therefore unnecessary to respond to all penetrations. The objective of the vertical obstacle avoidance logic in this case is to bring the rotorcraft as close to the pre-planned course altitude as soon as possible, as demonstrated in Fig. 14. If there are penetrations from both above and below, as long as there is navigable vertical distance between them, only the obstacle closest to the desired flight path altitude governs the deviation height command.

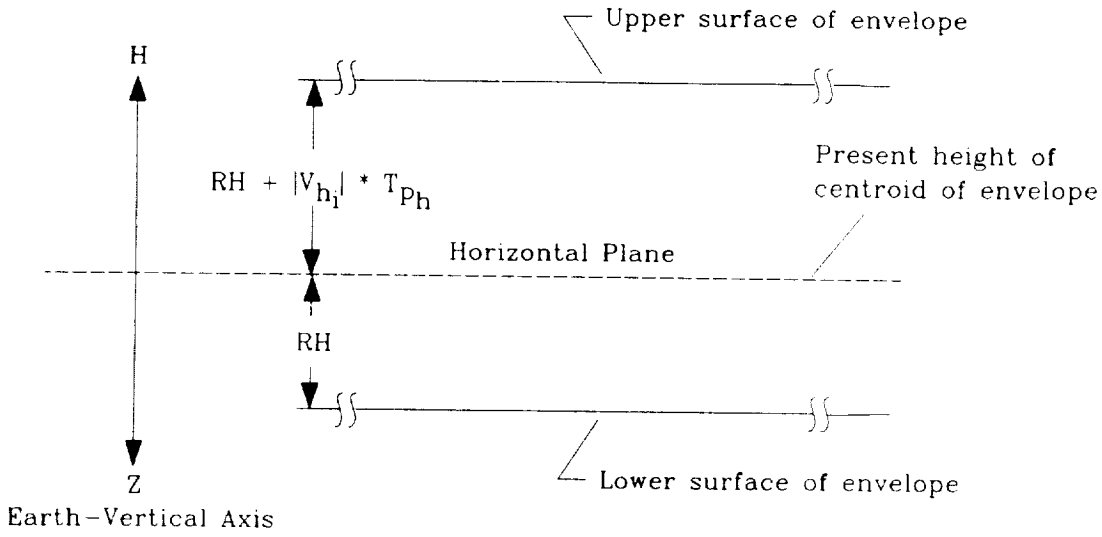

(1) Elevation of Anticipative Envelope, if Climbing ($V_{hi} > 0$)

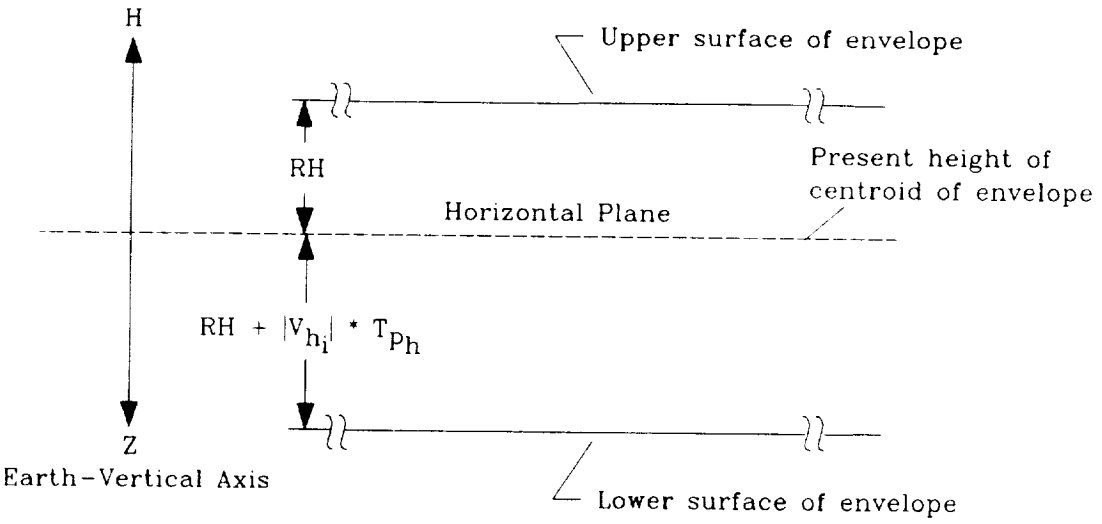

(2) Elevation of Anticipative Envelope, if Descending ($V_{hi} < 0$)

Figure 12. Flight Plan Showing Anticipative Geometry for Vertical Velocity Component with Safety Margin Envelope for Applying Sensed Data Base to Avoid Obstacles

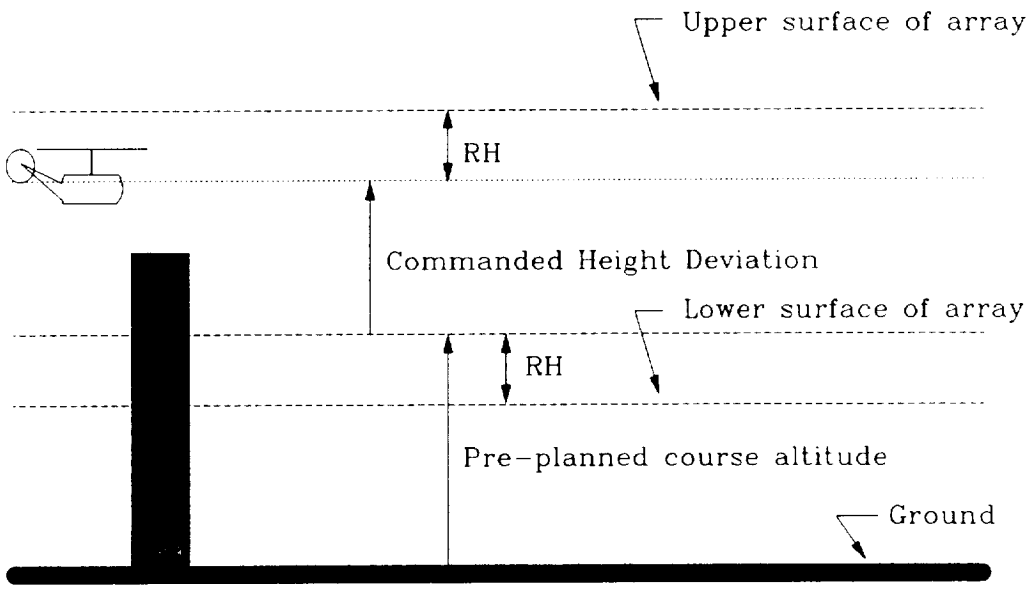

Figure 13. Positioning of Upper and Lower Surfaces of the Along-Course Anticipative Array with Current Commanded Height Deviation

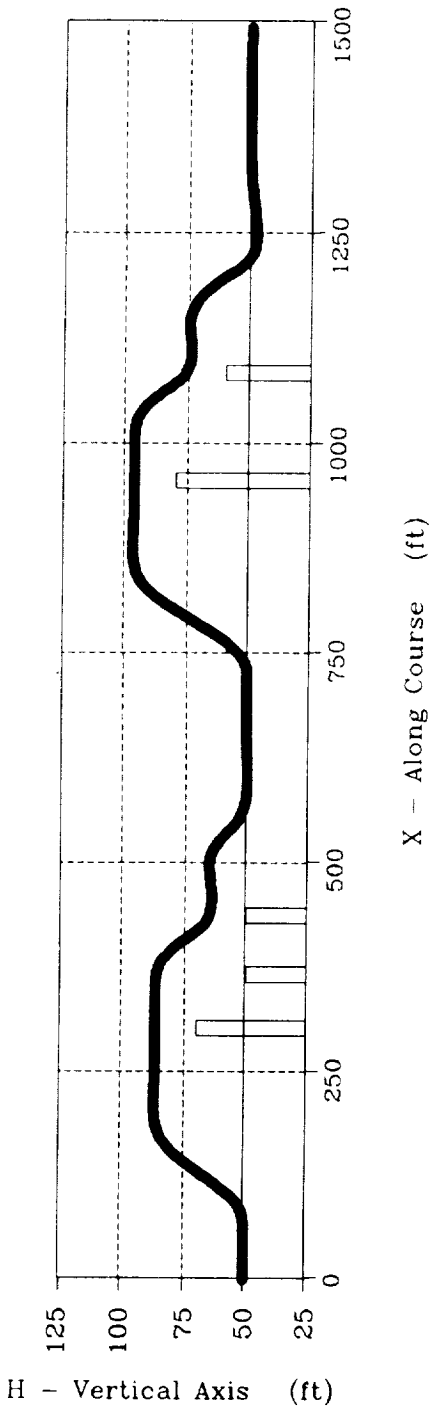

No obstacles completely obstruct flight path

(Vertical maneuvers will avoid obstacle without exposure to threats)

Planned course is ±16.5 ft high centered on the vertical course coordinate, H = 50. ft

Figure 14. Unexpected Obstacle Avoidance Using Vertical Evasive Maneuvers Only

SECTION IV

PURSUIT FEEDFORWARD GUIDANCE ALGORITHM (TASK 3)

Extraordinary precision in following guidance commands is required in NOE flight operations. This is dictated chiefly by two considerations:

1. The risk of becoming lost because the pattern and features of the sensed microterrain (e.g., streams, bushes, trees, rocks, and cultural features) may not be represented in the stored data base

2. The risk of damaging rotors, fuselage, empennage, and undercarriage in NOE operations.

In order to attain this level of precision, it is necessary to include pursuit feedforward guidance commands in the anticipative trajectory coupler. The pursuit feedforward guidance algorithms are contained in the "Task 3" block in Fig. 2.

Pursuit feedforward guidance will enhance pilot acceptance of ANOE flight operations, because the pursuit technique is the same as that employed by the pilot in manual curved course-and-profile guidance under visual meteorological conditions (VMC) if sufficient preview is available. Simulation experiments involving human operators have examined varying preview distances in the external visual field in the context of vehicular guidance along curved courses (Ref. 14) to determine conditions that promote pursuit guidance. The results show that an experienced human operator will adopt a pursuit feedforward guidance command input when sufficient preview of course curvature is available with the consequent reduction in curved course-following error. Pursuit feedforward guidance therefore provides a well-defined and validated form of guidance for corresponding manually and automatically controlled NOE flight operations.

A. DESIGN OF PURSUIT GUIDANCE CONTROL

A simplified block diagram of the ANOE controller is depicted in Fig 15. In a decoupled system, the depicted matrices are all diagonal, and the system equations simplify to four (4) independent equations, one each for the heave, sway, surge, and yaw axes. Given the simplified position response transfer function of

$$Y_c(s) = \frac{K_c}{s\left(s + \frac{1}{\tau_c}\right)}$$

where K_c is the high frequency gain (1/sec) of the controlled element displacement response to a velocity command, τ_c is a velocity command time lag (sec), and s is the Laplace operator (1/sec)

For each of the four independent axes, it is shown in Refs. 14 and 15 that it is ideally possible to negate the error, $\bar{e}(s)$, allowing position response, $\bar{y}(s)$, to follow commanded reference position, $\bar{r}(s)$, exactly with the inclusion of the higher order derivatives of the input, $\bar{r}(s)$ in the feedforward pursuit guidance control matrix $\bar{Y}_{pp}(s)$

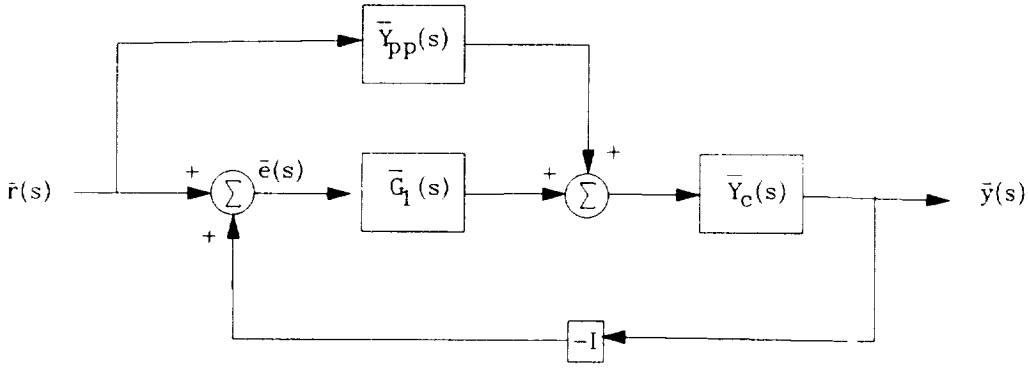

where $\bar{G}_1(s)$ represents the compensatory control matrix
$\bar{Y}_{pp}(s)$ represents the feedforward pursuit guidance control matrix
$\bar{Y}_c(s)$ represents the velocity command controlled element matrix
I represents the identity matrix

Figure 15. Simplified Block Diagram of the ANOE Controller

This can be demonstrated in the vertical guidance of the rotorcraft where it is desirable in NOE flight operations to maintain a minimum height above the terrain dictated by the terrain ground cover. The absolute course height profile, therefore, is the sum of the terrain elevation and the minimum navigable height, or

$$h_c = h_{min} + h_E(x,y)$$

where h_C is the commanded altitude, h_{min} is the minimum navigable height above the terrain, and $h_E(x,y)$ is the terrain elevation at the latitudinal and longitudinal geodetic coordinates (x,y). The required weighted linear combination of predicted commanded acceleration and velocity can be readily derived with a

low noise level from the continuous approximation of the terrain discussed previously. The resulting equation for the vertical velocity command signal, $\dot{h}_{ref}$, the input to Y_C, is

$$\dot{h}_{ref}(s) = \underbrace{\left[k_1\left(1+\frac{a_1}{s}\right)\right]}_{G_1(s)}\left[\underbrace{[h_c(s)-h(s)]}_{e(s)}\right]+\left[\underbrace{\frac{1}{K_c}\left(s^2+\frac{s}{\tau_c}\right)}_{Y_{pp}(s)}\right]\left[\underbrace{h_c(s)}_{r(s)}\right]$$

or, in the time domain

$$\dot{h}_{ref}(t) = k_1\left[(h_c-h)+a_1\int(h_c-h)dt\right]+\frac{1}{K_c}\left(\ddot{h}_c+\frac{1}{\tau_c}\dot{h}_c\right)$$

Since $a_1 \ll 1$, the compensatory guidance bandwidth $1/T_b$ is approximately

$$\frac{1}{T_b} = \frac{1}{2\tau_c}-\frac{1}{2}\sqrt{\frac{1}{\tau_c^2}-4K_c k_1}$$

The ability of this guidance algorithm to follow precisely a prescribed NOE height profile is demonstrated with the following example (Fig. 16) in which $1/T_b \doteq 0.5$ rad/sec, if $1/\tau_c = 2.5$ rad/sec, and $K_c = k_1 = 1$ rad/sec. A truncated sum of sinusoids was developed to simulate the terrain profile based on power spectra of sample terrain profiles presented in Ref. 15. The spatial break frequency of the envelope of the sum of sinusoids is approximately 0.0061 rad/(ft traversed). The sum of sines used contained three frequencies at or below the break and two frequencies above.

$$h_E = 120.57 \sum_{i=1}^{5} A_i \sin(\omega_i t) + 990\text{ft}$$

$$h_c = h_E + 10\text{ft}$$

$$\dot{h}_c = \dot{h}_E = 120.57 \sum_{i=1}^{5} A_i \omega_i \cos(\omega_i t)$$

$$\ddot{h}_c = \ddot{h}_E = -120.57 \sum_{i=1}^{5} A_i \omega_i^2 \sin(\omega_i t)$$

where

$\omega_i = \Omega_i v_T$

v_T = ground track velocity

The magnitude of A_i is determined by the expression

$$|A_i| = \frac{0.0061}{\sqrt{\Omega_i^2 + 0.0061^2}}$$

The sign of A_i, as well as the values for Ω_i, were determined such that $\dot{h}_c(0) = 0$. This was done to prevent the intrusion of transients in the test runs.

i	A_i (ft)	Ω_i (rad/ft)	$\omega_i(v_T = 20$ kts) (rad/sec)
1	-1.0	0.00131	0.0442
2	-1.0	0.00296	0.100
3	0.70	0.0061	0.206
4	0.464	0.0131	0.442
5	-0.215	0.0283	0.956

A batch simulation was then performed in which the rotorcraft was required to fly at a constant forward velocity of 20 kt over the defined terrain profile. Using this guidance algorithm, the maximum error realized was less than 0.3 m (1 ft).

B. LATERAL/DIRECTIONAL COURSE FOLLOWING

The flight plan is defined using waypoints within the gaming area and will, in general, meander with respect to the gaming area course. Each waypoint has associated with it the properties of latitudinal and longitudinal geodetic position and along-waypoint-course velocity. The waypoint course is defined as the straight legs connecting these sequenced waypoints. This course definition, however, yields discontinuities in both the first and second derivatives of the lateral position and heading commands at the waypoints. A prescribed transition leg is thus required in order to take advantage of the pursuit guidance algorithm defined previously.

A hyperbolic arc was chosen to represent this transition leg because of the relatively gradual entrance and exit characteristics of a turn along such a profile (Ref. 12). There remain slight discontinuities in the derivatives of the lateral and directional commands at the entrance and exit from the transitional hyperbolic legs, but the effects of these have been shown in batch simulations to be minimal. An example of a typical waypoint transition is presented in Fig. 17.

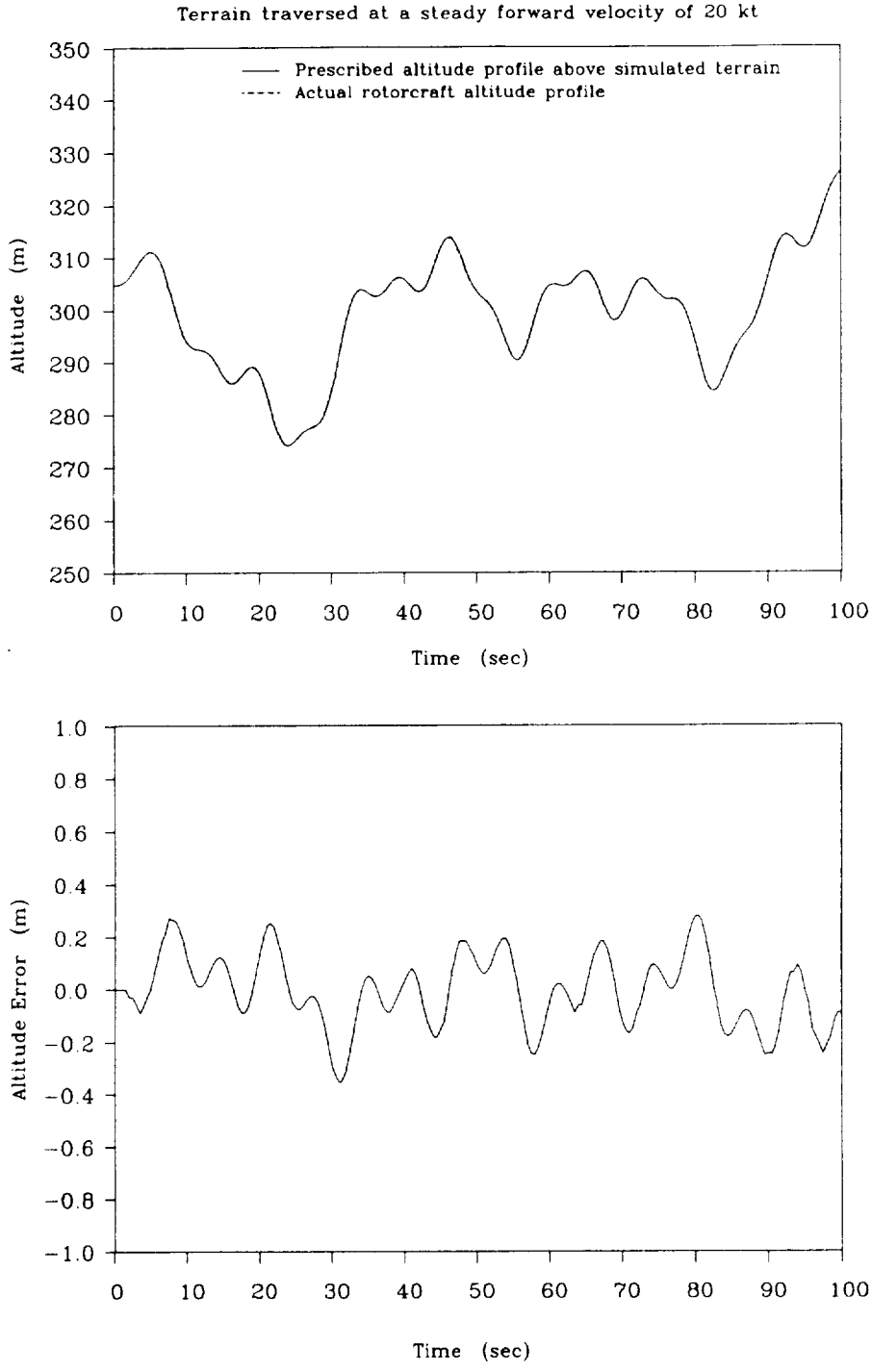

Figure 16. Terrain Following Test over Simulated Terrain

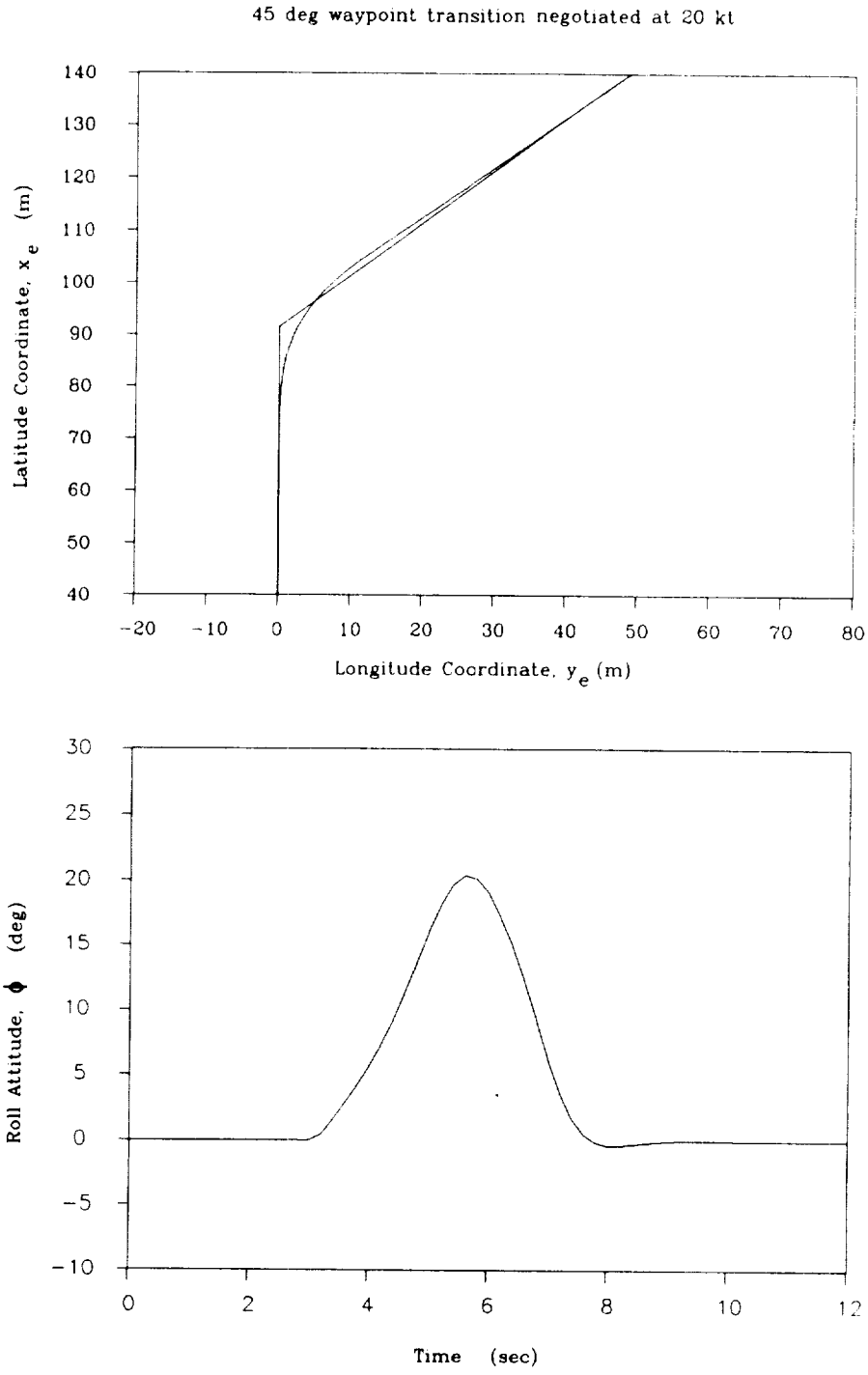

Figure 17. Sample 45-deg Heading Change at Waypoint Transition using Hyperbolic Transition Leg

SECTION V

CONSTRAINED TIME-OPTIMAL EVASIVE MANEUVERS (TASK 4)

As previously asserted, rapid response obstacle avoidance maneuvers are required for automatically-piloted NOE flight operations. This section presents a general description of the development of these maneuvers, which are represented as the "Task 4" block in Fig. 2. The four maneuvers chosen, each involving primarily one of the four independent axes of the rotorcraft, were (a) the bob-up and -down, (b) the hover turn, (c) the lateral sidestep, and (d) the longitudinal acceleration/deceleration maneuver. These maneuvers are intrinsic to the completion of most NOE flight operations and must, in order to ensure pilot acceptance when performed automatically, emulate the pilot's own guidance tactics and techniques. Recent Black Hawk (UH-60A) flight tests and simulation tests have shown the ability of a pilot to perform a nearly time-optimal maneuver when circumstances warrant aggressive response (Refs. 16 through 18). Based on these results, the automatic rapid response obstacle avoidance maneuvers were defined as constrained time-optimal maneuvers.

The main consideration in the design of automatic constrained time-optimal maneuvers is the definition of the constraining limits. As an example, the constraining limits in the case of a vertical maneuver are limits in vertical velocity, acceleration, and acceleration rate or jerk. These limits exist both as performance limits of the rotorcraft and as acceptance limits for the pilot, the latter of which can be considered most constraining in an automatically-piloted vehicle flying in NOE conditions. The constraining limits chosen for this project (as given in Table 2) were based on the most benign of those exhibited in the flight tests presented in Refs. 16 through 18.

Figure 18 presents the constrained time-optimal velocity command profile required to attain the maximum allowable vertical velocity in the least amount of time subject to limits on vertical acceleration and jerk. This command signal is designed to take full advantage of the constraining limits. To extend this technique into a constrained time-optimal bob-up maneuver, a multistage command response is in general required. In the first phase of the response, the rotorcraft builds vertical acceleration at the maximum acceptable positive jerk until the maximum acceptable vertical acceleration is achieved. The rotorcraft then continues to accelerate at this maximum until a maximum negative jerk brings the rotorcraft to a steady climb at the vertical velocity limit. These stages of the response are achieved using the velocity command profile of Fig. 18. The maximum rate of climb is continued until the position error passes through a switching error criterion that represents the minimum vertical stopping distance given the deceleration and jerk limits. Thereafter, the command sequence reverses polarity until the position error is nulled.

TABLE 2. CONSTRAINING LIMITS FOR RAPID RESPONSE MANEUVERS

Vertical $\begin{cases} \dddot{h}_{max} = 20 \text{ ft/sec}^3; \quad \ddot{h}_{max} = 16 \text{ ft/sec}^2; \quad \dot{h}_{max} = 20 \text{ ft/sec} \\ \dddot{h}_{min} = -15 \text{ ft/sec}^3; \quad \ddot{h}_{min} = -10 \text{ ft/sec}^2; \quad \dot{h}_{min} = -15 \text{ ft/sec} \end{cases}$

Lateral*

$$\ddot{\phi}_{max}(I,J) = \begin{bmatrix} 10 & 15 & 20 & 30 \\ 20 & 25 & 40 & 50 \\ 30 & 40 & 50 & 50 \end{bmatrix} \text{deg/sec}^2$$

$$\dot{\phi}_{max}(I,J) = \begin{bmatrix} 5 & 7.5 & 10 & 15 \\ 10 & 15 & 20 & 25 \\ 15 & 20 & 30 & 30 \end{bmatrix} \text{deg/sec}$$

$$\phi_{max}(I,J) = \begin{bmatrix} 10 & 10 & 10 & 15 \\ 10 & 15 & 20 & 25 \\ 15 & 20 & 30 & 30 \end{bmatrix} \text{deg}$$

$y_{max} = 50.667$ ft/sec (30 kt)

Longitudinal $\ddot{\theta}_{max} = 20$ deg/sec^2; $\dot{\theta}_{max} = 10$ deg/sec; $\theta_{max} = 10$ deg

Directional $\ddot{\psi}_{max} = 0.25$ rad/sec^2; $\dot{\psi}_{max} = 0.5$ rad/sec

---

*Lateral maneuvers are constrained, based on a two-digit maneuver urgency factor determined by the ODAMS. The matrix indices correspond to the digits of this factor (Ref. 12).

* * * * * * * * * * * * * * * * * * *

This constrained time-optimal response is realized via a model following scheme. For each maneuver, a simple single-axis model in which the states are directly controllable performs the prescribed maneuver. The model states are fed forward into the rotorcraft flight control system (FCS) with appropriate gains to force the rotorcraft to follow the model through the maneuver. An example of such a constrained time-optimal bob-up maneuver is presented in Fig. 19.

Similar guidance concepts were employed in the design of the other three maneuvers, and a more thorough description of these maneuvers is presented in Ref. 12.

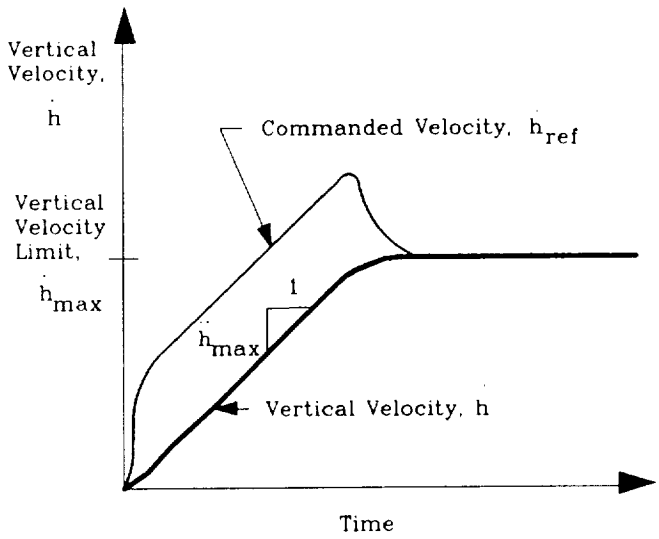

Figure 18. Constrained Time-Optimal Vertical Velocity Profile

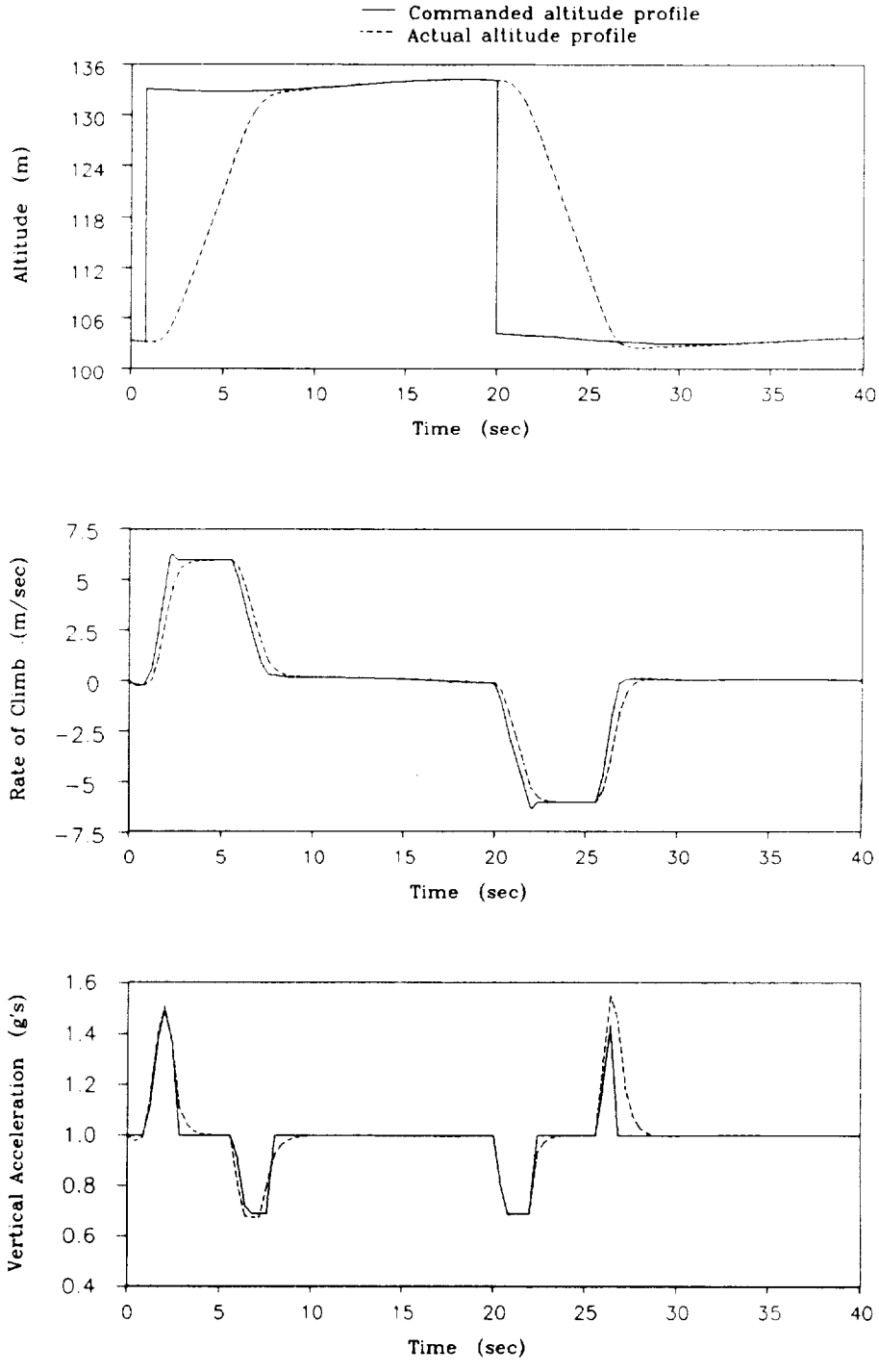

Figure 19. 30 m Constrained Time-Optimal Bob-Up Maneuver

SECTION VI

MAJOR COMPONENTS OF THE NASA ARC SIMULATION

The major components of the NASA ARC simulation are summarized in Table 3.

TABLE 3. MAJOR COMPONENTS OF THE REAL-TIME PILOTED SIMULATION PERFORMED AT THE NASA ARC

Motion System	Six-degree-of-freedom Vertical Motion Simulator (Refs. 9 and 10)
Visual System	Three window, Evans & Sutherland CT-5A, with a field of view of 38 deg vertical by 140 deg horizontal. The plan view of the terrain used for this simulation is shown in Fig. 20.
Rotorcraft Model	The characteristics of the rotorcraft were modeled with a translational rate-command flight control system in each axis of control. See the text and table under Subtopic A for a summary of the rotorcraft's bandwidths in each axis of control.
Atmospheric Disturbances	Steady winds, boundary layer wind shear, and turbulences were simulated. See Ref. 12 for details.
Head-Up Display	Multi-mode HUD with different options for NOE traveling and hovering. See the text under Subtopic B and Figs. 21 and 22 for details.
Force Feel System	A full authority McFadden hydraulic control feel loading system was used for all control axes (collective, longitudinal and lateral cyclic, and pedals). See Table 4 for the feel system characteristics in each axis.
Moving Map	A Silicon Graphics IRIS workstation was used to display an inside-out, course-up plan view of the terrain moving beneath the centered rotorcraft. The pilot could adjust the scale of the display to be 5, 20, or 100 dm/in (0.025, 0.1, or 0.5 nmi/in). Digital heading and time, together with a moving scale of heading, were provided across the top of the map (shown in Fig. 23).
Head-Down Instruments	The head-down instruments were arranged to be close to that of an Apache. See Fig. 24 for a pictorial description of the instruments.
Aural Display	A Votrax system was used to generate audio announcements of impending evasive maneuvers. Rotor flapping background noise was also provided.
Side Tasks	Three different side tasks were used as surrogates for mission tasks other than flight guidance and control. See the text in Section VII.A.3 for descriptions of the side tasks.

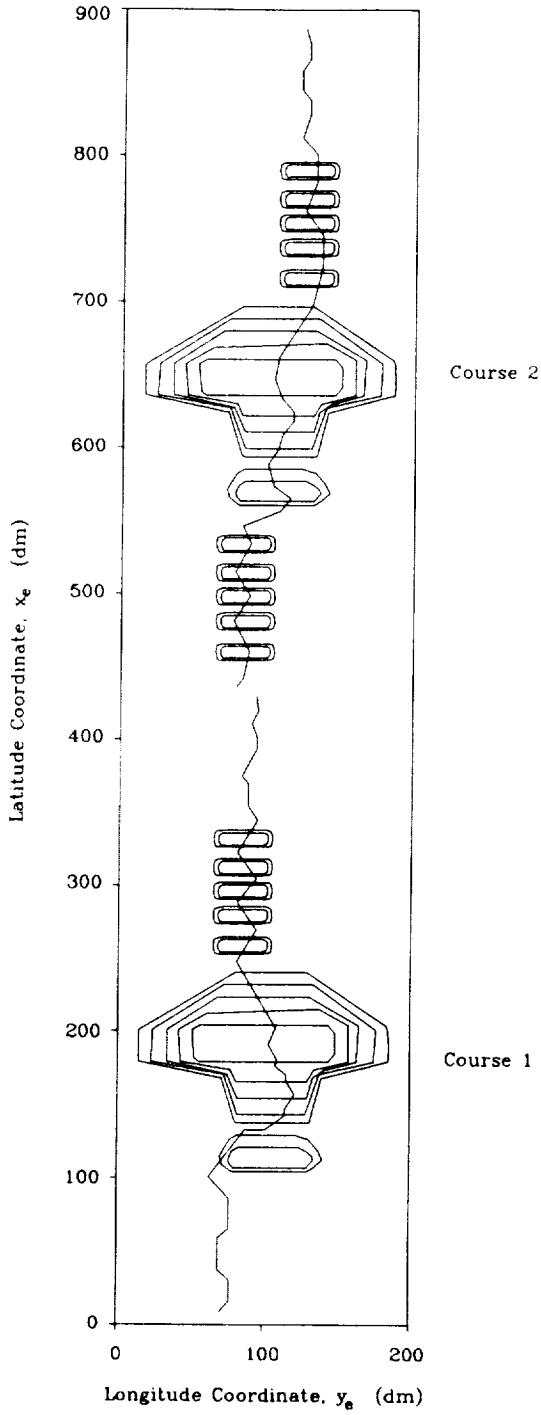

Figure 20. CT-5A Gaming Area Course for Automated NOE Simulation Flight Tests at ARC

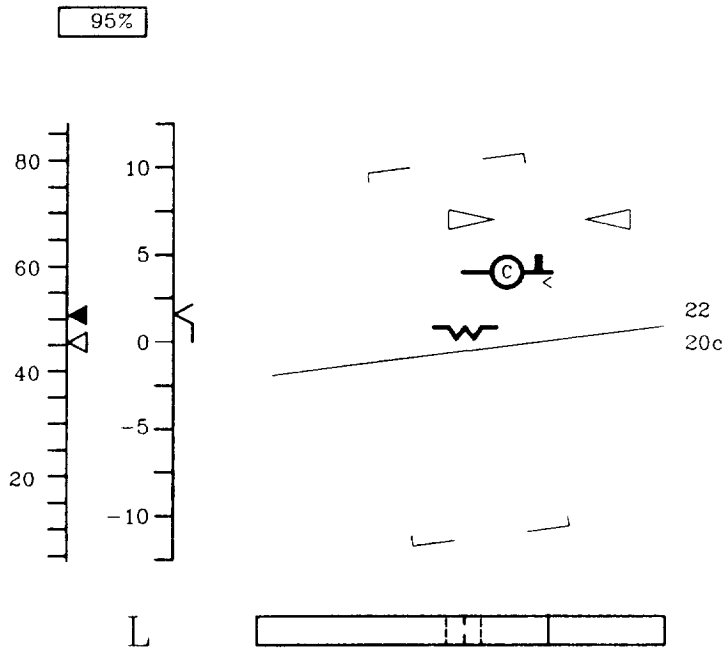

a. Monitoring HUD Configuration

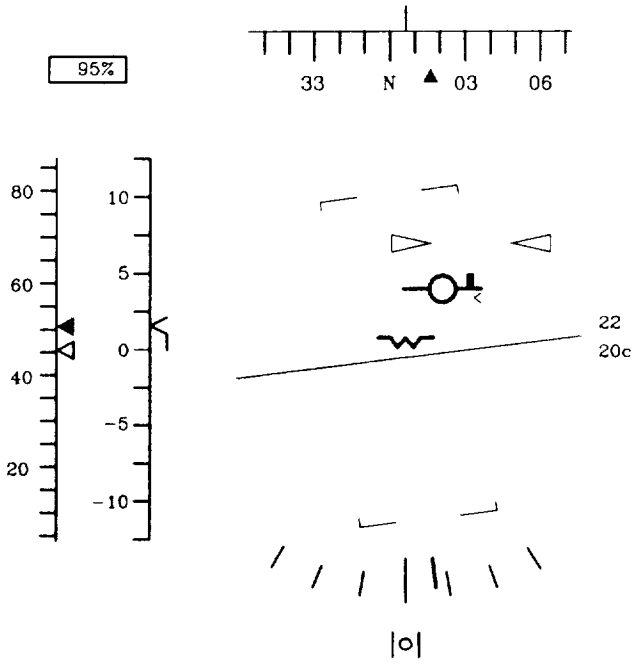

b. Manual Guidance HUD Configuration

Figure 21. Azimuth-Elevation Display for NOE Traveling

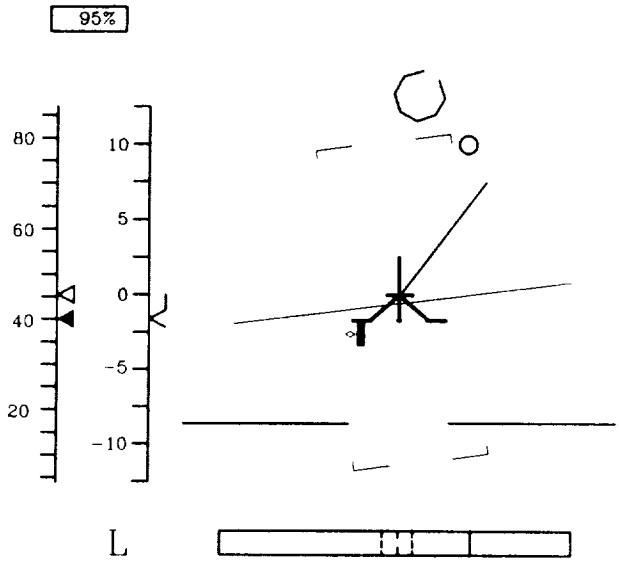

a. Monitoring HUD Configuration

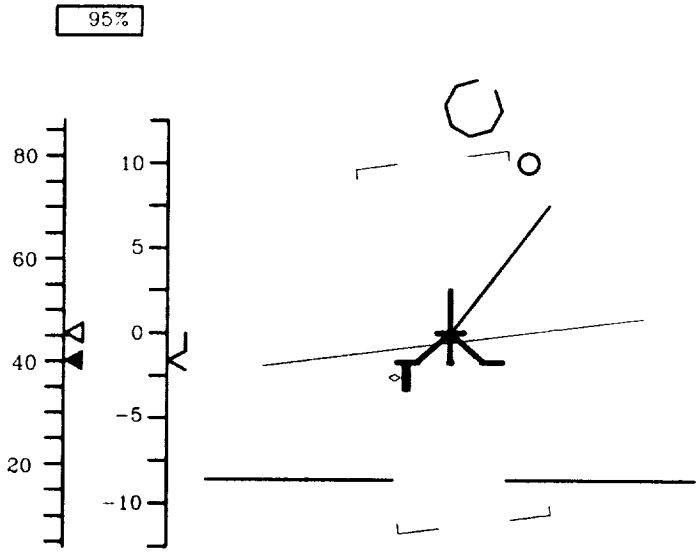

b. Manual Guidance HUD Configuration

Figure 22. Plan View Hover Task Display with Attitude Overlay

TABLE 4. CONTROL FEEL LOADING CHARACTERISTICS

AXIS	GRADIENT (lb/in)	BREAKOUT (lb)	DAMPING (lb/in/sec)	FRICTION (lb)
Longitudinal	2.0	1.25	0.1	0.5
Lateral	1.0	0.75	0.1	0.5
Collective	2.4	2.0	0.3	1.4
Yaw	6.0	2.75	0.0	1.0

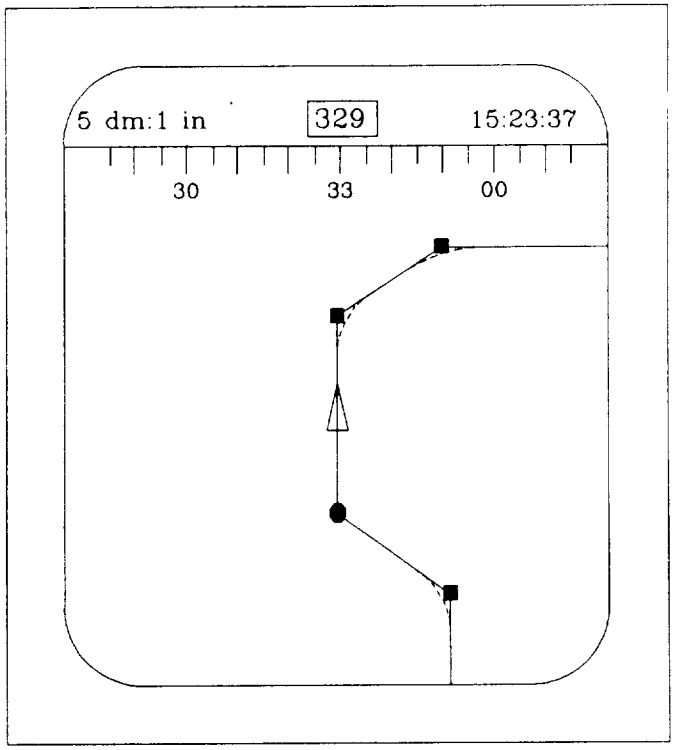

Figure 23. Moving Map Display

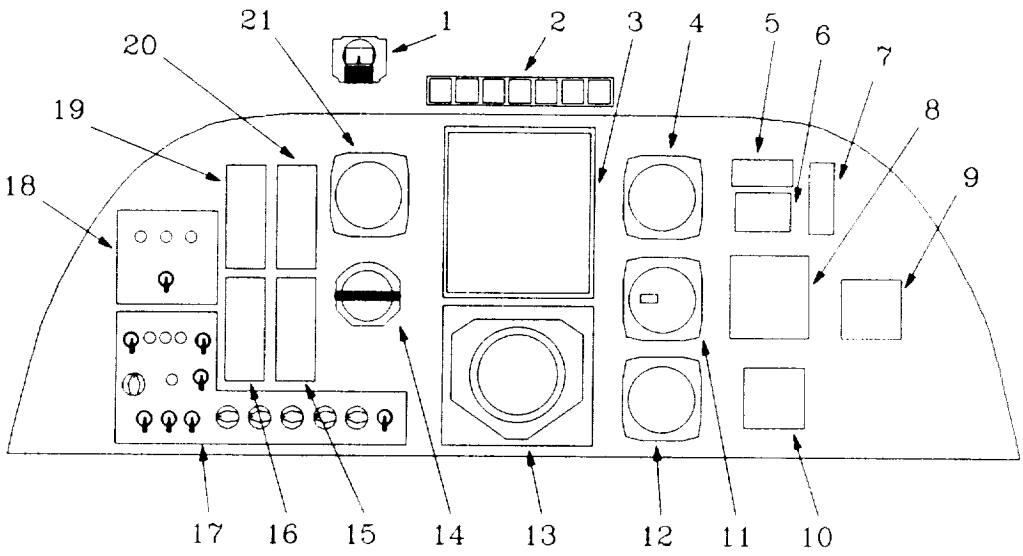

Figure 24. AH-64 Pilot Station Instrument Layout

Numbers indicate the following:

1 Standby magnetic compass

2 Master caution/warning panel (contains lighted auto-guidance toggle)

3 CRT for moving map display

4 Radar altimeter

5 Radio call placard

6 Stabilator position indicator

7 Stabilator/airspeed placard

8 Radar warning display

9 Clock

10 Accelerometer

11 Barometric altimeter

12 Instantaneous vertical speed indicator (IVSI)

13 Horizontal situation indicator (HSI)

14 Standby attitude indicator

15 Engine (N_P), rotor (N_R) indicator

16 Engine gas generator (N_G) indicator

17 Fire control panel

18 Choice reaction time side-task control panel

19 Engine turbine gas temperature (TFT) indicator

20 Engine torque indicator

21 Airspeed indicator

A. ROTORCRAFT MATHEMATICAL MODEL WITH TVC-SCAS

The model of the rotorcraft dynamics was simulated using small perturbation stability and control derivatives. The model was designed to simulate a highly augmented vehicle having translational velocity command, position hold capabilities. The transfer functions for vehicle response to cockpit control (i.e., for the controlled element, $\overline{Y}_c(s)$, without any of the pursuit feedforward or compensatory feedback terms shown in Fig. 15) are shown in Table 5.

TABLE 5. TRANSFER FUNCTIONS FOR VEHICLE RESPONSE TO COCKPIT CONTROL

Cockpit Controller	Vehicle Response	Transfer Functions for Manual Control Under:	
		Rate Command	Position Hold
Collective	Vertical Velocity	$\frac{\dot{h}}{\dot{h}_{R_p}} = \frac{2.0}{(s+2.0)}$	$\frac{h}{h_c} = \frac{1.0}{(s+0.5)(s+2.0)}$
Pedals	Yaw Rate	$\frac{\dot{\psi}}{\dot{\psi}_{R_p}} = \frac{4.0}{(s+4.0)}$	$\frac{\psi}{\psi_c} = \frac{4.0}{(s+1.0)(s+4.0)}$
Longitudinal	Forward Speed	$\frac{\dot{x}}{u_{R_p}} = \frac{0.8}{(s+0.8)}$	$\frac{x}{x_c} = \frac{0.16}{(s+0.2)(s+0.8)}$
Lateral	Lateral Speed	$\frac{\dot{y}}{v_{R_p}} = \frac{0.8}{(s+0.8)}$	$\frac{y}{y_c} = \frac{0.16}{(s+0.2)(s+0.8)}$

B. HEAD-UP DISPLAY

Two display configurations and two display modes were available to the evaluation pilot. The symbols to be presented by each of these configuration-mode combinations are presented in Figs. 21 and 22. The first configuration was an azimuth-elevation display format designed for forward flight at the very low speeds typical in NOE operations. One mode of this configuration was the monitoring display (Fig. 21a), for use in the pilots' monitoring of the automated flights. The side-task displays for divided attention were included in this display format. The other azimuth-elevation display mode (Fig. 21b) omitted the side-task displays, including instead additional aircraft state information to

aid in the manual guidance of the rotorcraft in NOE flight conditions. The following is a description of how the pilots were expected to use the manual guidance mode of the azimuth-elevation display configuration.

1. **Use of the Azimuth-Elevation Format**

a. **Heading**. The heading tape at the top of the HUD (Fig. 21b) provides the pilot with current and commanded heading information. The vertical "lubber line" in the center of the displayed tape is the reference marker. The heading tape slides along the top of the display, disappearing at and appearing from the display limits of the tape, such that the current heading is indicated by the reference marker. A solid triangular caret affixed to the sliding tape indicates commanded heading. The task of the pilot is to maintain the solid command caret aligned with the reference marker using the pedal controllers.

b. **Altitude**. Two scales on the left side of the display provide altitude and altitude rate information in a compatibly scaled "state-and-rate" format. The left-most scale is a sliding radar altitude tape. An open triangular marker is fixed in the display to provide the reference marker. The radar altitude tape slides vertically, disappearing at and appearing from the display limits of the tape, such that the current radar altitude is indicated by the reference marker. An adjustable solid triangular caret affixed to the sliding tape indicates commanded radar altitude.

The scale immediately to the right of the sliding radar altitude tape is the vertical velocity scale. This scale is fixed in the display. Vertical velocity is indicated via the left pointing marker, including a "tail" which extends to the zero vertical velocity point. The purpose of the tail is to provide the pilot with an aid to make a rough estimate of the vertical velocity with only a cursory glance at the symbology.

c. **Longitudinal Velocity**. A digital display of the actual and commanded longitudinal velocity (in kt) is located half-way up the far right side of the HUD. The commanded velocity is presented below the actual value together with the letter "c". Additional longitudinal velocity cues are available in the vertical error bar and acceleration caret located on the right-hand side of the pseudo-flight path symbol (Fig. 21). The length of the growing and shrinking longitudinal velocity error bar is proportional to the error, and the longitudinal acceleration caret provides information about the rate of change of the longitudinal velocity error. The pilot's task is to null the velocity error using longitudinal control inputs.

d. **Path/Terrain Following Guidance**. A "ghost" aircraft symbol (the two opposing isosceles triangles in the central portion of the display) provides vertical and lateral velocity commands relative to the "w" fixed in the center of the HUD. Actual vertical and lateral velocities are displayed relative to the "w" by the pseudo-flight path symbol. The velocity commands are calculated

to ensure accurate path/terrain following. The pilot's task is to maintain the pseudo-flight path symbol between the opposing triangles of the ghost aircraft symbol using the collective controller and the lateral axis controller.

2. **Use of the Plan-View Format**

The second display configuration was a plan-view format designed for hover tasks in low visibility NOE conditions. One mode of this configuration was the monitoring display (Fig. 22a), again for use in the pilots' monitoring of the automated flights. The side-task displays for divided attention were included in this display format. The other plan-view display mode omitted the side-task displays for use in the manual guidance of the rotorcraft (Fig. 22b). The following is a description of how the pilots were expected to use the manual guidance mode of the plan-view display configuration.

a. **Heading**. The heading error is displayed via the orientation of the octagonal hover location symbol. The pilot uses the pedal controllers to orient the hover location symbol such that the opening of the symbol is facing directly down in the HUD.

b. **Altitude**. As with the azimuth-elevation display configuration, the two scales on the left side of the display provide altitude and altitude rate information in a compatibly scaled "state-and-rate" format. The left-most scale is a sliding radar altitude tape. An open triangular marker is fixed in the display to provide the reference marker. The radar altitude tape slides vertically, disappearing at and appearing from the display limits of the tape, such that the current radar altitude is indicated by the reference marker. An adjustable solid triangular caret affixed to the sliding tape indicates commanded radar altitude.

The scale immediately to the right of the sliding radar altitude tape is the vertical velocity scale. This scale is fixed in the display. Vertical velocity is indicated via the left pointing marker, including a "tail" that extends to the zero vertical velocity point. The purpose of the tail is to provide the pilot with an aid to make a rough estimate of the vertical velocity with only a cursory glance at the symbology.

The task of the pilot is to maintain the solid command caret aligned with the reference marker using the collective controller. The pilot may use both displays to aid in this task by providing control inputs through the collective such that the vertical velocity indicator tracks the commanded radar altitude marker, as shown in the figure. In this way, as the rotorcraft approaches the desired radar altitude, the vertical velocity will approach zero, and the desired altitude will be maintained.

Additional height information is provided via a growing and shrinking vertical error bar on the left side of the center-fixed trident symbol. The vertical acceleration is displayed via an open diamond, and indicates the rate of change of the altitude error. The commanded altitude is displayed by the location of two horizontal bars relative to the bottom of the trident symbol.

c. **Longitudinal and Lateral Position Control.** A Position-Velocity-Acceleration (PVA) display format is used in the plan-view display configuration. The position error is indicated via the octagonal hover location symbol. The velocity is displayed by the velocity vector, a line emanating from the center of the trident symbol. The acceleration cue is realized by the circular acceleration symbol. This symbol is referenced to the tip of the velocity vector such that when the rotorcraft is translating at a constant velocity, the acceleration symbol is at rest on the tip of the velocity vector. The control strategy to be utilized by the pilot to null a position error is to use longitudinal and lateral control inputs to minimize the distance between the center of the hover location symbol and the center of the acceleration symbol. The controller inputs necessary to realize this minimization also result in the minimization of the position error in an exponential fashion.

SECTION VII

SIMULATION TEST PLAN

This section describes the simulation test plan in terms of two topics: (A) the independent variables and (B) the dependent variables (i.e., data measurements and records).

A. INDEPENDENT VARIABLES

The test plan experimental design is depicted in Table 6. The cells are ranked in the table (circled numbers) to provide a priority for conducting the experiment. There are four classes of independent variables, i.e.. (1) guidance and control technique, (2) course-profile combination, (3) divided attention (workload) level, and (4) pilot's visibility. The run numbers corresponding to the cell for each pilot and each course are tabulated in Appendix H.

1. Guidance and Control Technique

Pilot acceptance of flight governed by an automatic guidance system or by manual control was evaluated. With the automatic guidance system, the evaluation pilot was responsible for monitoring the flight operation as well as performing defined side tasks (described in detail in a subsequent section), which were surrogates for mission tasks. The manual flights were made for the purpose of rating the flying qualities of the task and were performed with no side tasks to distract the pilot from the guidance and control of the rotorcraft.

An additional guidance and control technique is a combination of automatic and manual guidance and control in the event of a failure in the obstacle sensor systems or when the obstacle detection logic commands pilot intervention. In Table 6, this is referred to as the supervisory override guidance and control technique. Some of these consisted of automatic runs in which several prearranged but unannounced sensor failures were dispersed randomly throughout the course. Following the recovery from the failure, the pilot had to stabilize the rotorcraft on the course, and initiate the automatic guidance recapture logic. The evaluation pilot was not told in advance that the data run will contain prearranged failures.

TABLE 6. EXPERIMENTAL DESIGN FOR PILOTED SIMULATION AT NASA ARC

		NOE Traveling and Aggressive Maneuvering While on Watch				
Pilot's Visibility:		1000 ft RVR		500 ft RVR		200 ft RVR
Guidance and Control Technique		Divided Attention Level 0	Divided Attention Level 1	Divided Attention Level 0	Divided Attention Level 1	Divided Attention Level 1
Data Runs	Automatic		1 cell (1)		1 cell (4)	1 cell (6)
	Supervisory Override		1 cell (2)			
Manual		1 cell (3)		1 cell (5)		

RVR = Runway Visual Range

Data Runs: 4 cells · 2 replications = 8 runs/pilot/course

Manual Runs: 2 cells · 2 replications = 4 runs/pilot/course

Total Runs: 12 runs/pilot/course · 3 courses · 4 pilots = 144 runs

Circled numbers indicate priority of that cell.

2. Three-Dimensional Course-Profile Combinations

Three three-dimensional waypoint course-profiles were used by reversing the direction of travel on one of two courses shown in Fig. 20. The waypoint course-profiles meandered within the gaming area course in a fashion similar to that depicted in Fig. 20, a contour diagram of the section of the CT-5A data base known as "Hunter-Liggett Special" terrain defining the gaming area course used in the ARC simulation. Each course was approximately 500 dm long and could be traversed in about 500 sec at 20 kt. The waypoint courses were designed in the plan view, with the altitude of each waypoint and threat exposure height defined as heights above the continuous surface approximating the actual digitized terrain. This course was partially delineated from surrounding terrain with the use of tree rows and contained at least one waypoint that commanded zero velocity. Upon arrival at this waypoint, the rotorcraft was commanded to perform an unmask-mask maneuver utilizing a bob-up/down procedure. Upon completion of this aggressive maneuver, the waypoint course was resumed. The threat exposure height was defined as the average height of the trees in the data base.

Unexpected obstacles were placed strategically along the courses. An ODAMS algorithm indicated to the pilot by way of an audio annunciator the course of evasive action prior to its execution. In the manual flights, these announcements were followed by a commanded course of evasive action using the symbology in the HUD shown in Fig. 21b and/or the height command caret (solid triangular pointer on Radar Altitude Tape) in the HUD shown in Fig. 22b. For the automatic flights, the automatic guidance system performed the announced evasive maneuvers, and the pilot monitored the guidance using the HUD symbology shown in either Fig. 20a or Fig. 21a, whichever was appropriate for the maneuver.

3. Divided Attention Level

To simulate the NOE flight environment, three workload-intensive side tasks were included in the simulation tests to serve as surrogates for mission tasks other than flight guidance and control. It was the responsibility of the evaluation pilot both to perform these side tasks and to monitor the rotorcraft's operational performance. The divided attention level "1" referred to in Table 6 was provided through the use of side tasks, which consisted of a Choice Reaction Time side task, a "Sternberg" recognitive task, and a sub-critical tracking task.

For the Choice Reaction Time side task, three lights in a row on the cockpit instrument panel were illuminated randomly, two at a time. The pilot was to respond by toggling the specified switch on the cockpit instrument panel only to the illumination pattern ON-OFF-ON. This correct action extinguished the lights. The scoring of this task was based on the average response time over the duration of the run relative to the maximum allowable response time, τ_p. Incorrect pilot responses (i.e. toggling the switch in response to other

illumination patterns) resulted in the assessment of the maximum allowable response time while correct pilot responses were assessed the time of illumination of the correct pattern.

The Sternberg recognitive task (Ref. 19) simulates a target recognition task. The pilot was asked to memorize a limited number of items from a much larger set. Members of the large complete set of items were then randomly presented to the pilot. The pilot was to respond one way when members of the set of relatively few memorized items were presented, and another when any other items were presented. For this simulation, the large, complete set of items was the English alphabet. As the number of memorized items increases, the workload on the pilot increases. One level of divided attention was realized by selecting random sets of three from these twenty-six items for the pilots' memorized sets.

The letters from the alphabet were presented in the lower left-hand corner of the HUD (Figs. 21a and 22a). Two toggle switches on the instrument panel were required for this task. Upon presentation of members of the memorized set, the pilot toggled the left switch, and upon presentation of any other letter, the right switch. Following a correct response, the presented symbol disappeared; following an incorrect response, the letter remained in the display for 2 sec following the response. To indicate the error, the letter flashed.

The sub-critical tracking task (Ref. 20) was implemented using a short vertical bar travelling horizontally along the bottom of the HUD (Figs. 21a and 22a). A null position was displayed using a horizontally centered vertical marker, and the acceptable position boundaries for the vertical bar are depicted by dashed vertical marks. The limits of travel of the vertical bar were also shown as the bounding box. The positioning of the vertical bar was a sub-critical unstable process, with the pilot's controlling inputs delivered through a joy stick mounted on the right arm rest. One level of divided attention was realized by setting the magnitude of the unstable pole in the process to 0.5 rad/sec. The subject pilots were trained using the critical task (i.e., the value of the unstable pole is increased until control is lost; this value is then defined as the critical task score). The pilots' mean critical task scores ranged from 4.5 to 5.5 rad/sec; thus, the divided-attention level was approximately 10 percent of the pilots' mean critical task scores.

4. Pilot's Visibility

Three different levels of the pilot's visibility occluded by fog were simulated, i.e., 200 ft, 500 ft, and 1000 ft RVR. At 20 kt, 200 ft, 500 ft, and 1000 ft translate to roughly 6 sec, 15 sec, and 30 sec of visibility, respectively. With the ODAMS reference preview interval T_{p_x} = 6 sec and the speed at 20 kt, the obstacle avoidance logic will preview the terrain, obstacles, and threats up to 16 sec ahead of the rotorcraft's present position (see Fig. 16). Thus, with 200 ft of pilot's visibility, the automatic guidance system is basing its

TABLE 7. DEPENDENT VARIABLES (I.E., MEASUREMENTS)

1. Flight Plan Performance Errors
   a. Ground speed or longitudinal position error with respect to commanded flight profile, whichever is appropriate
   b. Lateral distance error with respect to commanded course
   c. Altitude error with respect to commanded altitude
   d. Elapsed time between waypoints in flight plan
   e. Three dimensions of terrain and obstacle clearance with respect to rotorcraft envelope

2. Other rotorcraft motion and control variables
   a. Pitch and roll attitudes
   b. Pitch and roll rates
   c. Heading
   d. Turn rate
   e. Airspeed
   f. Inertial velocity
   g. Course and path angles (or ground and vertical velocities)
   h. Translational and rotational accelerations
   i. Control displacements and rates
   j. Rotor torque and speed

3. Subjective Ratings
   a. Utility of displayed status information
   b. Display clutter
   c. Display attentional workload
   d. Confidence level in automatic guidance system
   e. Pilot Commentary
4. Cooper-Harper Flying Quality Ratings Under Manual Control

obstacle avoidance evasive maneuver commands on information beyond the pilot's range of visibility. With 500 ft of pilot's visibility, the automatic system sees obstacles and threats just 1 sec before the pilot does, according him nearly equivalent information with which to judge the appropriateness of the obstacle avoidance maneuver commands. With 1000 ft of pilot's visibility, the pilot may have at least the opportunity to preview terrain, obstacles, and threats 14 sec before the automatic system acts.

B. DEPENDENT VARIABLES (I.E., DATA MEASUREMENTS AND RECORDS)

Each of the types of measurements referred to in Table 7 has a specific role to fulfill in the subsequent analysis and presentation of the results of this investigation. We shall outline each type of measurement more specifically and discuss its role in this subtopic.

1. Flight Plan Performance

This group of measurements comprises three dimensions of flight plan error performance: (a) ground speed and (b) lateral and (c) vertical position with respect to the commanded flight plan stored in the guidance system. The elaspsed time between waypoints in the flight plan (d) was recorded on the end-of-run printout. Limitations in coding the obstacle and threat data base made it impossible to identify (e) obstacle and threat clearance.

2. Pilot Acceptance

The "other rotorcraft motion and control variables" listed in Table 7 represent motions whose variability from trimmed values or steady-state norms can be judged by comparison with standards of pilot acceptance.

3. Subjective Rating

Three simple pilot rating scales for use in research on and evaluation of manual control displays were derived and used in the pilot experiments reported in Refs. 21 and 22 and are well suited to the present investigation. In addition, a scale for use in the evaluation of pilot confidence in the automatic guidance system was derived for the present investigation. The scales shown in Table 8 are of interval-scale quality and will permit averaging and other standard parametric statistical analyses. The use of four trait categories: (a) status utility, (b) clutter, (c) attentional demand, and (d) confidence in the automatic guidance system will help to separate subjective identification of these effects. For manual operations, each pilot was asked to provide a Cooper-Harper rating (Table 8b) based on the desired and adequate performance error levels specified in Table 8c.

TABLE 8. PILOT OPINION RATING SCALES

Rating Scale for Utility of Status Information

CRITERIA	DESCRIPTIVE PHRASE	RATING
Usefulness[1] of the information supplied, on the specified display unit, on the vehicle status – especially the relevant flight path vector states, such as: altitude, speed, heading, attitude, path error, etc.	All desired states presented with adequate resolution and readability	S1
	Many of desired states presented, with a few deficiencies in scaling, resolution, or readability	S2
	Some desired states presented, and/or some problems with scaling, resolution, or readability	S3
[1]Useful with respect to the mission phase, task criteria, and operator's sense of vehicle safety	Inadequate number of states, or serious deficiencies in scaling, resolution, or readability	S4
	No direct status information or unusable	S5

Rating Scale for Clutter

CRITERIA	DESCRIPTIVE PHRASE	RATING
Degree of subjective symbol-background clutter on specified display unit	Completely uncluttered – e.g., only one pair of elements	K1
	Mostly uncluttered – no confusing or distracting elements	K2
	Some clutter – multiple elements competing for attention	K3
	Quite cluttered – difficult to keep track of desired quantities among competitors	K4
	Completely cluttered – nearly impossible to tell desired elements or quantities due to competing elements	K5

Rating Scale for Confidence[2] in Automatic Guidance

CRITERIA		DESCRIPTIVE PHRASE	RATING
Autoguidance acceptable	Confidence level		
Yes	High	Very high level of confidence – no instances tempting manual intervention	C1
		High level of confidence – few instances tempting manual intervention	C2
	Low	Low level of confidence – instances requiring manual intervention	C3
		Marginally acceptable level of confidence – several instances requiring manual intervention	C4
No		Complete lack of confidence in automatic guidance system	C5

Rating Scale for Display Attentional Workload

CRITERIA	DESCRIPTIVE PHRASE	RATING
Demands on the operator attention, skill, or effort	Completely undemanding and relaxed	D1
	Mostly undemanding	D2
	Mildly demanding	D3
	Quite demanding	D4
	Completely demanding	D5

[2]Factors to be considered in rating confidence level high:
- Acceptable precision of following flight plan
- Timely comunication of unexpected departure from flight plan to avoid obstacles
- Timely execution of obstacle avoidance maneuvers
- Relative benignity of obstacle avoidance maneuvers in the light of their timeliness
- Precision and timeliness of recovery of flight plan
- Similarity of automatic guidance and control technique to your personal techniques
- Acceptability of excursions in attitudes, attitude rates, heading, yaw rate, accelerations, control authority used, control rates

a. Rating Scales for Monitoring Automatic Guidance Using the Displays Provided

TABLE 8 (CONCLUDED)

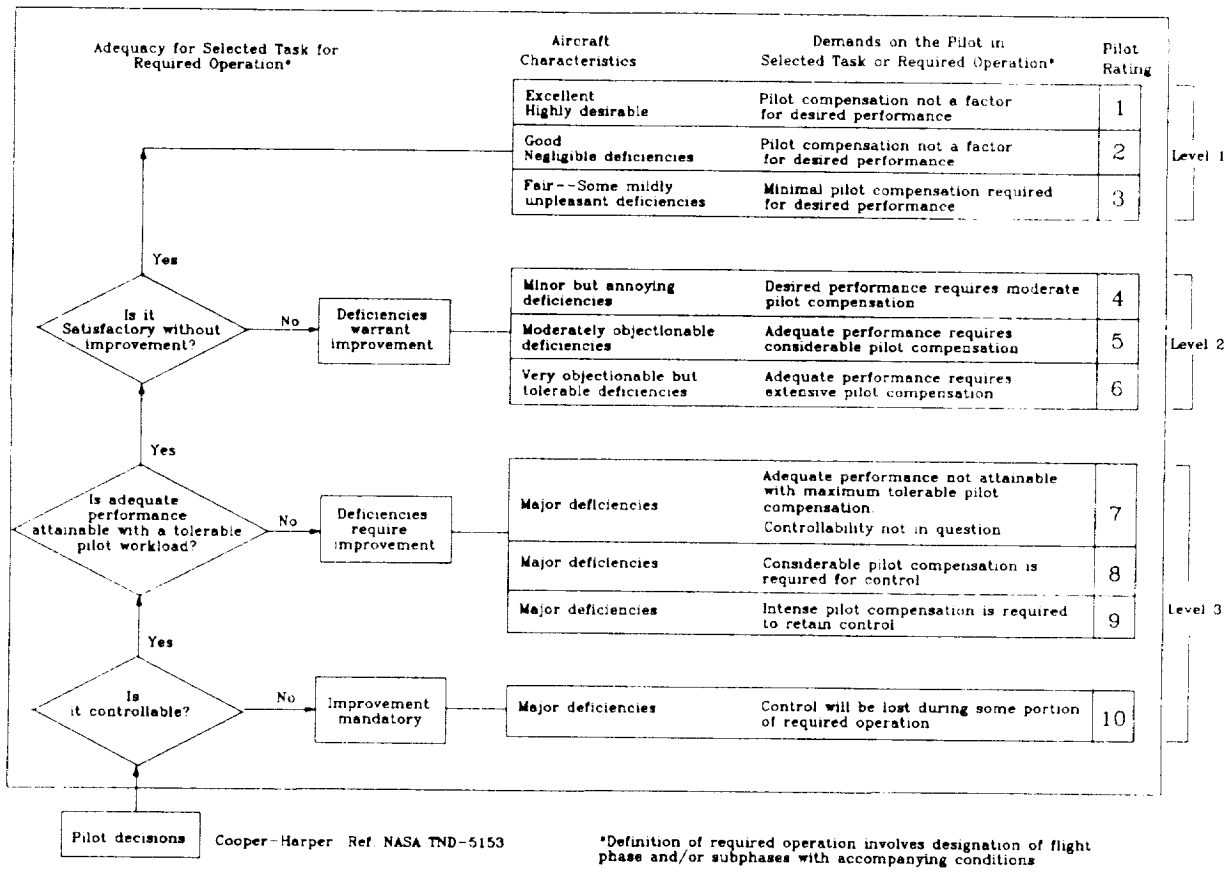

b. Cooper-Harper Scale for Manually Controlled Flying Qualities

Axis	Desired	Adequate
Airspeed	±2 kt	±4 kt
Altitude	±5 ft	±10 ft
Heading	±10 deg	±15 deg
Lateral Deviation	±1/2 A/C symbol (±16 ft)	±1 A/C symbol (±32 ft)

c. Specifications for Performance Errors

SECTION VIII

SUMMARY OF RESULTS

This summary of results from the NASA ARC piloted simulation is partitioned into three topics: (A) simulation results per se, (B) simulation design limitations, and (C) inherent conceptual design limitations.

A. SIMULATION RESULTS

1. Successful Completion of the Stated Tasks

In the following paragraphs, the successful completion of each simulation task is described:

a. Interpolation Within the Resolution of the Stored Data Base (Task 1). The peak errors between the actual and modelled terrain of the CT-5A data base were less than 6 ft, and these errors were on the perimeter of the data base. Typical peak errors in modelling the waypoint course were less than 2 ft. However, there was a limitation associated with the CT-5A data base in that the layered polygonal representation of the terrain led to discontinuities in the first and second derivatives of the altitude with respect to horizontal position. This is unlike typical Defense Mapping Agency (DMA) data base representations of terrain in which the terrain surface undulates continuously rather than discretely. Nevertheless, with minimal adjustments (smoothing the abrupt discontinuities in terrain slope), it was possible to obtain acceptable values of the derivatives that are used by the pursuit guidance algorithm.

b. Obstacle Detection and Avoidance Maneuver Selection Logic (Task 2). The ODAMS algorithm proved to be trustworthy and acceptable to the pilots. Although not all of the ODAMS logic options were exercised during the time-limited piloted simulation, off-line testing of the ODAMS logic did not reveal any cases that posed a threat to the rotorcraft under ANOE flight.

c. Pursuit Feedforward Guidance Algorithm (Task 3). The pursuit guidance algorithm helped to guide the rotorcraft along the course with extremely small errors through simulated turbulence having 2.5 ft/sec root-mean-square (RMS) velocity, and the algorithm was universally accepted by the evaluation test pilots. The maximum tracking errors on waypoint legs having no obstacles or aggressive maneuvers are given in Table 9.

TABLE 9. MAXIMUM ERRORS IN FOLLOWING COURSE COMMANDS*

	Ground Speed	Cross Track Displacement	Heading
Automatic	± 1.00 ft/sec	± 8.00 ft	± 0.05 rad (± 3.0 deg)
Manual	± 5.0 ft/sec	± 50.0 ft	± 0.4 rad (± 23 deg)

*Height error could not be obtained because of a defective radar altitude recording channel.

* * * * *

d. Constrained Time-Optimal Evasive Maneuvers (Task 4). The constrained time-optimal algorithms performed accurate, smooth, repeatable, aggressive evasive maneuvers. The evaluation pilots were initially skeptical regarding these maneuvers, especially the bob-down maneuvers at such a low altitude. However, after the pilots experienced the maneuvers a number of times, they gained confidence in the automatic system. The aggressiveness of the maneuvers had to be reduced in going from the fixed-base MDHC simulation to the moving-base ARC simulation.

2. Pilot Opinion Ratings

The Cooper-Harper pilot opinion ratings (CHPORs) of the manual flight task are summarized in Table 10. Note that only three of the five ARC evaluation pilots gave ratings (two had insufficient time to become familiar with the task). The results indicate that, under manual operation, the aircraft/task combination is Level 2 for some tasks and Level 3 for others. Three possible reasons for the poor ratings may be that the pilots were not sufficiently trained for the display/control configuration, that the HUD was not optimized, and/or that the acceptable performance limits were too tight for manual operation. There was insufficient time to investigate these possibilities, since the main objective of the research was to evaluate pilot acceptance of automatic flight.

The pilot ratings for utility of displayed status information (Sn), display clutter (Kn), attentional workload (Dn), and confidence in the automatic guidance system (Cn) are summarized in Table 11. The table includes results for the head-up display (HUD) and the head-down moving map display (MMD). Figure 25 illustrates the pilot ratings for Sn, Kn, and Dn. The MMD was nearly always rated superior to the HUD. The ratings for Cn, which are very promising, are plotted in Fig. 26. The confidence ratings of one and two indicate there were no or few instances in which the pilot was tempted to intervene and take control of the rotorcraft. It is true, however, that the confidence of a pilot in an automatic guidance system for nap-of-the-Earth flight operations would be affected by the real-world environment. In the simulation environment, no possible harm

TABLE 10. COOPER-HARPER PILOT OPINION RATINGS

Pilot	Rating	Pilot Comments or Explanation
1	5	For acceleration task
	4	For straight and level task
	7	For deceleration task
	6	For turning task
	7	For aggressive maneuver
2	5	
3	7	I think the acceptable performance limits are too tight

TABLE 11. PILOT RATINGS FOR UTILITY OF DISPLAYED STATUS INFORMATION (Sn), DISPLAY CLUTTER (Kn), ATTENTIONAL WORKLOAD (Dn), AND CONFIDENCE IN THE AUTOMATIC GUIDANCE SYSTEM (Cn)

Pilot	Rating	Display	Pilot Comments or Explanation.
1	S3/S4	HUD	
	K4	HUD	
	D3/D4	HUD	I'm confused as to which control to use with the symbols.
	S2	MMD	
	C1/C2		I attempted manual intervention, but it had no effect. I can't judge clearances very well.
2	S3	HUD	Readability problem with altitude.
	K3	HUD	h and ḣ cluttered
	D3	HUD	All associated with altitude control.
	S1	MMD	
	K1	MMD	
	D1	MMD	
	C2		I was tempted to manually intervene in one instance. Satisfactory, but somewhat abrupt in turns.
3	S1	HUD	But difficult to use them in the manual mode at this point.
	K4	HUD	If not the decluttered mode.

TABLE 10 (CONCLUDED)

Pilot	Rating	HUD/MMD	Pilot Comments or Explanation.
	D4	HUD	In the manual mode it is a real challenge. It is not a very demanding task in the auto-mode because it is so perfect.
	S2	MMD	Do not always see rising terrain.
	K2	MMD	
	D1	MMD	No situations occur to increase anxiety
	C?		As the simulation is set up "no" and "few" interventions does not equate to "high" confidence levels as defined by the bulleted items in this table: There is no timely communication of unexpected departure, and it seems to come pretty close to obstacles. $\ddot{\theta}$ is too abrupt to achieve a_x.
4	S1 & S4	HUD	All desired states presented (S1), but not flight path centered, symbols not limited, and scaling is not optimum (S4).
	K4	HUD	Information not flight path centered: requires scanning all over cockpit and display.
	D5	HUD	Do not feel that I have enough time left to monitor trajectory.
	S2	MMD	No altitude information on MMD.
	K2	MMD	
	D2	MMD	
	C?		Pilot 4 did not give a confidence rating.
5	S2	HUD	
	K3	HUD	
	D3	HUD	
	C2		

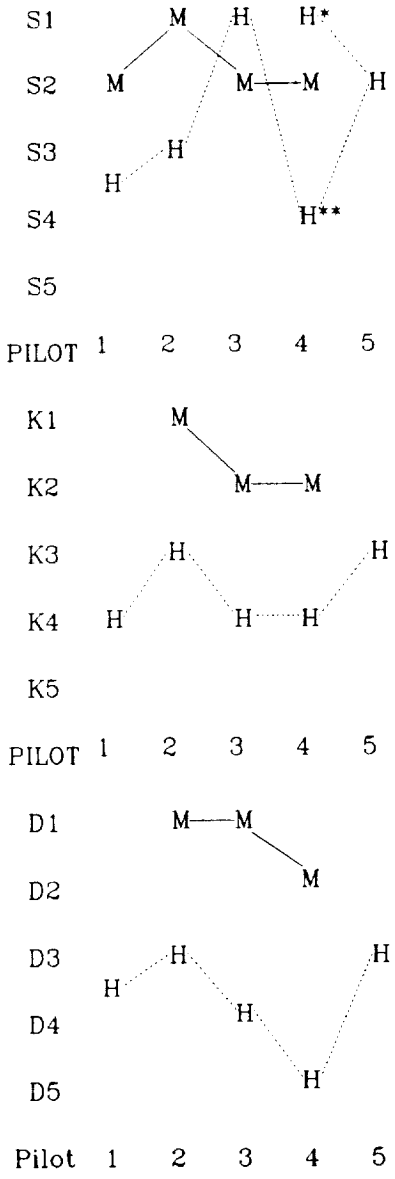

NOTES: H* pilot comment: all desired states presented
H** pilot comment: scaling not optimum; states not flight-path centered
H = Head-Up Display (HUD in Table 10)
M = Moving Map Display (MMD in Table 10)

Figure 25. Pilot Ratings from Table 10

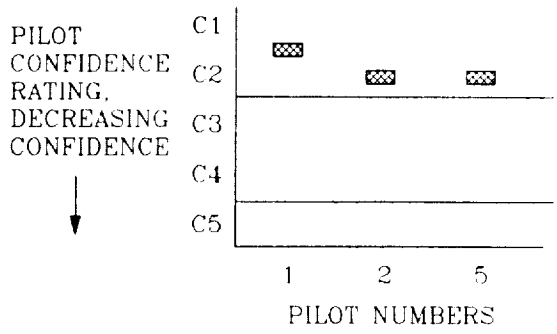

Figure 26. Evaluation Pilots' Confidence Ratings

could come to the evaluation pilot. In the particular simulators used for this investigation, it was not possible to indicate instances, such as rotor strikes, where harm could have come to the rotorcraft and/or the pilot. Nevertheless, the high confidence of the evaluation pilots in the automatic guidance system reflects the adherence of the system to the precision and safety requirements necessary for automated nap-of-the-Earth flight operations.

3. Side Task Results

There were mixed opinions on the validity and usefulness of the side tasks, which were included in this simulation to give the evaluation pilots, who were not actually flying the aircraft, something to do besides watching what the automatic system was doing. One pilot stated that the side tasks were "interesting, well thought out, and kept the automatic flight interesting." Some of the pilots thought that the side tasks were unrealistic (that is, they were not "face valid"), while others tended to ignore the side tasks. One pilot stated , "I can't keep track of what's going on and do the side tasks ... it's too much." In a later section on recommendations, we present suggestions on how the side tasks might be improved for future simulations.

As the pilots gained confidence in the automatic guidance system and therefore had more time to concentrate on other tasks, we expected that their side task scores, which had no inherent value, would improve. With a few exceptions, however, the data did not support this hypothesis (see Appendix I for details). This could have been the result of fatigue and/or disdain for the side tasks in general.

B. SIMULATION DESIGN LIMITATIONS

1. Manual Flight Task

The simulated head-up and head-down displays were designed primarily for monitoring the ANOE guidance and control system; therefore, little effort was expended to optimize them for the four-axis manual guidance task. As a result, only two of the five NASA ARC test pilots were able to fly the course manually with the precision needed for Level 2 CHPORs.

Following commands in all four axes simultaneously proved to be difficult for some of the evaluation pilots, while others had no difficulty at all. One pilot expressed his limitation: "... two axes are about as much as you can really handle, with one axis being active and the other being a kind of passive one."

2. Computer-Generated Imagery

The CT-5A computer-generated imagery (CGI) was incapable of providing the level of tree density necessary to simulate concealed NOE flight. As a result, the chosen meandering course through the data base was not delineated in the NASA ARC simulation as it was in the MDHC simulation, and the turns in the course appeared to be without reason. Consequently, the ARC pilots perceived the manual flight task as unrealistically confining, because the pilots were asked to follow a meandering course with a high level of accuracy through wide open areas. One pilot complained that asking the pilot to follow a planned course even in real NOE conditions is unrealistic. In contrast, the data base set up on the Compuscene IV CGI for the MDHC simulation did present a well defined course, with trees closely bordering the path on both sides. Neither CGI, however, treated trees as physical obstacles in the correlated obstacle data base.

It was very difficult to judge clearance distances and forward distances to objects because of deficient depth perception. Pilot 4 stated: "The trouble is, you don't get a feel for how scary it really is." All pilots experienced considerable difficulty in judging distances and speeds from the CT-5A CGI data base due to a lack of texture.

The CT-5A CGI data base was not a threatening NOE environment. Even if the rotorcraft impacted an object, no collision was recognized.

3. Automated Flight Path Monitoring Task

The HUD was designed to allow the pilot to monitor the states of the rotorcraft fully during automated flight. In forthcoming iterations of the ANOE design process, the HUD should provide only supervisory, overview information (i.e., pathway in the sky). This is discussed more fully in the section on recommendations.

4. Side Tasks

As mentioned above, the evaluation pilots, with the exception of Pilot 5, complained that the tasks were unrealistic. This was especially true of the sub-critical tracking task (SCTT), which required the pilots to perform a non-flying continuous task. Most considered this not only an unrealistic but also an unacceptable task.

Another complaint was that the side tasks could not be performed while allowing the pilots to keep their hands on the flight controllers. Most pilots agreed that no pilot would accept an automated NOE guidance system unless he could keep his hands on the flight controllers.

5. Aggressiveness of Automatic Evasive Maneuvers

The ANOE guidance system was deemed too aggressive by some of the pilots. This is attributable to the deficiencies in the visual scene, which was unable to display sufficient features and obstacles that would necessitate the programmed level of urgency. In addition, aggressive pitch attitude maneuvering tended to disorient the pilot in low visibility conditions and to promote vertigo, as noted by Pilot 3. Since the aggressiveness could be adjusted easily, it was changed during the simulation to the pilots' satisfaction.

6. Audio Annunciator

Although the pilots' consensus was that audio announcements of impending maneuvers would be highly desirable, if not a necessary feature of an ANOE guidance system, the Votrax voice synthesizer that was available for the NASA ARC simulation was inadequate for this purpose. The messages were unintelligible, and, even if they could be understood, the system was so slow that even concise messages took too long to announce if multiple maneuvers were to be performed.

7. Cab Controllers

The dynamics of the cab controllers (i.e., gradients, breakouts, detents, etc.) were criticized by the pilots in the NASA ARC simulation, because they made the manual flight task more difficult. This was a limitation that could not be removed easily if at all. The full authority flight control system was implemented using a McFadden hydraulic system to back-drive the controller of each axis during the automatic test flights. However, there was delay between

the commanded and actual stick position, and this demanded large deadbands on the controllers so that the delays would not accidentally trip the supervisory override. These delays, coupled with pilot's desire to maintain his hands on the controllers and the inevitable risk of inadvertently tripping the supervisory override due to this contact, necessitated such great deadbands on the controllers that unacceptably large discontinuities resulted upon disengagement of the automatic guidance system.

C. CONCEPTUAL DESIGN LIMITATIONS

1. Supervisory Override and Automatic Recapture

As mentioned previously, imposed deadbands on the controllers caused unacceptable discontinuities upon disengagement of the automatic guidance system by the supervisory override. The supervisory override feature was not designed to disengage any one controller axis while allowing the automatic guidance system to maintain control of the other axes; instead, it disengaged all of the axes at once. The control stick steering solution in the recommendation section should be considered to correct this problem.

The implementation of the automatic recapture algorithm was never debugged thoroughly. It was unreliable and sometimes erratic.

2. Constrained Time-Optimal Evasive Maneuver Aggressiveness

Satisfactory limitation of the aggressiveness of the longitudinal constrained time-optimal acceleration/deceleration maneuvers in reduced visibility conditions has already been discussed. See the recommendations section for further comments.

3. Obstacle Detection and Avoidance Maneuver Selection Algorithm

There are three limitations of particular significance. First, the obstacle detection and avoidance maneuver selection (ODAMS) algorithm allows only for a set number of discrete lateral evasive maneuver commands rather than a continuous range of lateral maneuver commands. Although consistent with the discrete resolution of the DMA data base, this limits its capability to identify all possible evasive paths, if the sensor(s) has (have) finer resolution than the DMA data base and may cause the ANOE guidance system to stop unnecessarily. Second, the height control portion of the ODAMS algorithm did not continue throughout the lateral evasive maneuvers (discussed subsequently under Recommendations); and third, the off-course anticipation array for ODAMS was developed but not incorporated in the off-line or real-time simulations.

SECTION IX

RECOMMENDATIONS

Recommendations resulting from the NASA ARC piloted simulation are divided into five areas presented in this section: (A) automatic nap-of-the-earth head-up display development, (B) control stick steering, (C) flight test, (D) necessary prerequisites for another simulation, and (E) obstacle detection and avoidance maneuver selection algorithm generalization.

A. AUTOMATIC NAP-OF-THE-EARTH HEAD-UP DISPLAY DEVELOPMENT

A supervisory head-up display (HUD) presenting only long range guidance information should be developed for use in automatic nap-of-the-earth (ANOE) guidance systems. An ideal concept to this end is a pathway-in-the-sky approach, in which a sequence of crossbars is presented to identify the planned trajectory of the rotorcraft. A ghost aircraft flies ahead of the rotorcraft to present lateral and vertical lead information, as shown previously in Figs. 21a and 21b. Alterations to the planned flight profile necessitated by unexpected obstacles would be indicated by another set of crossbars, differing from the original set in color and/or intensity, that would circumnavigate the obstruction. Intrinsic to this HUD design concept is the assumption that any failures in the ANOE guidance system will be sensor failures. If undetected by the pilot, these errors would result in the rotorcraft impacting an undetected obstacle. The pilot is therefore presented with information that will enable him to identify sensor failures. If an obstruction intersects the planned flight path and no alternate flight path has been presented, the pilot knows that the sensors have not identified that obstruction. Another HUD concept worthy of consideration for ANOE application is the Obstacle Avoidance System (OASYS) developed by the MDHC (Ref. 23)

The ANOE HUD should be developed in a workstation environment, where concepts can easily be tested and revised. The Silicon Graphics IRIS Workstation facility at the NASA ARC Guidance and Navigation Branch is a suitable site. Once a "final" design has been developed, another exercise should be conducted on the VMS to familiarize the pilots with the HUD.

B. CONTROL STICK STEERING

Most of the problems encountered with the supervisory override and automatic guidance recapture logic could be overcome with the inclusion of a "Control-Stick-Steering" feature, with which pilot inputs are added to the automatic guidance commands to form the overall commands to the rotorcraft flight control system. In this way, the pilot can at any time augment the control input of any axis or all axes without disengaging the automatic guidance. Alternatively,

he can, with the push of a button, entirely disengage the automatic guidance system and assume complete control of the rotorcraft. A design for such a system is presented in Ref. 12. Once designed and programmed, such a system should be checked out in the VMS.

C. FLIGHT TEST

Based on the simulation results, parts of the ANOE guidance system are ready for flight testing.

1. Terrain Following

The terrain following algorithm can be tested safely in flight over moderate terrain. A necessary prerequisite would be a source for the rotorcraft's inertial velocity and position in a known digital data base.

2. Constrained Time-Optimal Maneuvers

These can easily be tested without the ODAMS algorithm to assess pilot reaction to automatically flown aggressive maneuvers. An outcome of such an investigation could be guidelines for levels of acceptable aggressiveness for the maneuvers. If possible, aggressiveness should also be based on visibility, that is, as visibility decreases, so should the aggressiveness of the maneuver.

3. Course Tracking

Again, inertial position and velocity would be required. A simple slalom course across the runway at Crows Landing would be suitable. Two candidate rotorcraft for these flight tests would be the following variable stability "flying simulators" with the capability in place for computer-aided guidance and control: (a) a suitably equipped AH-60 Black Hawk or (b) the variable stability CH-47 Chinook operated by NASA Ames Research Center Flight Dynamics and Controls Branch.

D. NECESSARY PREREQUISITES FOR ANOTHER SIMULATION

To respond to some of the pilots' complaints of unrealistic side tasks, new but similar side tasks should be developed that closely resemble actual pilot responsibilities on a mission. These could be responding to a fire light, identifying targets, and guiding radio-controlled missiles to a designated target. It might be possible to modify the operation of the existing side tasks to make them more realistic without going all the way to "face-valid" tasks (i.e., we should not have to simulate war games in order to evaluate ANOE concepts). First, make the sub-critical tracking task (SCTT) intermittent with no more than 30 sec of tracking, and disable the Sternberg and choice reaction tasks while the SCTT task is being performed. (The SCTT could be interpreted as a radio-controlled guided missile task.) Second, put the SCTT controller on the cyclic controller,

perhaps using a thumb wheel controller. Third, motivate the pilots to perform the side tasks with feedback of their scores and/or penalties for not doing the side tasks. The research pilots should be consulted with respect to side task modifications and their comments and suggestions should be solicited.

A collision detection system should be developed that would identify instances of contact between the rotorcraft and the surrounding environment and that would abort the mission (read "crash") when appropriate.

It would be preferable to use a better CGI (e.g., Compuscene IV or an equivalent) to alleviate some of the problems noted previously. In any case, a data base should be designed expressly for an ANOE simulation. This data base should have at least one well-defined covert course that is bordered closely on both sides by cultural features (such as trees, cliffs, buildings, etc.) and that preferably follows a stream or highway for realism. Also, multiple threats and targets should be available for random placement throughout the course.

Since a major problem with this piloted simulation of an automated guidance system was one of evaluation pilot motivation, creating more interesting side tasks, providing the possibility of a crash, and creating a generally more threatening environment through which the pilot is flown should improve motivation in future investigations.

E. OBSTACLE DETECTION AND AVOIDANCE MANEUVER SELECTION ALGORITHM GENERALIZATION

The first improvement that should be addressed is removal of the limitation of the ODAMS algorithm in selecting discrete lateral evasive maneuver commands. This could, as has been stated previously, result in unnecessary stop commands being issued by the ODAMS when a navigable path circumventing the obstacle does exist but is not one of the selectable paths.

A second improvement to the ODAMS would be the separation of the lateral and vertical axes in the decision logic. The vertical axis portion of the ODAMS should be run continuously, regardless of the state of the lateral decision logic. This is not currently the case. The vertical decision logic, as well as the lateral decision logic, is discontinued during lateral evasive maneuvers. As a result, the vertical situation during and following the maneuver is analyzed to determine the acceptability of proposed lateral evasive maneuvers. This could disallow acceptable evasive maneuvers simply because one altitude would not be suitable for the entire maneuver. If the vertical decision logic were separate, the maneuver would be allowed, and the altitude would be varied appropriately.

REFERENCES

1. Cheng, V. H. L., And B. Sridhar, "Considerations for Automated Nap-of-the-Earth Rotorcraft Flight," Proceedings of the American Control Conference, Atlanta, GA, June 15-17, 1988.

2. Pekelsma, N. J., And R. V. Denton, "Pilot Oriented Aids for Helicopter Automatic Nap-of-the-Earth Flight," Proceedings of the AHS National Specialists' Meeting in Flight Control and Avoinics, Cherry Hill, NJ, October 13-15, 1987.

3. Deutsch, O. L., M. Desai, and L. A. McGee, "Far-Field Mission Planning for Nap-of-the-Earth Flight," Proceedings of the AHS National Specialists' Meeting in Flight Control and Avionics, Cherry Hill, NJ, October 13-15, 1987.

4. Denton, R. V., And L. A. McGee, "Automation of Guidance for Nap-of-the-Earth Flight," Proceedings of the Autonomous All-Weather Navigation and Landing Workshop, Monterey, CA, January 27-30, 1988.

5. Swenson, H. N., "Simulation Evaluation of Helicopter Terrain Following/Terrain Avoidance Concepts," Proceedings of the 8th Digital Avionics Systems Conference, San Jose, CA, October 17-20, 1988.

6. Cheng, V. H. L., "Obstacle-Avoidance Automatic Guidance," Proceedings of the AIAA Guidance, Navigation and Control Conference, Minneapolis, MN, August 15-17, 1988.

7. Cheng, Victor H. L., and Banavar Sridhar, "Considerations for Automated Nap-of-the-Earth Rotorcraft Flight," 1988 American Control Conference, Vol. 2, Atlanta, GA, June 15-17, 1988, pp. 967-976.

8. Cheng, Victor H. L., and Banavar Sridhar, "Integration of Active and Passive Sensors for Obstacle Avoidance," IEEE Control System Magazine, Vol. 10, No. 4, June 1990, pp. 43-50.

9. Jones, A. David, Operations Manual: Vertical Motion Simulator (VMS) S.08, NASA TM 81180, May 1980.

10. Cook, Anthony, "Simulation World Moves Up to V/STOL," Aerospace America, November 1985, pp. 46-48.

11. Gorder, Peter J., and Wayne F. Jewell, Stored Flight Profiles for the Compuscene IV Display of Automatically Guided Rotorcraft Nap-of-the-Earth Flight, Systems Technology, Inc., Working Paper No. 1254-7, January 1989.

12. Gorder, Peter J., Warren F. Clement, and Wayne F. Jewell, Mathematical Model of a Fully Automatic Guidance System for Rotorcraft Nap-of-the-Earth (NOE) Flight Following Planned Flight Profiles, Systems Technology, Inc., Techical Report No. 1254-2, September 1990.

13. Clement, Warren F., Field of Coverage for Sensed Terrain and Obstacles in Automatically Guided Rotorcraft Nap-of-the-Earth Flight, Systems Technology, Inc., Working Paper No. 1254-3, February-April 1988.

14. Allen, R. Wade, and Duane McRuer, "The Man/Machine Control Interface--Pursuit Control," Automatica, Vol. 15, No. 6, November 1979, pp. 683-686.

15. Clement, Warren F., Duane T. McRuer, and Raymond E. Magdaleno, Some Data Processing Requirements for Precision Nap-of-the-Earth (NOE) Guidance and Control of Rotorcraft, Systems Technology, Inc., Technical Report No. 1239-1, December 1986, Revised February 1987.

16. Ferguson, Samuel W., Warren F. Clement, William B. Cleveland, and David L. Key, "Assessment of Simulation Fidelity Using Measurements of Piloting Technique in Flight," Systems Technology, Inc., Paper No. 347, Presented at the 40th Annual Forum of the American Helicopter Society, Arlington, Virginia, May 1984.

17. Clement, Warren F., William B. Cleveland, and David L. Key, "Assessment of Simulation Fidelity Using Measurements of Piloting Technique in Flight," Systems Technology, Inc., Paper No. 348, Presented at the AGARD Guidance and Control Panel 38th Symposium, Helicopter Guidance and Control Systems for Battlefield Support, Monterey, California, May 1984.

18. Ferguson, Samuel W., Warren F. Clement, Roger H. Hoh, and William B. Cleveland, "Assessment of Simulation Fidelity Using Measurements of Piloting Technique in Flight--Part II," Systems Technology, Inc., Paper No. 371, Presented at the 41st Annual Forum of the American Helicopter Society, Ft. Worth, Texas, May 1985.

19. O'Donnell, Robert D., "Standard Task Assessment of Cognitive Workload in Alternative Cockpit Configurations," in B. O. Hartman (ed.), Higher Mental Functioning in Operational Environments, AGARD Conference Proceedings No. 181, April 1976.

20. Jex, Henry R., "A Proposed Set of Standardized Sub-Critical Tasks for Tracking Workload Calibration," in Moray, Neville (editor), Mental Workload--Its Theory and Measurement, Plenum Press, 1977.

21. Clement, Warren F., R. Wade Allen, and Dunstan Graham, Pilot Experiments for a Theory of Integrated Displays, JANAIR Report No. 711107, October 1971.

22. Clement, Warren F., Investigation of the Use of an Electronic Multifunction Display and an Electromechanical Horizontal Situation Indicator for Guidance and Control of Powered-Lift Short-Haul Aircraft, NASA CR-137922, August 1976.

23. Cerchie, P., A. C. Flackbert, and D. Reago, "Helicopter Obstacle Avoidance System: The Use of Manned Simulation to Evaluate the Contribution of Key Design Parameters," Presented as Paper #5, Session D, of the American Helicopter Society's 45th Annual Forum and Technology Display, Boston, MA, May 22-24, 1989.

APPENDIX A

COMPRESSION OF THE STORED DATA BASE REPRESENTING TERRAIN

An example of fitting the altitude of the terrain distributed over 1080 dm of X_{Crs} using the finite Fourier transform (FFT) program Y2DFFT.FOR (given in Appendix D of Ref. A-1) is shown in Fig. A-1 for Y_{Crs} = 50 dm and MX = 20 (i.e., only the first twenty sine waves of the summation containing NX/2 = 540 sine waves were used to compute the estimated altitude). Note that the error is always the greatest at the beginning and end of the series (X_{Crs} = 0 and 993 dm). The effect of MX on the maximum error in altitude is shown in Fig. A-2. Note that when both the mean bias and trend are removed from the data, the maximum error for MX = 20 is reduced from 122 to 27 m and that the maximum error for Y_{Crs} = 0 is only 2.5 m. The choice for setting MX = 20 was based on the spectral analysis of this terrain. The analysis showed that 99 percent of the power in this terrain occurred over a (low-pass) spatial frequency bandwidth of 0.114 rad/dm, which corresponds to the twentieth harmonic for a series of length 1098. Using MX = 20 requires the storage of 43 numbers for each value of Y_{Crs}, which corresponds to a data compression factor along the course of 25 with respect to the original 1080 data points for one value of Y_{Crs}.

Figure A-3 contains a plot of maximum altitude error versus across-course position Y_{Crs} (for $0 \leq X_{Crs} \leq 1098$ dm) for all of the data and when the ten data points at each end of the series are ignored. Note that the maximum errors for $Y_{Crs} > 80$ dm are reduced by factors of three by ignoring the ten data points at each end. Since NY = 101 data points, using MY = 10 sinusoida across the course requires the storage of 23 numbers, which corresponds to a data compression factor across the course of 4.4. The overall data compression factor is thus $25 \times 4.4 = 110$.

a. Original and Fitted Altitude

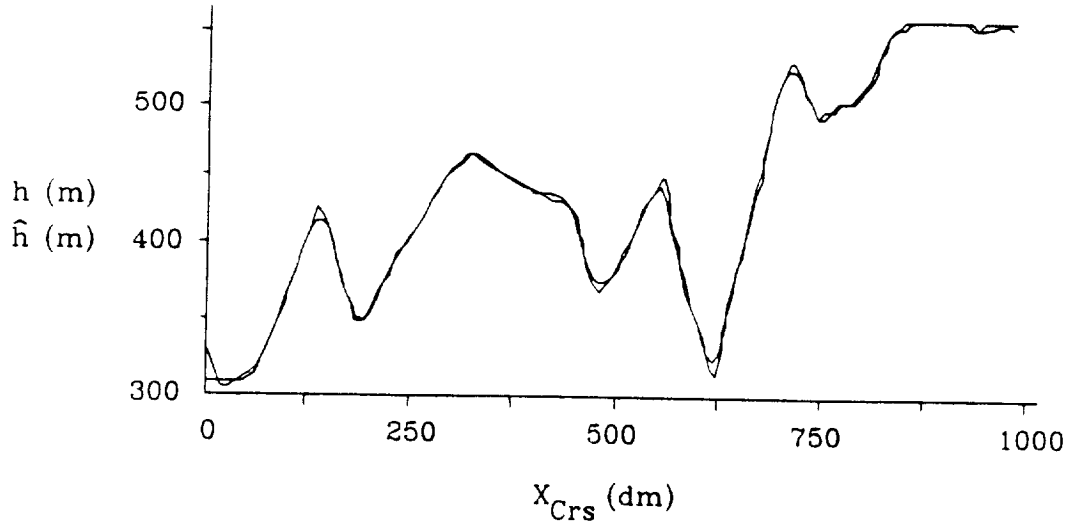

b. Error Between Original and Estimated Altitude

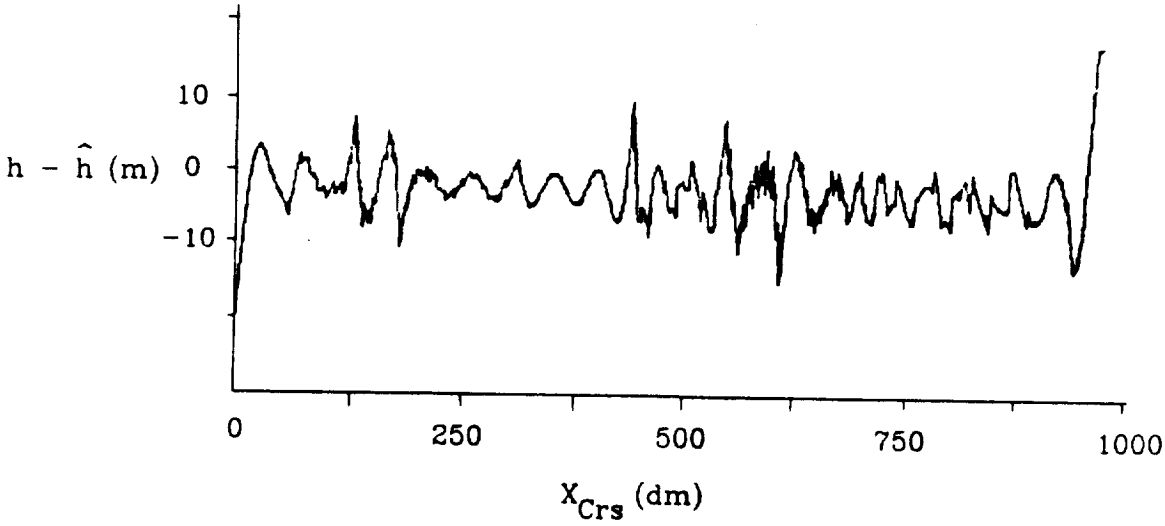

NOTES: 1. NX = 1080 data points distributed over 1080 dm of X_{Crs} and MX = 20 sinusoids

2. Data compression ratio is NX/(3 + 2MX):1 = 25.1:1 along the course

Figure A-1. Actual and Fitted Altitude Versus X_{Crs} for Y_{Crs} = 50 dm

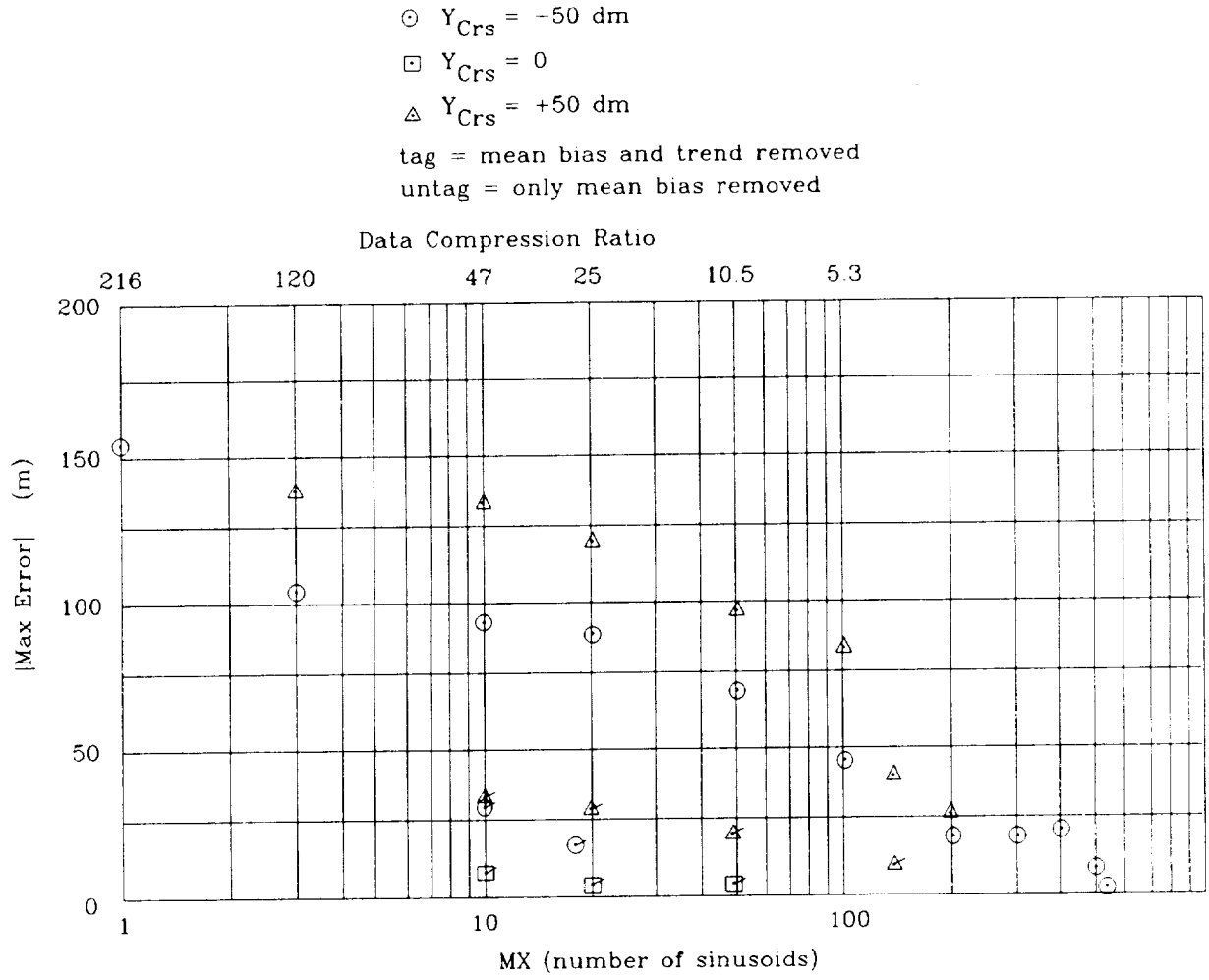

NOTES:
1. NX = 1080 points (distributed over 1080 dm along the course)
2. IPOLY = 0 or 1
3. Limit of MX is NX/2 = 540 sinusoids
4. Data compression ratio = NX/(3 + 2MX):1

Figure A-2. Maximum Error in Altitude Versus Number of Harmonics in the Sum of Sines, MX
(Example of terrain is from Figs. 1 and 4 in Ref. A-1)

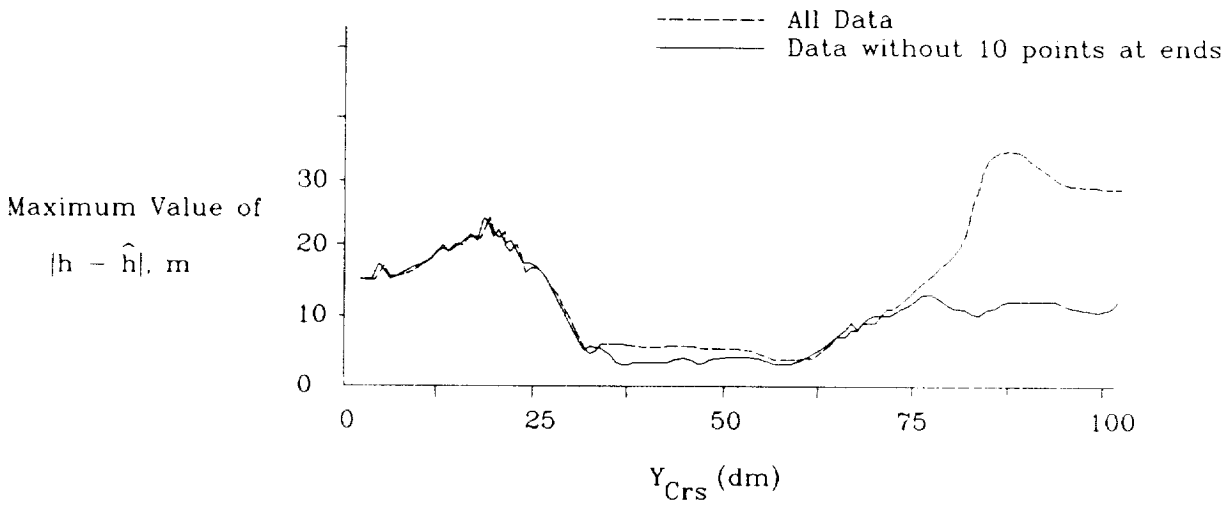

Figure A-3. Maximum Error in Altitude Versus Lateral Course Position for $0 \leq X_{crs} \leq 1098$ dm

REFERENCE

A-1. Gorder, Peter J., and Wayne F. Jewell, Stored Flight Profiles for the Compuscene IV Display of Automatically Guided Rotorcraft Nap-of-the-Earth Flight, Systems Technology, Inc., Working Paper No. 1254-7, January 1989.

APPENDIX B

SIMULATED GAMING AREA COURSE FROM THE GENERAL ELECTRIC (GE) COMPUSCENE IV COMPUTER-GENERATED IMAGE (CGI) DATA BASE AT McDONNELL-DOUGLAS HELICOPTER COMPANY (MDHC)

The compressed storage and real-time updating of terrain profiles and obstacles for automatic guidance were organized in gaming area course-oriented coordinates that were indexed to the defined gaming area course shown in Fig. B-1 from the GE Compuscene IV CGI Fulda Gap (Germany) data base at MDHC. The gaming area course was 1092 dm long (takes approximately 1092 sec to traverse at 20 kt) and 100 dm wide and was effectively straightened into a rectangular corridor (Fig. B-1) for compressed storage and real-time updating of the automatic guidance system. This coordinate conversion was transparent to the pilots.

Four three-dimensional waypoint course-profiles were planned within the gaming area terrain data base of the GE Compuscene IV CGI to shorten the simulation time for each run to about 273 sec (approximately 4.5 min) at 20 kt and to provide variety among routes for the pilots. The waypoint course-profiles meandered within the gaming area course in a fashion similar to that depicted in Fig. B-2. The waypoint courses were designed in the plan view with the altitude of each waypoint and threat exposure height defined as heights above the continuous surface approximating the actual digitized terrain. Each course was delineated from surrounding terrain with the use of tree rows and contained at least one waypoint that commanded zero velocity. Upon arrival at this waypoint, the rotorcraft was commanded to perform an unmask-remask maneuver utilizing a bob-up/bob-down maneuver. Upon completion of this aggressive maneuver, the waypoint course was resumed. The threat exposure height was defined as the height of the trees delineating the course. Unexpected obstacles were placed strategically along the courses together with alternate routes among the trees.

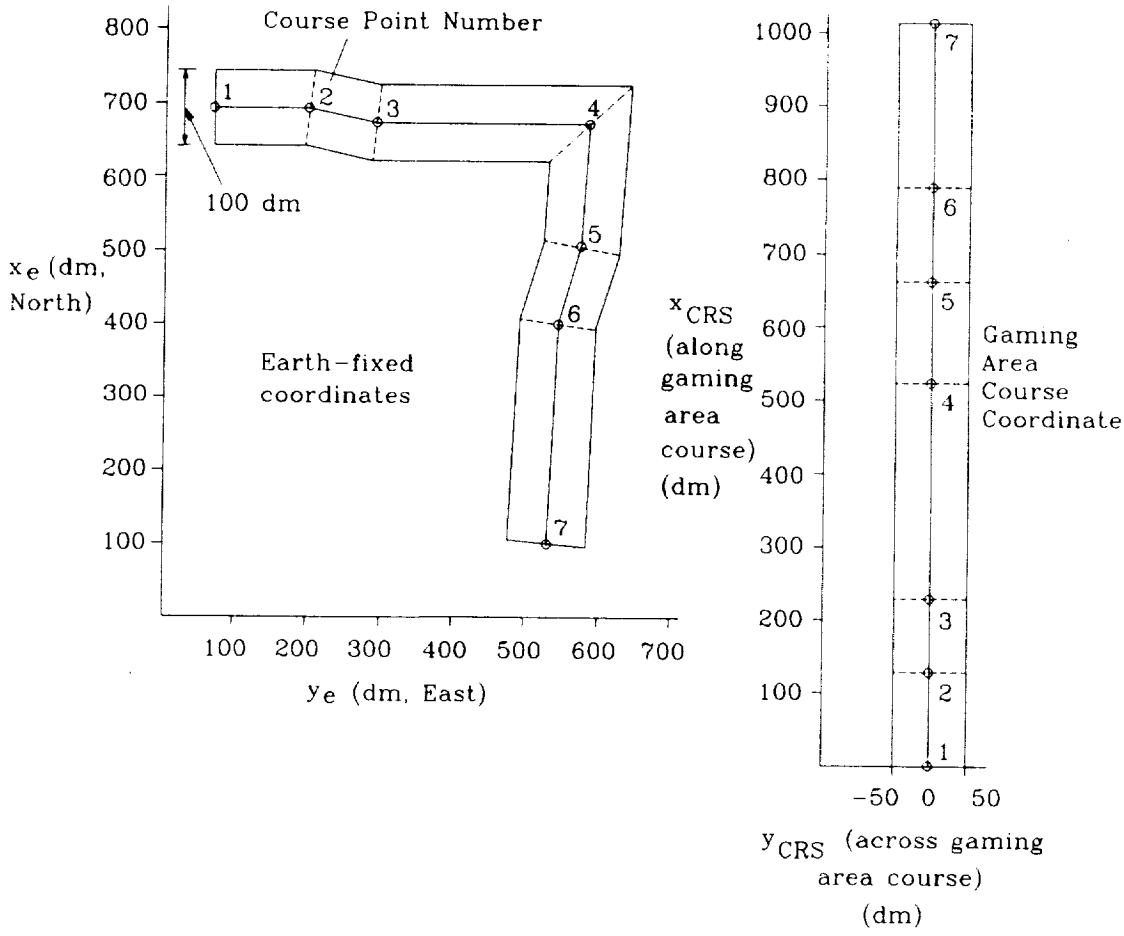

Figure B-1. Transformation of Gaming Area Course from Earth-Fixed Coordinates to Gaming Area Course Coordinates

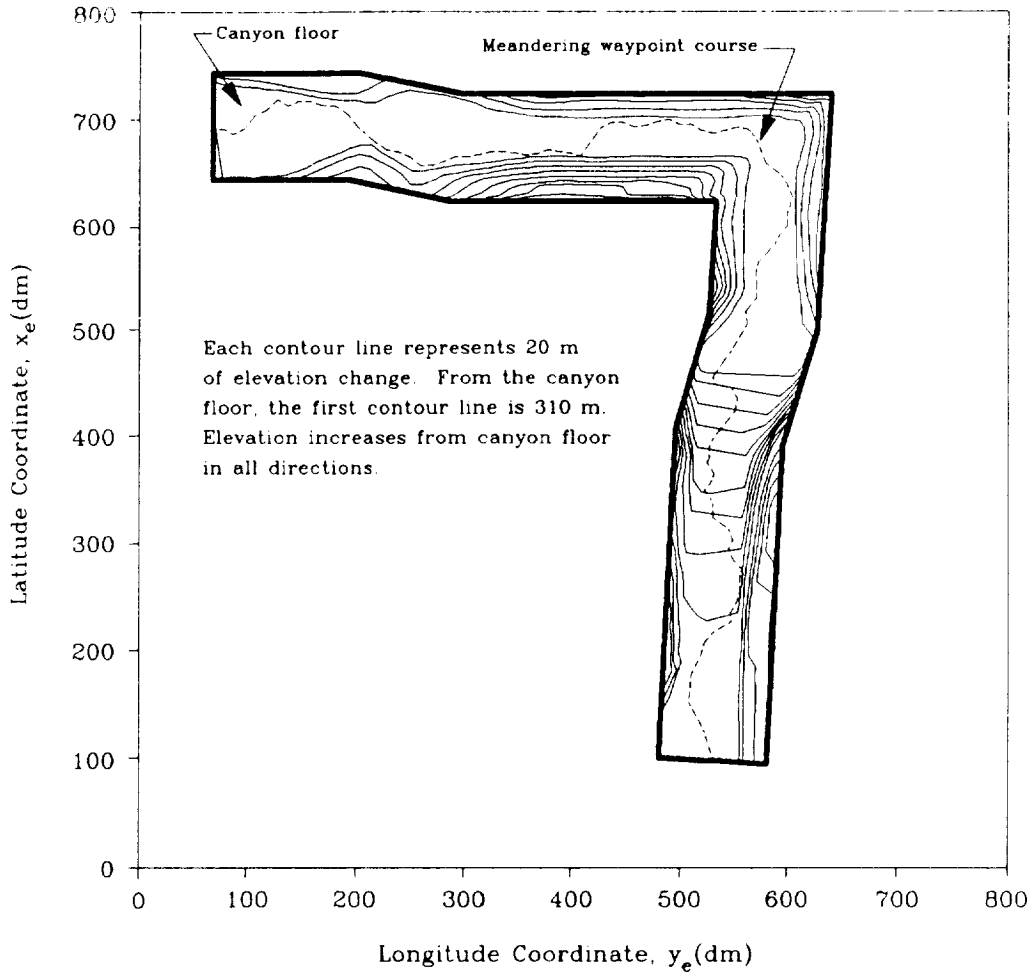

Figure B-2. Gaming Area Course for Automated NOE Flight Simulation Tests

APPENDIX C

McDONNELL-DOUGLAS HELICOPTER COMPANY
AUTOMATED FLIGHT PATH GUIDANCE/ADVANCED DIGITAL FLIGHT CONTROL SYSTEM

The McDonnell-Douglas Helicopter Company (MDHC) Advanced Digital Flight Control System (ADFCS) is an inertial acceleration-command, velocity-hold system that provides the pilot with direct control of the aircraft's three-dimensional flight path. The rate of change of the commanded flight path is determined by pilot stick inputs. In general, MDHC's ADFCS concept is an inertial flight path management control concept as opposed to the more traditional angular rate and attitude control.

This control system is algorithmically implemented in an inner-loop, outer-loop form. Inner loops serve as the aircraft's primary stabilization; whereas, the outer loops are used to provide control of flight path states. The types of control algorithms used for the outer-loop closures vary to provide the pilot with different levels of flight-path automation. Currently, the ADFCS contains several outer-loop control "modes," each providing different forms of flight-path augmentation. The "low speed" control mode is typically engaged at velocities below 20 kt, with lateral and longitudinal stick inputs to the system interpreted as translational acceleration commands that are integrated to provide velocity references. The resultant velocity commands are maintained in an inertial reference frame so that directional inputs do not affect the ground track. A transition into "cruise" mode is made as velocity increases through 20 kt. In this mode, lateral stick is interpreted as roll-rate command, and longitudinal stick remains a translational acceleration command. Cruise mode is characterized as being turn-coordinated flight, while low-speed mode is characterized as decoupled ground track/heading flight. Altitude control is vertical speed command, altitude hold below 20 kt, and vertical acceleration command, vertical speed hold above 20 kt. For most cases, this gives the pilot vertical rate control in low-speed mode and flight path angle pointing control in cruise mode. The command summary defining the transition regions for the MDHC ADFCS is shown in Fig. C-1.

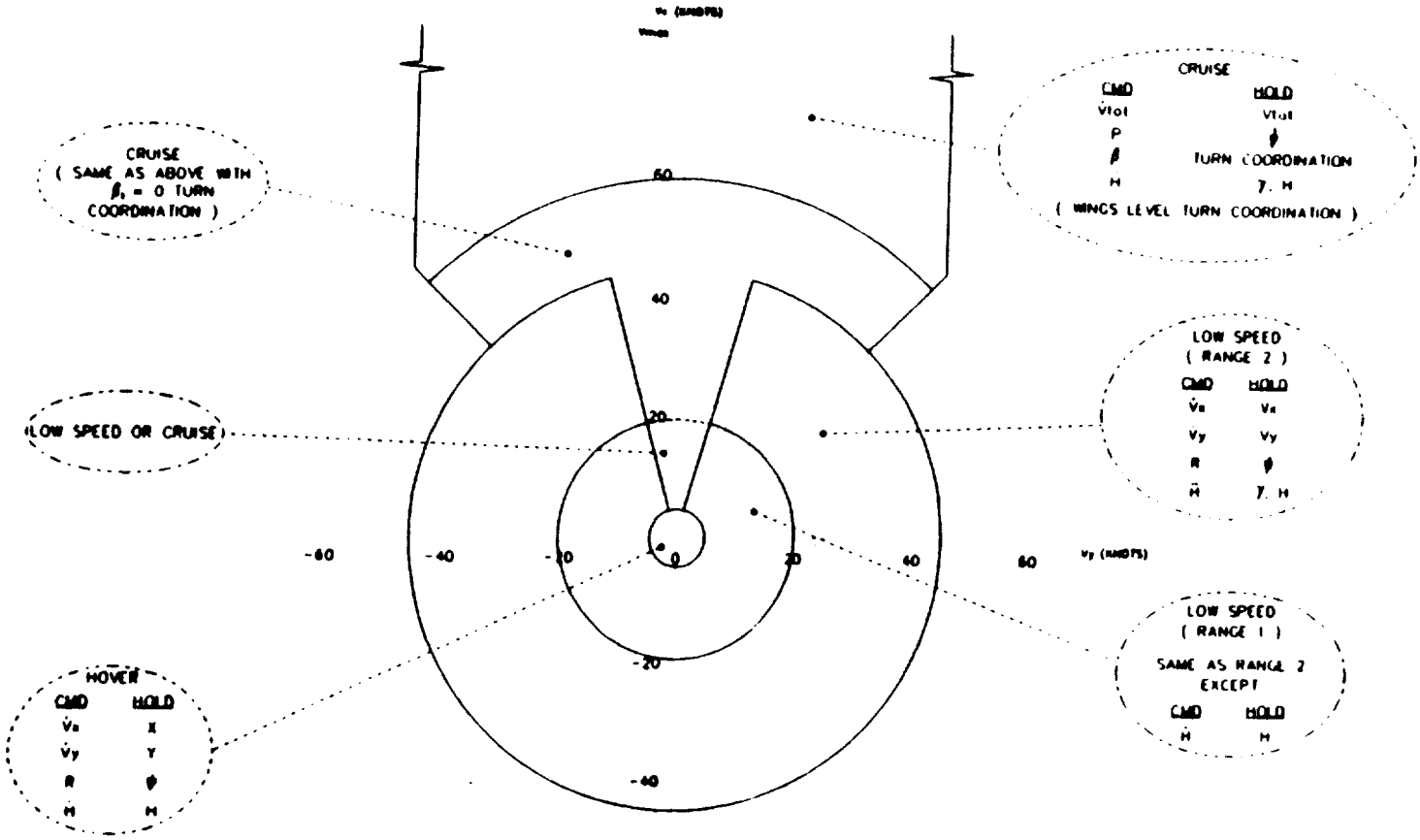

Figure C-1. MDHC Advanced Digital Flight Control System Command Summary

The PITCH, ROLL, and YAW inner-loop control modules implement the basic body axis rate stabilization loops as well as the first outer loop for vehicle attitudes. The VERTICAL control module provides a body-axis normal-acceleration command based on the altitude-rate command and feedback. The inner-loop control modules also include the switches and logic used to open integrators when actuator position and rate limits or aircraft performance boundaries are encountered and to initialize them for mode synchronization. Inputs are provided in each of these modules to allow predictive (or feedforward) commands from the outer-loop control modules. The outputs of these modules become inputs to the ACTUATOR module. This module conditions the angular- and normal-acceleration commands from the inner-loop modules based on aircraft performance functions and coupling effects, and it serves as the final software interface between the control laws and actuators.

The acceleration-command, velocity-hold concept of the ADFCS is incorporated in the outer-loop control modules. The outer loops are closed about estimated inertial states of the aircraft, with pilot inputs controlling the appropriate inertial references. Different outer-loop modules are sequenced as a function of control mode to provide the desired level of automation, such as coordinated flight, flight-path velocity-vector hold, or flight-path guidance. The mode supplying commands to the inner stabilization loops is automatically selected based on current flight conditions and aircraft states. This "auto-moding" feature separates the ADFCS from autopilots that require the pilot to select outer-loop augmentation modes.

Guidance algorithms in the previous Automatic Flight Path Guidance (AFPG) versions of the ADFCS were distributed throughout the manual control modules. Logic flags and integrator synchronization commands were added in each module to allow smooth transitions between automated guidance and manual control. Although this structure was effective for integrating AFPG and the ADFCS, complexity grew rapidly when integrating additional features, such as obstacle avoidance and time-optimal maneuver algorithms. The increased complexity made it difficult to modify the auto-guidance functions without inadvertently modifying the baseline manual control function. If additional automatic guidance algorithms were added to the ADFCS, the resulting logic necessary to distinguish between automatic algorithms could become unmanageable.

The current approach completely separates the manual and automatic controls. Each control mode of the automated system is derived from a baseline counterpart; that is, each affected baseline control module is modified appropriately to perform a specific guidance function. The modified modules form an additional group of control laws that are transparent to the baseline system until automated guidance is engaged. When automated guidance is selected or engagement is successful using flight-path capture, the mode control logic of the ADFCS diverts calculation of the automated flight-path solution to the modified control modules. In the event of a pilot supervisory override, control is returned to the baseline modules. With this approach, the baseline control configuration remains unchanged, and the automatic modules can be modified without affecting manual control.

This "multilevel" control concept is depicted by the flow chart shown in Fig. C-2. The first-level logic selects the baseline mode type; whereas, the second level selects the particular controller module based on the automation task. For example, lateral and longitudinal velocity vector control (low speed) or turn coordinated control (cruise) would be selected by the Level 1 auto-moding logic as described in the preceding paragraph. This is indicated in Fig. C-2 by the dashed sections marked "Level 1 Mode Control Logic." The choice between an automated module, such as the AFPG, or the pilot input "baseline" module would occur at Level 2. This selection process is indicated in Fig. C-2 as "Level 2 Mode Control Logic." For fully automated flight-path guidance, the AFPG module would be selected. If no alternate mode is selected, the system defaults to the baseline ADFCS, which accepts pilot stick inputs. Modules may be modified,

added, or removed without affecting either the baseline or AFPG control. Note that Level 1 is necessary only if control functions other than the baseline exist.

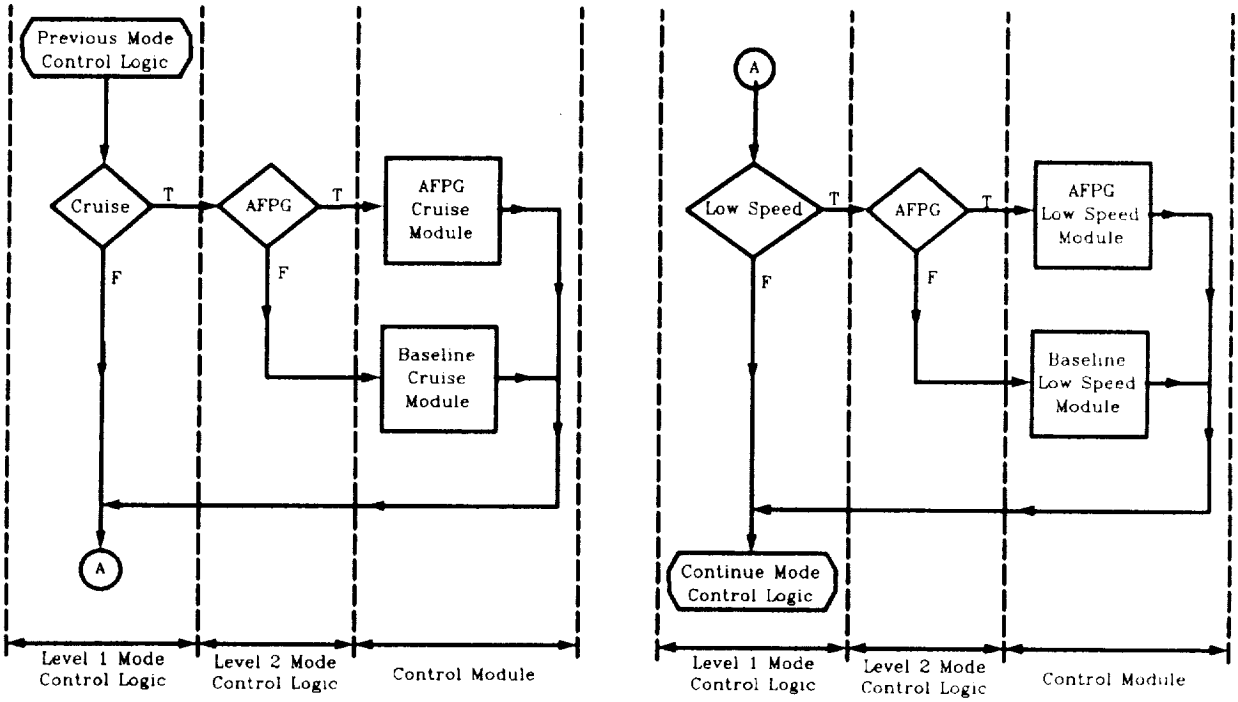

Figure C-2. Automatic Flight Path Guidance/Advanced Digital Flight Control System Multi-Mode Control Structure

The ADFCS Level 1 mode is completely automatic and requires no pilot action to select the outer-loop control mode. The Level 2 mode is pilot selectable, however, and must be activated by depressing a cockpit switch. Level 2 selection could be implemented automatically if the engagement criteria are properly defined.

Another feature of the multilevel mode control is the ability to sequence Level 2 modes while maintaining the same Level 1 mode. An example of this is the supervisory override feature of the AFPG. This feature enables the pilot to override the automated guidance and take control of the aircraft if he chooses to override the programmed flight path. Responding to a lateral stick input, the mode logic diverts control calculations from the AFPG module to the baseline modules. The pilot regains full control authority while the AFPG algorithms

transparently monitor his stick inputs and the aircraft states. When the proper re-engagement criteria are satisfied, control is returned to the AFPG modules. In general, the re-engagement criteria are satisfied when the pilot sets up an intercept to the pre-programmed course and releases all stick force; that is, those not commanding flight-path changes.

APPENDIX D

COCKPIT DISPLAYS IN THE McDONNELL-DOUGLAS HELICOPTER COMPANY SIMULATION

McDonnell-Douglas Helicopter Company (MDHC) displays for the Automatic Flight Path Guidance (AFPG) control consisted of a moving map of the Fulda Gap (West Germany) data base with the course superimposed and the AFPG cockpit display. The latter display is typically projected through the integrated helmet and display sight system (IHADDS) but can also be selected on a cockpit multifunction display (MFD).

An example of the cockpit display used for the AFPG/Advanced Digital Flight Control System (ADFCS) is shown in Fig. D-1. All display attributes are similar in function to those typically found on MFDs with the exception of the ghost aircraft, the pilot side tasks, and the AFPG system cues.

Waypoint tracking is accomplished by comparing the geometry defined by the temporary data stack with the aircraft's current position. Referring to Fig. D-2, the North (N_{CTE}) and East (E_{CTE}) errors between the aircraft and the $(i+1)^{th}$ waypoint are calculated and rotated through the $(i)^{th}$ leg bearing (Ψ_m) to give the following expressions for the lateral ground track position error (Y_{CTE}) and rate ($\dot{Y}_{CTE}$). Also calculated for leg sequencing logic are the along-track distance (X_{CTE}) and closing rate ($\dot{X}_{CTE}$) on the $(i+1)^{th}$ waypoint. In equation form:

$$N_{CTE} = X_{(i+1)} - X_{a/c} \tag{D-1}$$

$$E_{CTE} = Y_{(i+1)} - Y_{a/c} \tag{D-2}$$

$$Y_{CTE} = -N_{CTE}\sin\Psi_m + E_{CTE}\cos\Psi_m \tag{D-3}$$

$$\dot{Y}_{CTE} = -U_{NTH}\sin\Psi_m + U_{EST}\cos\Psi_m \tag{D-4}$$

$$\Phi_c = -(Y_{CTE}K_Y + \dot{Y}_{CTE}K_{\dot{Y}}) \tag{D-5}$$

$$\dot{H}_c = (H_{min} - H_{RADAR})K_H \tag{D-6}$$

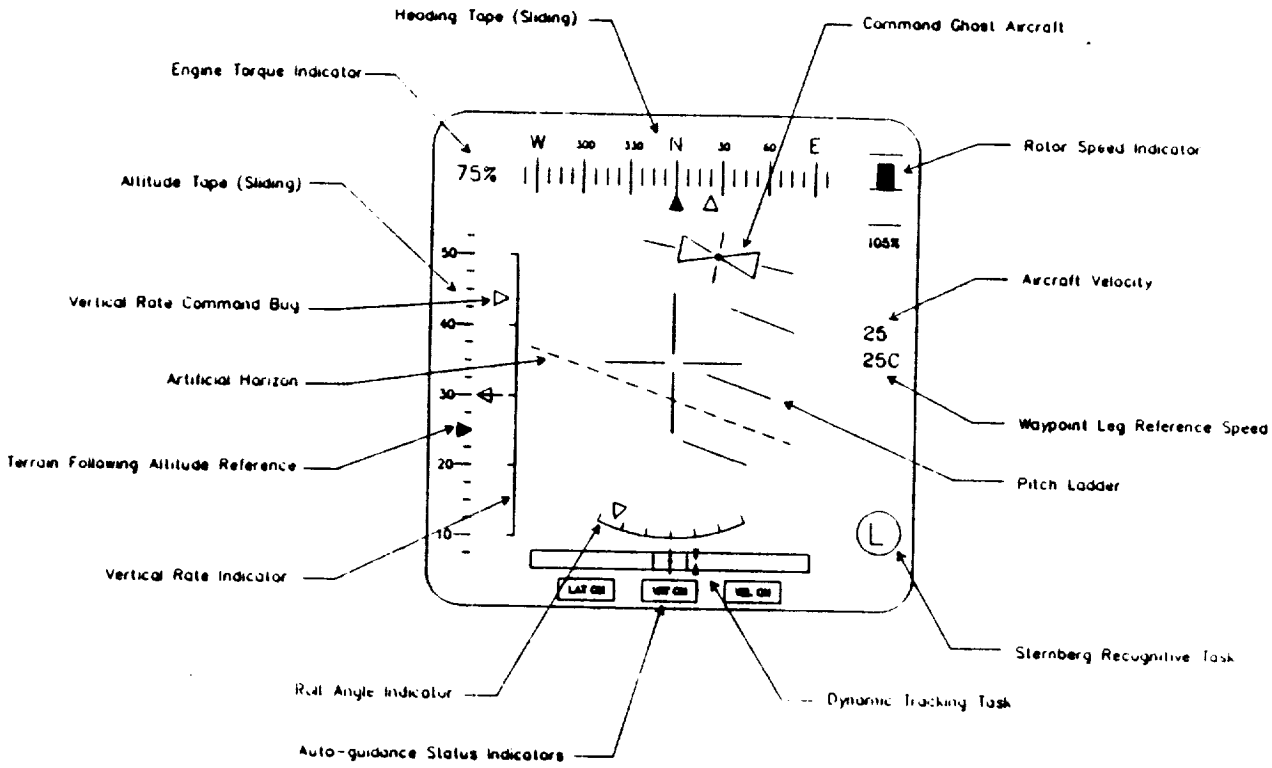

Figure D-1. Automatic Flight Path Guidance Cockpit Display

where Φ_c is the roll angle command in deg, K_y is the lateral track error gain in deg/ft, $K_{\dot{y}}$ is the lateral track rate gain in deg/ft/sec, H_c is the commanded vertical speed in ft/sec, H_{min} is the desired terrain following altitude in ft, H_{RADAR} is the aircraft radar altitude in ft, and K_H is the altitude error gain in sec^{-1}.

The $Y_{CTE}K_{\dot{y}}$ term in Eq. D-5 is limited by $K_{\dot{y}}V_c\sin(45°)$, where V_c is the commanded longitudinal velocity, to command a 45 deg capture angle where Y_{CTE} is large. Additionally, the total roll angle command Φ_c (Eq. D-5) is limited to a maximum of ± 20 deg and rate limited at ± 10 deg/sec.

The ghost aircraft symbol is driven horizontally and vertically by commands proportional to the lateral position error, as calculated by Eq. D-3, and the terrain following altitude error (Eq. D-6), respectively. Angular rotation of the ghost aircraft is governed by the roll angle command given by Eq. D-5. When the AFPG system is tracking the waypoint course, the ghost aircraft symbol remains centered on the display. In the event of a leg change or side-step maneuver,

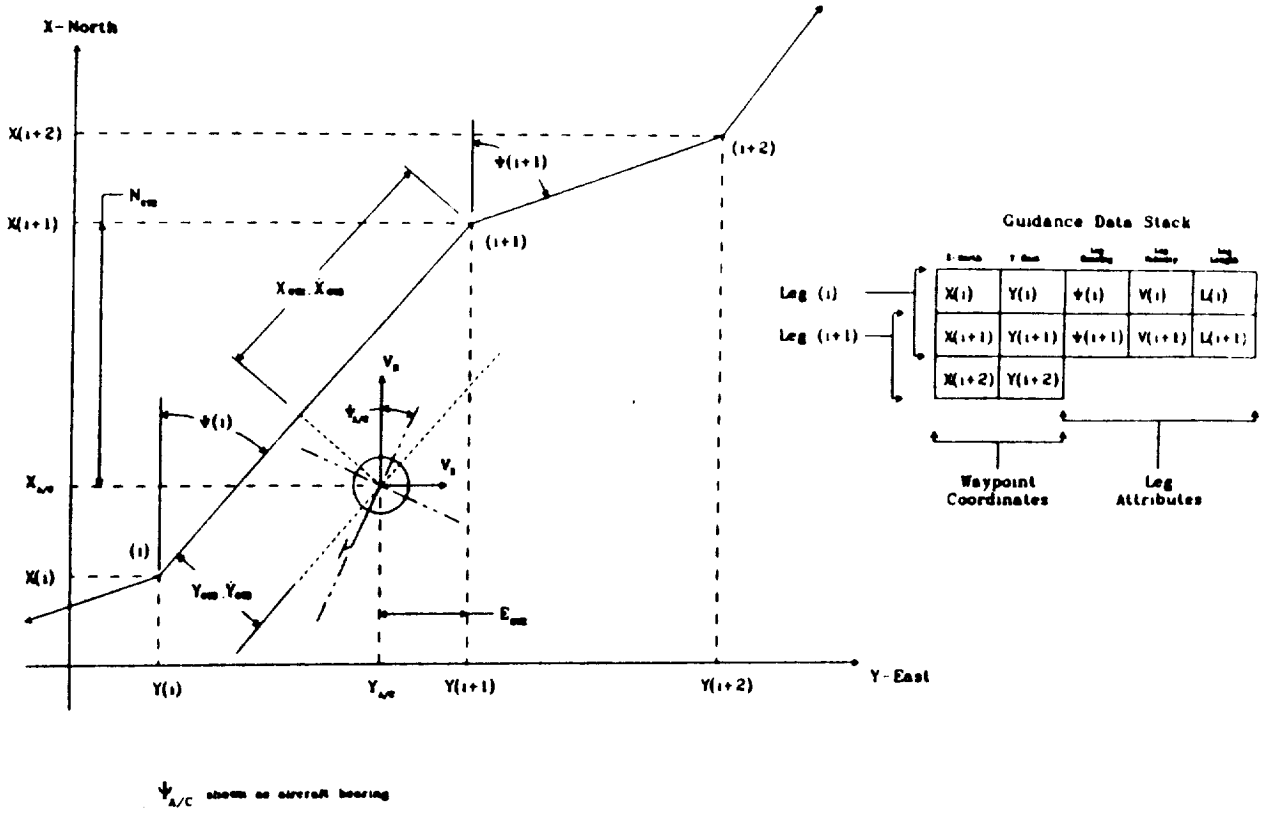

Figure D-2. Waypoint Course Tracking Geometry
($\Psi_{A/C} = \Psi_m$)

the ghost aircraft symbol moves a distance proportional to the magnitude and in the direction of the turn or maneuver. This provides the pilot with a cue that a maneuver is imminent, along with its magnitude and direction.

The sub-critical tracking and Sternberg recognitive tasks were also displayed on the MFD. The sub-critical tracking task, however, was not used for the simulation study. The choice reaction time side-task utilized three cockpit lights located directly below the MFD.

Not present on the MFD is a blinking turn indicator that warned the pilot of an upcoming leg change. This appeared on the upper left, directly below the torque readout.

An AFPG template, Fig. D-3, was also overlaid on the moving map display to indicate the programmed flight path with respect to the aircraft's relative position. This is most useful when attempting to re-engage the automated system by using the lateral capture routine. Once the valid intersection is obtained, a "phantom" leg is drawn on the display and maintained until the transition to the next leg. When the AFPG is engaged, the aircraft simply appears superimposed over the course, thus giving a rough visual estimate of current position. Figure D-3 includes examples of this template while tracking the programmed course and temporary leg, respectively.

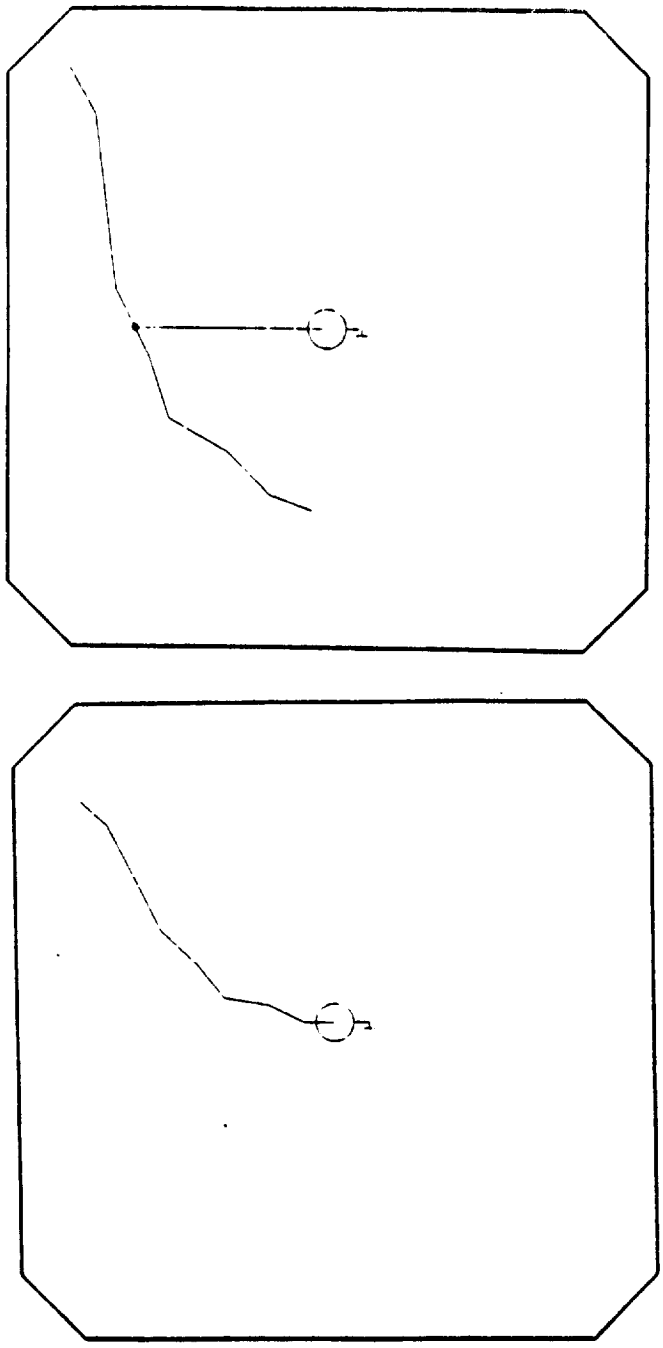

Figure D-3. Automatic Flight Path Guidance Moving Map Template

APPENDIX E

PILOT COMMENTS FROM THE PILOTED SIMULATION AT McDONNELL-DOUGLAS HELICOPTER COMPANY

This appendix presents pilot comments from the real-time piloted simulation of the combined Systems Technology, Inc., (STI) and McDonnell-Douglas Helicopter Company (MDHC) automated nap-of-the-earth guidance and control system negotiating the four prepared courses within the Fulda Gap gaming area from the Compuscene IV computer-generated image data base at MDHC in Mesa, Arizona, August 10 and 11, 1989.

1. OVERALL CONFIDENCE

Overall, the pilot seemed satisfied with the automated guidance and control algorithms, including the constrained time-optimal evasive maneuvers. Regarding the latter, he was impressed with the precision with which the automated system was able to perform these maneuvers. He stressed that, during the first few times experiencing these maneuvers, he was concerned because of the aggressiveness of the maneuvers; but, after this initiation, he was confident that the automatic guidance system was worthy of trust and was able to perform these aggressive maneuvers very precisely. He also commented on how smoothly the automatic guidance system performed the constrained time-optimal maneuvers, although he admitted that a moving-base simulator would provide a better vantage from which to judge this aspect of the maneuvers. He would prefer, however, a less aggressive bob-down when flying so close to the ground.

2. SPEED THROUGH THE COURSE

The commanded speed (20 kt) through these courses was deemed acceptable by the pilot, although he said he would not be comfortable at greater speeds. He said that, in such close confines (10 ft of rotor clearance) and with so many turns, he would feel comfortable flying manually through the course at approximately 5 kt less (15 kt); but, with the automatic system, he was comfortable traveling at 20 kt.

3. ALERTS OF IMPENDING DEVIATION FROM THE FLIGHT PATH

Main comments regarding the automated nap-of-the-earth (NOE) algorithms concerned the alerting (or lack thereof) of the pilot to impending departures from the planned flight profile as a result of detected obstacles. Impending lateral maneuvers were discernable due to the layout of the course, as the only breaks in the corridor of trees defining the course occurred at locations of lateral deviations from the flight profile, but there was no similar indication preceding vertical evasive maneuvers.

4. AUTO-GUIDANCE SYMBOLOGY

Lateral maneuvers via banked turns, NOE, were clearly displayed. The phantom aircraft symbology indicated with adequate predictability, the lateral maneuver prior to execution. The pilot was alerted that: (a) the guidance system had determined a lateral maneuver was necessary and (b) the particular maneuver was about to take place.

Climbs and descents for obstacle avoidance were not clearly displayed to the pilot. The choice of the climb or descent option prior to the maneuver was not apparent. The pilot could not discern whether the system had detected an obstacle requiring a vertical maneuver or what option to clear the obstacle would be used. It was recommended that the displays also indicate climbs and descents by vertical movement of the phantom aircraft. Later, displays were changed to include the vertical maneuver cues. This was a welcome change and proved to be quite useful.

Although lateral maneuver cues were displayed with the phantom aircraft, they did not discriminate between coordinated turns from one leg to the next and side-step maneuvers around obstacles. After becoming more familiar with the displays, it could be determined which maneuver was imminent; however, it wasn't readily apparent. The pilot should be cued explicitly by the system to distinguish coordinated turns from side steps.

Velocity control displays were very good. The leg's commanded velocity displayed below the aircraft's actual ground speed, provided an ideal cue to engage the velocity control.

In general, the phantom aircraft used to display commands from the guidance system proved very usable. It conveyed adequate information of the action about to be taken, while remaining uncluttered.

The suggestion was to include the vertical maneuver command in a central feature of the head-up display (HUD), that is, the ghost aircraft symbol. In the McDonnell-Douglas Helicopter Company (MDHC) HUD, the ghost aircraft symbol consists of a circle with a dashed perimeter between two opposing triangles (Fig. E-1). A vertical displacement of the opposing triangles with respect to the center of the circle could be used to indicate a vertical position command.

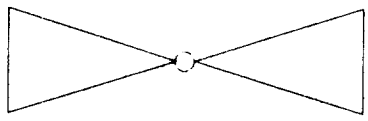

Figure E-1. Ghost Aircraft Symbol Used in MDHC Head-Up Display

5. MONITORING RPM DROOP AND CONTROL AUTHORITY

The pilot was asked how he kept track of the control authority used up by the automatic guidance system, since the simulation provided him with a series side arm controller without authority indicators. He did not monitor the control authority and accepted that it was not possible for him to do so either visually or tactually, Similarly, there was no instrument by which the pilot could monitor the rotor RPM, but rather a warning light illuminated only as an indication of a problem. Again, the pilot indicated that the lack of RPM information was acceptable to him in the simulator.

6. SPECIFICATION OF VERTICAL CLEARANCE

Another suggestion from the pilot concerned the vertical clearance of obstacles. He suggested that the pilots be told the clearance requirements and whether these requirements are fixed or may vary. This suggestion was motivated by the fact that the MDHC implementation of the obstacle detection and avoidance maneuver selection logic seemed to call for vertical evasive maneuver magnitudes that resulted in varying clearances of the obstacles with no apparent reason for this variance.

7. SIDE TASKS

The dynamic tracking side task should be included in addition to the Sternberg and choice reaction time tasks to provide a task that demands the pilot's attention at all times. Incrementing the workload level necessary to stabilize an unstable system is a better indicator of maximum pilot workload when combined with the other tasks.

8. STERNBERG RECOGNITIVE TASK

The evaluation pilot had some difficulty performing the Sternberg recognitive task as it was set up for the MDHC simulation. This task calls for the pilot to memorize a set of letters, and, as letters are presented randomly in the corner of the HUD, he is to flip a thumb toggle upward in response to the presentation of a member of the memorized set and downward in response to the presentation of all other letters. Unfortunately, because the member letters are presented so infrequently, the pilot grew accustomed to flipping the toggle downward; and then, when a letter from the memorized set was presented, even though the pilot correctly identified the letter as a member of the set, his habitual reaction was to flip the toggle downward. He recommends that the task be changed so that the pilot is to respond only to the presentation of members of the memorized set.

STI tried to avoid the problems encountered by the subject pilot not by eliminating response to nonmembers, but by presenting members and nonmembers at more nearly equivalent frequencies. The main problem identified by the pilot was the fact that, because the presentation of members of the memorized set is so infrequent (each letter of the alphabet has the same chance of being presented, yet only three or six are members of the memorized set), he found himself automatically responding as if the presented letter were not a member of the memorized set even if he had correctly identified the letter as a member. By experiencing the member and nonmember letters presented at more nearly equivalent frequencies, the pilot should not find himself responding spontaneously.

9. AIRCRAFT MANEUVERING

The aircraft roll rates and bank angles were comfortable. The guidance system control inputs were positive/decisive maneuvers that seemed to be very close to what the pilot would input for manual flight. The simulated system maintained near perfect nose/tail alignment for NOE flight. An attempt was made to evaluate roll rate and acceleration limit changes for the side-step maneuvers. Most changes were benign in a fixed-base visual cue simulation except at the highest rates. It is recommended that this type of evaluation be accomplished in a motion-base simulator.

Lateral maneuvers were acceptable after the pilot learned to discriminate between side-step and coordinated turn autoguidance commands. Again, the pilot must be alerted to the particular type of maneuver prior to execution by the guidance system. It is recommended that further investigation into types of turning and side-step display cues be undertaken.

The commanded ground speed of 20 kt and a terrain following altitude of 25 ft above ground level (AGL) were almost perfectly maintained during the simulation. The guidance system inputs for these commands were also comfortable and accomplished smoothly.

The guidance climb control input was comfortable. The descent command, however, resulted in an approximate 1,200 ft/min descent rate. For a 50-ft change in altitude, the descent rate appeared to remain at 1,200 ft/min until the instant of reaching the target altitude of 25 ft AGL. The high rate of descent at low altitude was somewhat disconcerting to the pilot because he was not sure (a) if the guidance system was indeed going to arrest the descent and (b) at which point he should enter the loop to recover if the guidance failed. This concern subsided after observing that the system consistently "stopped on a dime" at the commanded altitude. The initially high rate of descent to regain mask is tactically sound. Further investigation is necessary to ascertain if the real aircraft can duplicate the almost instantaneous arrest of the descent rate seen in the simulation and if the pilot could successfully recover if a guidance system failure occurred at that point.

Inconsistent vertical clearance of obstacles almost resulted in manual overrides until the pilot ascertained that the obstacle was indeed cleared. The clearance envelopes around obstacles will have to be clearly understood by pilots prior to flying this type of guidance system.

Vertical control inputs were not predictable while performing the manual flights. It was very difficult for the pilot to stop at a desired altitude or to maintain a constant altitude, and pilot-induced oscillation in the vertical axis resulted. Excessive time was used by the pilot in attempting to maintain desired vertical tasks, causing other side-tasks to suffer. It was apparent that the radar altitude hold feature of the ADFCS was not entirely functional. This was isolated to a mistake made when transferring the off-line AFPG/ADFCS code to the real-time simulation. The problem was corrected in later simulations, which greatly reduced the workload in the vertical axis.

10. PLANNED INSTANCES REQUIRING SUPERVISORY OVERRIDE

To "keep the pilots honest," the evaluation pilot suggested that, at some point in the automatic runs, unannounced instances should be arranged that would require pilot intervention to avoid a collision. To incorporate this suggestion into the STI simulation of automated NOE and yet prevent these instances from weakening the pilot's confidence in the automatic system, the addition of prearranged failures will be considered an independent variable in the experiment. Several simulation runs will include a variety of prearranged failures without the pilot's foreknowledge. The pilot will be asked to rate the controllability and margin of safety of the manual intervention via supervisory override using the decision tree and fine point scale in Table 5 of Ref. E-1. This will provide an opportunity to test the supervisory override feature as well as the automatic guidance recapture logic.

11. AUTOMATIC GUIDANCE RECAPTURE

The pilot had trouble engaging the automatic system using MDHC's recapture logic. This logic undoubtedly works well in an up-and-away scenario with very long waypoint legs, but, in the NOE environment, it was very difficult to use. The main problem was that the waypoint course had to be approached nearly perpendicularly in order to insure engagement of the lateral flight path guidance, and, in the confines of the navigable corridor, this was nearly impossible.

12. PILOT OPINION RATING SCALES

Neither evaluation test pilot was willing to fill out the provided pilot opinion rating scale forms (Table 2 in Ref. E-2) after each run. To do so would be repetitive, one stated, as his responses would not vary from run to run. He preferred to fill out the rating form once, following the simulation session.

STI agrees that the three of the rating scales concerning attributes of the display units need not be filled out by the evaluation pilots following every run. In fact, it is the intention of STI to have the pilots respond to these rating scales only twice: at the beginning and end of the simulation. The rating scale concerning the pilot's confidence in the automatic guidance system should, however, be filled out following every data run. In addition, a fifth rating scale has been created to analyze the pilot's opinion concerning controllability and margin of safety during manual intervention via supervisory override (Table 5 in Ref. E-1). The pilot will be asked to respond to this rating scale only after runs in which he has exercised his ability to take over control from the automatic guidance system.

13. KINETOSIS

A potential problem with the MDHC simulation was vertigo leading to kinetosis due to wide fields of view of dynamic imagery in fixed-base simulation. The Compuscene IV provides a lateral field angle of 120 deg and an elevation field angle of 90 deg. Representatives of MDHC confirm that it induces vertigo in pilot subjects consistently within one-half to three-quarters of an hour exposure. As the demonstration on August 11 lasted two-and-one-half hours, it was likely that the evaluation pilot would experience vertigo leading to kinetosis, and that this might have had a decidedly negative impact on his acceptance of the simulation. Possibly because the actual time during the demonstration spent flying was limited to approximately three-quarters of an hour broken into 10 to 15 min intervals, the pilot made no mention of the effect of vertigo.

In a follow-up telecon, the pilot did acknowledge that, in the past, he has been troubled by kinetosis resulting from simulation flights in the fixed-base MDHC simulation cabs, often delayed for up to 6 hrs following the simulation flight but that he experienced no such discomfort following any of his simulation sessions associated with this project. He suggested that the fact that the flight monitoring task required of him during a majority of the simulation test flights afforded him more time to scan inside the stationary cockpit was a possible explanation.

14. GENERAL COMMENTS

The simulation test flights conducted during the demonstration included the first tests of the MDHC prerecorded flight feature. Unfortunately, it was quickly recognized that the evaluation pilot was unable to perform the side tasks during the playback of the recorded flight, since all pilot inputs from the manual flight were inadvertently recorded, including the inputs to the side task switches. This invalidated comparison of the recorded flights with the automated flights, compromising the double blind aspect of the test plan. There is some debate whether the double blind can be valid anyway, since the evaluation pilot indicated that the differences between manual and automatic flight profiles were easily discernable due to the precision with which the automated system guided the

rotorcraft through the course. The MDHC simulation did not include turbulence, however, and this may help to disguise runs with the automatic guidance system in the simulation at Ames Research Center.

A feature of the MDHC HUD that was deemed a valuable addition to the STI HUD was the digital presentation of the commanded airspeed below the digital airspeed on the right side of the display (see Ref. E-3). This velocity command information will also be displayed analogically by the relative vertical location of the ghost aircraft symbol in the HUD.

The simulation schedule of Saturday, August 12, was intended to address two questions that arose from the demonstration (a) how the pilot will react to variations in the maneuver urgency factor (MUF) in lateral evasive maneuvers and (b) whether the addition of vertical command information in the ghost aircraft symbol would satisfy the pilot's requirement of information alerting him to impending vertical maneuvering.

The first result from the simulation was that the variation of the MUF was transparent to the evaluation pilot. He suggested that this would probably not be the case in a motion-based simulator, but, with only visual cues, the differences among lateral evasive maneuvers with varying MUFs were not discernible.

The pilot also indicated that the addition of height deviation commands in the movement of the ghost aircraft symbol did help to provide indication of impending vertical maneuvers.

REFERENCES

E-1. Gorder, Peter J., Warren F. Clement, and Wayne F. Jewell, Fully Automatic Guidance for Rotorcraft Nap-of-the-Earth Flight Following Planned Profiles. NASA Ames Research Center Simulation Test Plan, Systems Technology, Inc., Working Paper No. 1254-8, August 1989.

E-2. Gorder, Peter J., And E. Chris Nehls, Pilot Briefing for Real-Time Simulation Testing of Fully Automatic Guidance for Rotorcraft Nap-of-the-Earth (NOE) Flight Following Planned Flight Profiles. MDHC Simulation, Systems Technology, Inc., Working Paper No. 1254-10, June 1989.

E-3. Gorder, Peter J., Constrained Time Optimal Obstacle Avoidance Maneuvers, Systems Technology, Inc., Working Paper No. 1254-2, February 1988.

APPENDIX F

McDONNELL-DOUGLAS HELICOPTER COMPANY (MDHC) PILOTED SIMULATION SIDE TASK RESULTS

Two of the three proposed side tasks were presented to each MDHC evaluation pilot during both automatically and manually guided simulation runs; these side tasks were the Sternberg recognitive task and the choice reaction time task. The subcritical dynamic tracking task, although shown on the automated flight path guidance (AFPG) display example, was not used in the MDHC simulation. These side tasks are described in detail in Section VII in the main body of this report.

The Sternberg side task was displayed on the lower right corner of both the look-down multi-function display (MFD) and the IHADSS helmet-mounted display (HMD). The pilot was given the choice of which display method he preferred. Thumb switches on the side-arm controller were used for pilot response inputs. The pilot was instructed to respond to correct (valid) letters by depressing the inner thumb switch and incorrect (invalid) letters by depressing the outer thumb switch.

The choice reaction time display utilized three cockpit lights located slightly below the MFD. This forced the pilot to use a scanning procedure that divided his attention among out-the-window and various instrument monitoring tasks. The trigger switch on the side-arm controller was used for pilot response inputs. The pilot was instructed to respond by depressing the switch only when the center lamp was illuminated.

Both side tasks were presented to the pilot at light- and heavy-loading levels. The Sternberg task consisted of three valid letters for light loading and six valid letters for heavy loading, with new letters displayed every 20 sec. Pilot response inputs would clear the current letter until another was presented. The choice reaction side task utilized mean times between light illuminations of 48 sec for light loading and 8 sec for heavy loading. Pilot response to this task would extinguish all lamps whether correct or incorrect. The center lamp remained illuminated indefinitely until an input was sensed; whereas, the outer lamps would dim after 10 sec with no pilot response.

The proposed waypoint route consisting of 101 points was divided into four routes each having approximately 40 points. This was done to shorten the simulation times per run while providing variety for the pilot.

1. STERNBERG SIDE TASK RESULTS

The means and standard deviations of the responses for the Sternberg side task during manually and automatically guided runs over each of the four courses by each of the two pilots are presented in Figs. F-1 and F-2, corresponding to individual responses in Tables F-1 and F-2.

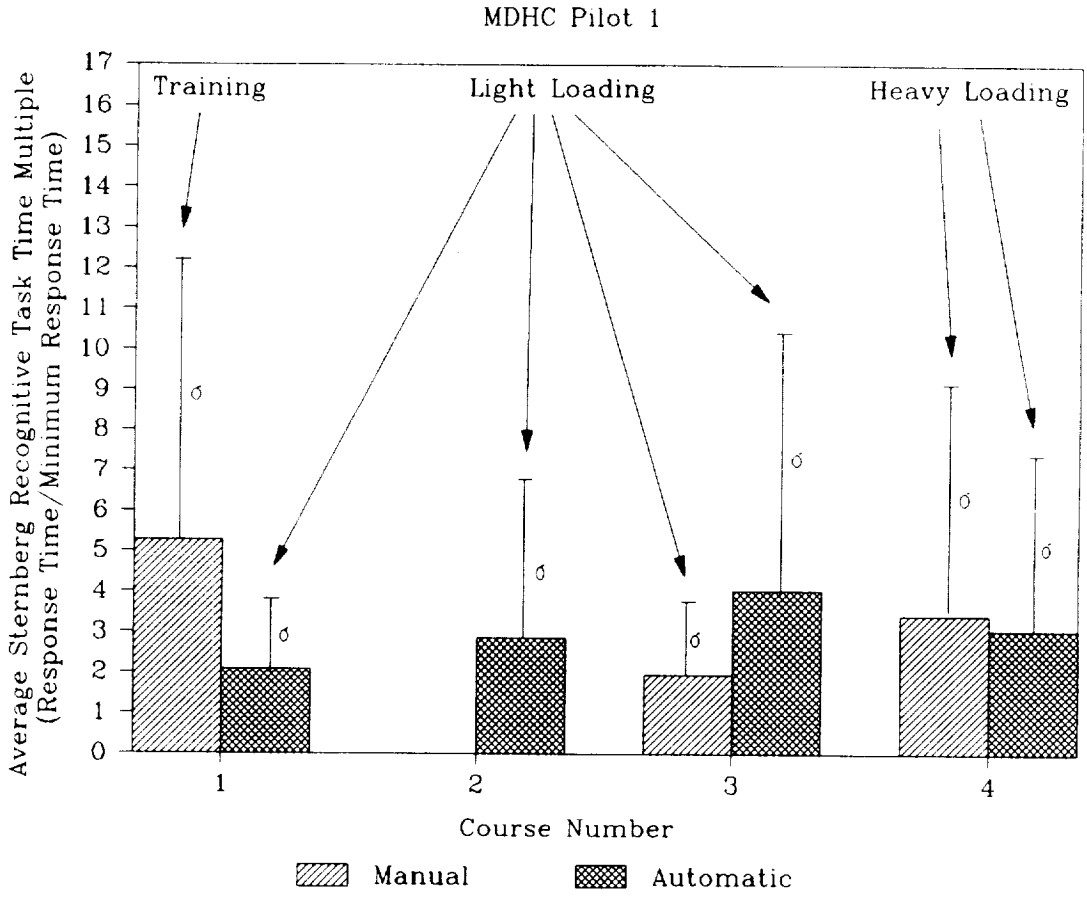

Loading: Light (3 valid characters out of 26, time between stimuli is 20 sec)
Heavy (6 valid characters out of 26, time between stimuli is 20 sec)

Minimum Response Time is 1 sec
Maximum Response Time is the Time Between Stimuli

(Incorrect responses were assessed the maximum response time)

Figure F-1. Means and Standard Deviations of Responses by MDHC Pilot 1 to Sternberg Side Task During Manually and Automatically Guided Runs Over Each of Four Courses

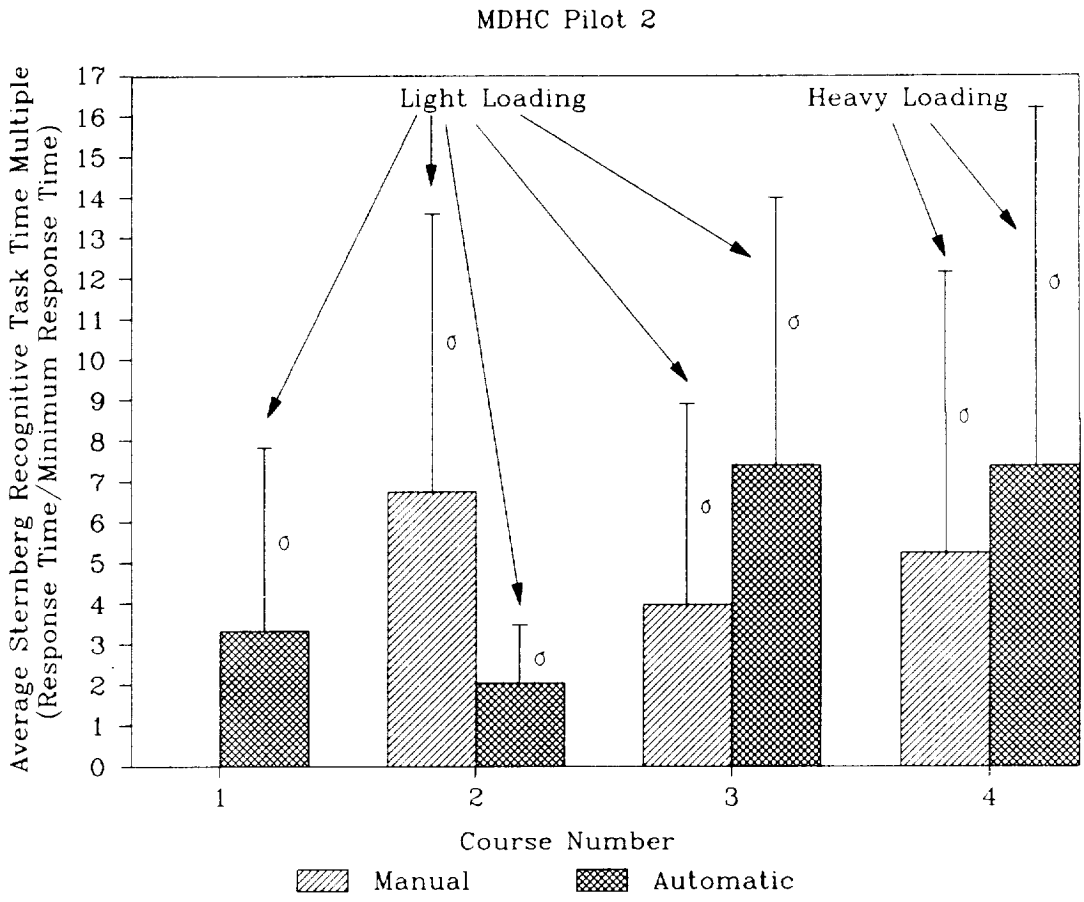

Loading: Light (3 valid characters out of 26, time between stimuli is 20 sec)
Heavy (6 valid characters out of 26, time between stimuli is 20 sec)

Minimum Response Time is 1 sec
Maximum Response Time is the Time Between Stimuli

(Incorrect responses were assessed the maximum response time)

Figure F-2. Means and Standard Deviations of Responses by MDHC Pilot 2 to Sternberg Side Task During Manually and Automatically Guided Runs Over Each of Four Courses

TABLE F-1. STERNBERG REACTION TIMES, MEANS, AND STANDARD DEVIATIONS (SD) OF RESPONSES (IN SEC) BY MDHC PILOT 1

Course 1		Course 2	Course 3		Course 4	
Manual Time	Automatic Time	Automatic Time	Manual Time	Automatic Time	Manual Time	Automatic Time
2.1	2.73	2.13	8.03	3.33	1.63	5
17.27	5.03	3.13	4.57	1.8	2.03	2.53
1.03	1.77	1.7	1.93	16.63	2.37	5.87
1.23	0.93	1.37	0.93	20	2.47	2.23
1.73	1.17	1.23	5.3	2.67	1	3.07
1.6	4.03	0.83	2.17	20	3.63	1.2
2.8	1	1.27	1.57	20	20	3.6
3.1	6.5	20	2.83	2.67	2.23	1.4
1.77	1.3	1.97	1.57	1.57	1.47	1.97
1.07	1.43	1.37	1	3.07	1.27	20
2.3	1.13	1.43	1.2	0.93	1.97	1.5
1.17	4.5	4.13	1.4	0.93	1.37	1.77
1.63	0.97	2.6	3.87	0.9	3.03	1.33
1.5	1	3.03	1.67	1.27	1.43	2.8
3.93	1.07	1.2	2.67	1.33	20	1.17
3.67	2.97	1.83	1.37	1.5	1.33	1.57
2.07	1.13	4.07	0.83	2.07	1.37	3.13
6.77	1.47	1.1	1	3	2.77	1.47
20	1.17	3	1.87	0.87	1.67	1.27
20		5.07	1	2.53	1.13	1.2
20		1.1	0.7	0.97	1	
2.1		1.43	1.13	1.77		
1.17		0.87	0.87	1.23		
11.8		2.1	1.93	1.23		
		1.5	1.5	2.1		
		7.37	1.03	1		
			0.8	0.53		
				0.8		
Mean: 5.27 SD: 6.92	Mean: 2.07 SD: 1.80	Mean: 2.85 SD: 3.88	Mean: 1.96 SD: 1.75	Mean: 4.02 SD: 6.40	Mean: 3.42 SD: 5.61	Mean: 3.05 SD: 4.28

TABLE F-2. STERNBERG REACTION TIMES, MEANS, AND STANDARD DEVIATIONS (SD) OF RESPONSES (IN SEC) BY MDHC PILOT 2

Course 1	Course 2		Course 3		Course 4	
Automatic Time	Manual Time	Automatic Time	Manual Time	Automatic Time	Manual Time	Automatic Time
2.37	20	1	20	20	3.07	1.57
1.53	18.1	2.33	1.8	20	20	2.33
1.87	11.57	1.63	2	8.6	20	3.4
1.5	20	1.93	3	2.77	2.73	3.9
1.17	20	4.13	1.27	6.1	1.73	3
20	2.17	1.07	3.5	1.5	1.83	3.53
4.23	3.97	3.13	1.1	1.57	2.27	1.97
1.43	1.43	1.37	3.77	14.63	1.7	1.23
3.1	4.17	2.7	2.93	12.3	10.2	20
2.7	1.67	3.2	20	4.03	0.97	20
2.83	1.1	1.5	3	11.87	2.53	2.5
3.2	4.5	1.7	4.93	6	2.43	1.97
4.07	9.37	2.63	2.73	2.27	3.83	20
2.57	1.7	2.53	1.93	4.07	4.93	2.83
2.63	16.4	1.1	3.5	10.1	1.77	20
2.13	4.13	4.47	1.1	4.57	20	4.53
2.03	12.57	1.07	1.5	5	1.03	20
3.9	8.6	1.13	1.03	2.67	3.07	
	3.1	1.37	4.1	1.53	2.53	
	4.27	1.67	2.7	3.47	3.3	
	2.4	0.93	5	9.33		
	1.2	2.23	2.43	5.23		
	1.8	0.93	3.97	20		
	5.17	5.3	3.43			
	9.37		4.6			
	1.8		3.5			
	1.17		2.17			
	3.83					
Mean: 3.33 SD: 4.37	Mean: 6.74 SD: 6.76	Mean: 2.04 SD: 1.35	Mean: 3.96 SD: 4.85	Mean: 7.40 SD: 6.49	Mean: 5.23 SD: 6.77	Mean: 7.38 SD: 8.57

In Fig. F-1 for Course 1, the manually guided training run included three occasions out of 24 presentations on which no choice was made and therefore each was assessed the maximum response time of 20 sec, one occasion with a response time over 17 sec, and one occasion with a response time nearly 12 sec. Hence the difference in mean response times between the manual training run and the automatically guided run over Course 1 was significant with a 99 percent level of trust based on Behrens' test (Ref. F-1). Although a longer mean response time with manual guidance is theoretically reasonable, the difference in mean response times on Course 1 may be substantially a training effect, because the opposite sense of the difference in means occurred on Course 3.

In Fig. F-1 for Course 3, the automatically guided run included three occasions out of 28 presentations on which no choice was made and therefore each was assessed the maximum response time of 20 sec, and one occasion with a response time over 16 sec. Hence the difference in mean response times between the manually and automatically guided runs over Course 3 was significant with a 99 percent level of trust based on Behrens' test (Ref. F-1). The longer mean response time with automatic guidance is counterintuitive and remains unexplained, unless there were unusual (and unrecorded) circumstances involving supervisory override and recovery on Course 3.

In Fig. F-1 for Course 4 with heavy loading, the difference in mean response times between manually and automatically guided runs was not significant.

In Fig. F-2 for Course 2, the manually guided runs included three 20 sec response times out of 28 presentations and four response times between 11 and 20 sec. Hence the difference in mean response times between the manually and automatically guided runs over Course 2 was significant with a 99 percent level of trust based on Behrens' test (Ref. F-1). The longer mean response time with manual guidance is theoretically reasonable.

In Fig. F-2 for Course 3, the manually guided runs included two 20 sec response times out of 23 presentations; whereas, the automatically guided runs included three 20 sec response times out of 23 presentations and six response times between 8 and 15 sec. Hence the difference in mean response times between the manually and automatically guided runs over Course 3 was significant with a 95 percent level of trust based on Behrens' test (Ref. F-1). Again, the longer mean response time with automatic guidance is counterintuitive and remains unexplained, unless there were unusual (and unrecorded) circumstances involving supervisory override and recovery on Course 3.

In Fig. F-2 for Course 4 with heavy loading, the manually guided runs included three incorrect responses out of 20 presentations, and the automatically guided runs included five incorrect responses out of 17 presentations for the reason discussed in Appendix C, Pilot Comments Regarding the Sternberg Recognition Task. The difference in mean response times between manually and automatically guided runs over Course 4 was not significant.

2. CHOICE REACTION TIME SIDE TASK RESULTS

The means and standard deviations of the responses for the choice reaction time side task during manually and automatically guided runs over each of the four courses by each of the two pilots are presented in Figs. F-3 and F-4, corresponding to individual responses in Tables F-3 and F-4.

In Fig. F-3 for Course 1, the manually guided training run included two occasions out of 14 presentations on which no choice was made, and therefore each was assessed the maximum response time of 3 sec, one occasion with a response time of 2.1 sec, and one occasion with a response time of 1.7 sec. The automatically guided runs for Course 1 included only one occasion out of five presentations with a response time of 2 sec, about twice those of the other four presentations. Hence the differences in mean response times between the manual training run and the automatically guided run over Course 1 was significant with less than a 90 percent level of trust based on Behrens' test (Ref. F-1). Although a longer mean response time with manual guidance is theoretically reasonable, the difference in mean response times on Course 1 may be substantially a training effect.

In Fig. F-3 for Course 3, the manually guided runs included two occasions out of seven presentations on which the response time was in excess of half the maximum response time of 3 sec: one occasion with a response time of 2.7 sec and one occasion with a response time of 1.7 sec. The automatically guided run for Course 3 included no occasions out of six presentations with an extreme response time. Hence the difference in mean response times between the manually and automatically guided runs over Course 3 was significant with less than a 90 percent level of trust based on Behrens' test (Ref. F-1). The longer mean response time with manual guidance is theoretically reasonable.

In Fig. F-3 for Course 4 with heavy loading, the manually guided run included ten occasions out of thirty-six presentations on which no response was made, and therefore each was assessed the maximum response time of 1.5 sec, one occasion with a response time of 1.5 sec, three occasions with a response time of 1.4 sec, and one occasion with a response time of 1.3 sec. The automatically guided run for Course 4 included six occasions out of thirty presentations on which no response was made, and therefore each was assessed the maximum response time of 1.5 sec, four occasions with a response time of 1.4 sec, and one occasion with a response time of 1.3 sec. Hence the differences in mean response times between the manually and automatically guided runs over Course 4 was not significant.

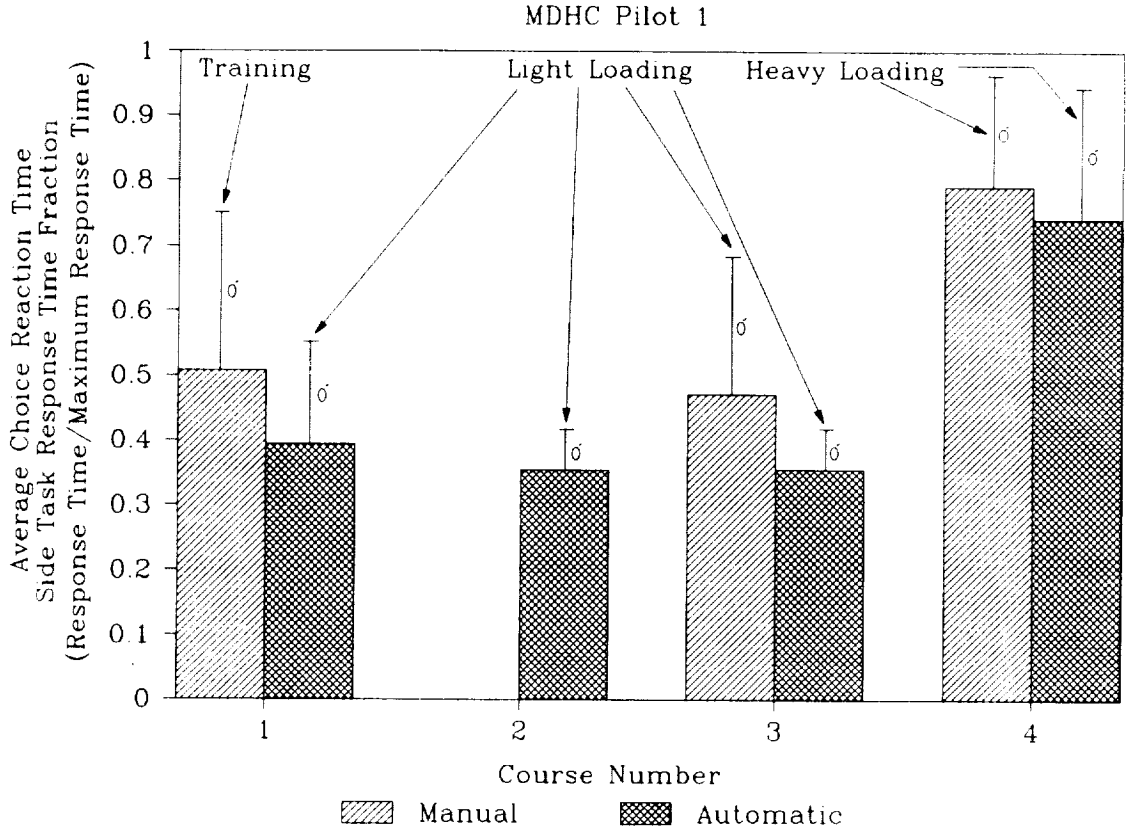

Figure F-3. Means and Standard Deviations of Responses by MDHC Pilot 1 to Choice Reaction Time Side Task During Manually and Automatically Guided Runs Over Each of Four Courses

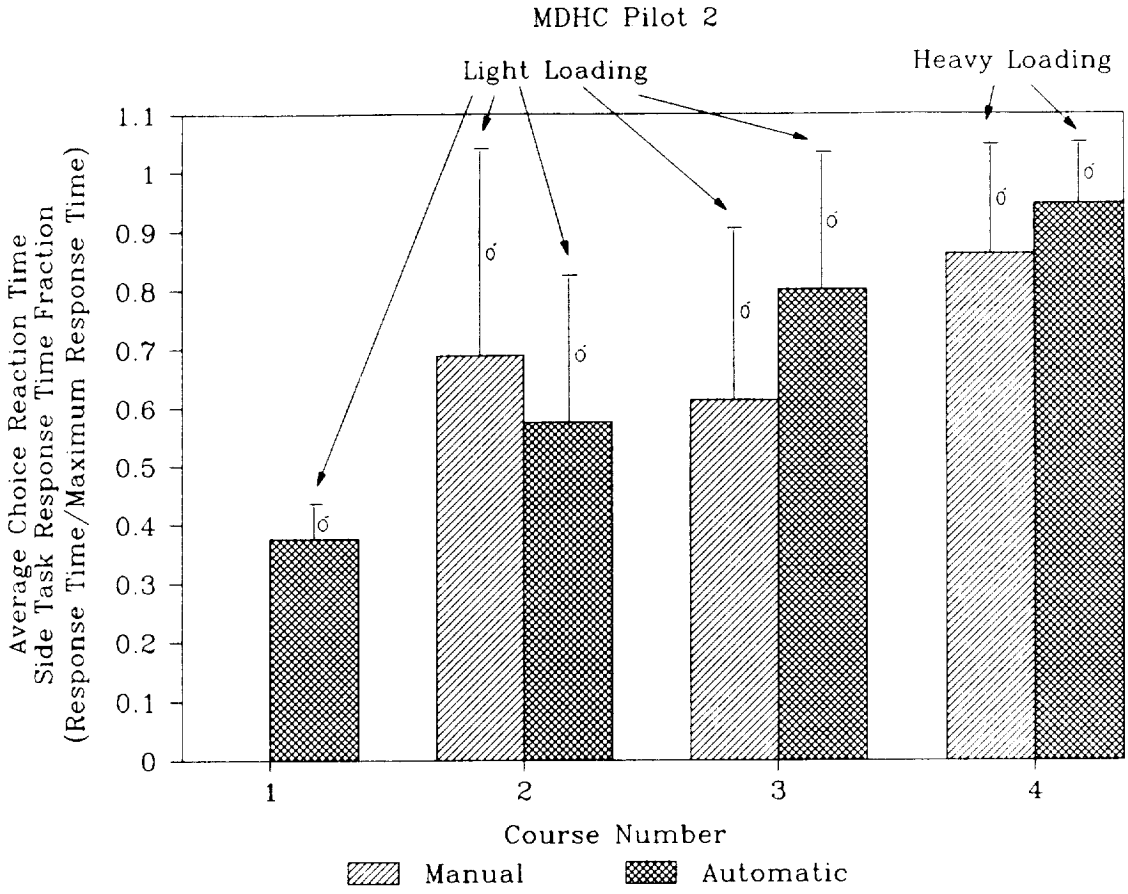

Loading: Light (mean time between stimuli is 48 sec; maximum response time is 3 sec)

Loading: Heavy (mean time between stimuli is 8 sec; maximum response time is 1.5 sec)

Figure F-4. Means and Standard Deviations of Responses by MDHC Pilot 2 to Choice Reaction Time Side Task During Manually and Automatically Guided Runs Over Each of Four Courses

TABLE F-3. CHOICE REACTION TIMES, MEANS, AND STANDARD DEVIATIONS (SD) OF RESPONSES (IN SEC) BY MDHC PILOT 1

Course 1		Course 2	Course 3		Course 4	
Manual Time	Automatic Time	Automatic Time	Manual Time	Automatic Time	Manual Time	Automatic Time
1.7	1.1	1.2	1.5	1.2	0.9	1.5
1.2	1	1.3	0.9	1.1	1.1	0.9
1.1	0.8	1.3	1.1	1.2	1	1.2
0.5	2	0.8	1	1.2	1	1.2
1.2	1	0.9	2.7	0.8	1	1.5
1		1.1	1	0.9	0.9	1
1.5		0.9	1.7		1.3	1
1.2		1			1.5	0.8
1.3					1	1.5
1.4					1.5	1.5
3					1.5	0.7
3					0.9	1.1
2.1					1	0.8
1.1					1	0.9
					0.8	1.3
					1	1.4
					1.5	0.8
					1.5	0.8
					1.2	1.2
					0.8	1.4
					1.4	0.9
					0.9	1.5
					1.2	1.5
					1.5	1.2
					1.1	0.8
					1.1	0.8
					1.5	1.4
					1.4	1.4
					0.8	1.1
					1.5	0.9
					1.5	0.6
					0.9	
					1.4	
					1.2	
					1.5	
					1.5	
					0.9	
(in seconds)						
Mean: 1.52 SD: 0.72	Mean: 1.18 SD: 0.47	Mean: 1.06 SD: 0.19	Mean: 1.41 SD: 0.64	Mean: 1.07 SD: 0.18	Mean: 1.19 SD: 0.27	Mean: 1.11 SD: 0.29
(dimensionless)						
Mean: 0.51 SD: 0.24	Mean: 0.39 SD: 0.16	Mean: 0.35 SD: 0.06	Mean: 0.47 SD: 0.21	Mean: 0.36 SD: 0.06	Mean: 0.79 SD: 0.17	Mean: 0.74 SD: 0.20

TABLE F-4. CHOICE REACTION TIMES, MEANS, AND STANDARD DEVIATIONS (SD) OF RESPONSES (IN SEC) BY MDHC PILOT 2

Course 1	Course 2		Course 3		Course 4	
Automatic Time	Manual Time	Automatic Time	Manual Time	Automatic Time	Manual Time	Automatic Time
1.3	3	1.2	1.3	1.8	1.2	1.5
1	3	3	3	1.8	1.5	1.5
1.2	1.5	1.4	0.9	3	1.5	1.5
1	0.9	1.1	2.2	3	1.5	1.5
	3	1.4	2.1		1.5	1.4
	1	2.1	3		1.5	1.5
		2.6	1.2		1.1	1.2
		1	1		1.5	1.5
					1.1	1.5
					1	1.3
					1.1	1.5
					1.2	1.1
					1.5	1.5
					1.5	1.5
					0.5	1.2
					1.5	1.1
					1	1.5
					1.5	1.5
					1.5	1.5
					0.8	1.5
					1	1.5
					1.5	
					0.9	
					1.5	
					1.4	
					1.5	
					1.2	
					1.5	
					1.5	
(in seconds)						
Mean: 1.13 SD: 0.15	Mean: 2.07 SD: 1.04	Mean: 1.73 SD: 0.75	Mean: 1.84 SD: 0.86	Mean: 2.53 SD: 0.86	Mean: 1.29 SD: 0.28	Mean: 1.42 SD: 0.14
(dimensionless)						
Mean: 0.38 SD: 0.05	Mean: 0.69 SD: 0.35	Mean: 0.58 SD: 0.25	Mean: 0.61 SD: 0.35	Mean: 0.8 SD: 0.23	Mean: 0.86 SD: 0.18	Mean: 0.95 SD: 0.1

In Fig. F-4 for Course 2, the manually guided runs included three occasions out of six presentations on which no response was made, and therefore each was assessed the maximum response time of 3 sec and one occasion with a response time of 1.5 sec. The automatically guided runs for Course 2 included one occasion out of eight presentations on which no response was made, and therefore it was assessed the maximum response time of 3 sec and two occasions with response times in excess of 2 sec. Hence the difference in mean response times between the manually and automatically guided runs over Course 2 was not significant with even a 90 percent level of trust based on Behrens' test (Ref. F-1). The longer mean response time with manual guidance is, however, theoretically reasonable.

In Fig. F-4 for Course 3, the manually guided runs included two occasions out of eight presentations on which no response was made, and therefore each was assessed the maximum response time of 3 sec and two occasions with response times in excess of 2 sec. The automatically guided runs for Course 2 included two occasions out of four presentations on which no response was made, and therefore each was assessed the maximum response time of 3 sec and two occasions with response times of 1.8 sec. Hence the difference in mean response times between the manually and automatically guided runs over Course 2 was not significant with even a 90 percent level of trust based on Behrens' test (Ref. F-1). The longer mean response time with automatic guidance is, however, counterintuitive, unless there were unusual (and unrecorded) circumstances involving supervisory override and recovery in Course 3.

In Fig. F-4 for Course 4 with heavy loading, the manually guided runs included sixteen occasions out of twenty-nine presentations on which no response was made, and therefore each was assessed the maximum response time of 1.5 sec and one occasion with a response time of 1.5 sec. The automatically guided runs for Course 4 included thirteen occasions out of twenty-one presentations on which no response was made, and therefore each was assessed the maximum response time of 1.5 sec, two occasions with response times of 1.5 sec, and one occasion with a response time of 1.4 sec. Hence the difference in mean response times between the manually and automatically guided runs over Course 4 was significant with a 95 percent level of trust based on Behrens' test (Ref. F-1). Again, the longer mean response time with automatic guidance is counterintuitive, unless there were unusual (and unrecorded) circumstances involving supervisory override and recovery on Course 4.

3. SUMMARY

In general, the pilots judged that the side tasks provided inadequate loading of attention level. The seven instances exhibiting longer mean response times with manual guidance were theoretically reasonable. There were, however, five instances exhibiting longer mean response times with automatic guidance that remain unexplained unless there were unusual (and unrecorded) circumstances involving supervisory override and recovery. The pilots were able to respond to the side tasks while rarely making mistakes under light loading. Under heavy

loading with both manual and automatic guidance on Course 4, however, Pilot 2 incurred eight incorrect responses to the Sternberg task for the reason discussed in Appendix D, Section 8: Sternberg Recognitive Task. There was also enough variability in the choice reaction response times by Pilot 2 on Courses 2 and 3 to render an inconsistency in mean trends not statistically significant.

REFERENCE

F-1 Fisher, R. A., and F. Yates, Statistical Tables for Biological, Agricultural and Medical Research, Hafner Publishing Co., New York, 1949, pp. 3, 4, 60, 61, and 62.

APPENDIX G

CONCLUSIONS AND RECOMMENDATIONS FROM THE SIMULATION AT McDONNELL-DOUGLAS HELICOPTER COMPANY

The MDHC Advanced Digital Flight Control System (ADFCS) has proven to be inherently adaptable to automated nap-of-the-earth trajectory generation techniques. This adaptability has been demonstrated by the integration of several automation concepts. First, MDHC's Automated Flight Path Guidance (AFPG) algorithms demonstrate the ability to fly waypoint courses while providing the pilot with override capabilities in the event of automated system failure. Second, STI's obstacle detection/time-optimal maneuver selection algorithms provide avoidance commands to the AFPG system if an obstacle is detected on or about the waypoint path. These two were combined to form a candidate auto-guidance algorithm for piloted evaluations. Specific conclusions concerning the integration of these algorithms and considerations of the real-time simulation follow.

1. PILOT ACCEPTANCE OF AUTOMATED NOE CONCEPT

MDHC pilots do not generally accept the fully automated NOE concept at this time due to current sensor technology limitations and reliability/redundancy considerations. However, if adequate sensors are assumed to complement the overall system, the automated NOE concept is considered tactically sound. Results from this study have led to the following conclusions concerning pilot acceptance:

- The sensor complement necessary for automated NOE operations must be defined before gaining full pilot acceptance of any system
- Automated system status and maneuver cues must be clearly displayed to the pilot
- The maneuver aggressiveness necessary to avoid obstacles must be defined.

2. REAL-TIME SIMULATION REALISM

The visual data base, used for the piloted evaluations, consisted of a waypoint course that was clearly delineated by a corridor of trees. Alternate routes were also marked by a corridor of trees at sections of the programmed flight path designated for the placement of obstacles. Once the pilots had flown the system several times, the alternate route provided a cue to the upcoming side-step maneuver. This may have affected the pilot's final evaluation of the system's obstacle detection and overall maneuver aggressiveness. In general, for an initial evaluation of auto-guidance algorithms, this type of data base

is adequate. For subsequent studies, however, it is recommended a more random spacing of terrain features and obstacles be used. This will limit the visual cueing of maneuvers and offer more versatility when programming waypoint courses and placing obstacles.

Maneuver aggressiveness evaluation is difficult to perform in a fixed-base simulation facility. The lack of acceleration cues limits the pilot's ability to judge the relative aggressiveness of maneuvers. Therefore, a motion base simulator should be used for this task.

3. TIME-OPTIMAL MANEUVERS

Time-optimal maneuvers do provide expedient obstacle avoidance; however, it has not been determined whether the increased complexity over simple compensatory controllers is justified. Compensatory and time-optimal methods should be compared with additional piloted simulations.

The time-optimal control algorithms performed satisfactorily only when implemented with model-following techniques. It is recommended that all control algorithms be implemented with this method.

APPENDIX H

AUTOMATIC NAP-OF-THE-EARTH TEST MATRIX FROM THE NASA AMES RESEARCH CENTER SIMULATION

	TECHNIQUE, RVR								
PILOT, COURSE	AUTO 200 FT	AUTO 500 FT	AUTO 500 FT	SUPOV 500 FT	SUPOV 500 FT	AUTO 1000 FT	AUTO 1000 FT	MANUAL 500 FT	MANUAL 1000 FT
Familiarization Run Numbers									
P2, 1N						9,10 FB*			
P1, 2N								13,15,16	22,23 (RVR ∞)
P3, 1N		19 FB*						44,45	29 FB*
2N									30 FB*
2S								31 FB*	
P5, 1N		1 FB*							
2N		7							
Data Run Numbers									
P2, 1N		12	52	40	50			37	
2N		11				51		41	
2S		43				39		36	
P1, 1N	18			54	57	24			
2N		53				55			
2S		17	56			25			
P4, 2N		28		60					
2S		58	59						
P3, 1N		22	48	33				20	
2N		32				47			
2S		21		46		49			

*FB = fixed base.

APPENDIX I

SIDE TASK RESULTS FROM THE NASA AMES RESEARCH CENTER SIMULATION

This appendix presents the results of (1) the Sternberg and choice reaction time side tasks and (2) the subcritical tracking task.

1. STERNBERG AND CHOICE REACTION TIME SIDE TASKS

The mean responses for the Sternberg and choice reaction time (RT) side tasks during automatically guided runs are presented in chronological order for each of the four pilots in Figs. I-1 through I-4 from Table I-1. The means were calculated on-line at the end of each run; standard deviations were not calculated. The side task loading was light, because the subcritical tracking task (SCTT) was also being performed.

Following what appears to be skill development in the first two runs by Pilot 1 in Fig. I-1, the mean results for both tasks exhibit substantial variation, excepting initial Run 22. The mean Sternberg RT multiple, RT/RT_{min}, varies between 1.1 and 1.6 (dmls), and the mean choice RT fraction, RT/RT_{max} varies between 0.3 and 0.6 (dmls). There is no evident correlation with course number and/or visibility expressed in terms of runway visual range (RVR).

In Fig. I-2 for Pilot 2, the mean Sternberg RT multiple shows evidence of skill development throughout the entire sequence of runs. The trend might also reflect increasing confidence in the automatic guidance. The mean choice RT fraction fluctuates between 0.54 and 0.33 (dmls) with a mean trend reflecting skill development and/or increasing confidence in the automatic guidance. Again, there is no evident correlation with course number and/or visibility.

In Fig. I-3 for Pilot 3, both the mean Sternberg RT multiple and the mean choice RT fraction show evidence of skill development in the first three runs, followed by variability in the two subsequent runs. Among the five runs, the mean Sternberg RT multiple varies between 1.09 and 1.34 (dmls), and the mean choice RT fraction varies between 0.25 and 0.56 (dmls). There is no evident correlation with course number and/or visibility.

In Fig. I-4 for Pilot 4, the three responses (one for each course 2N, 2S, and 1N in chronological order) exhibit limited variability. The mean Sternberg RT multiple varies between 1.75 and 2.07 (dmls), and the mean choice RT fraction varies between 0.46 and 0.68 (dmls). The chronological trends happen to be complementary in that the shortest response on one task is accompanied by the longest on the other and vice versa.

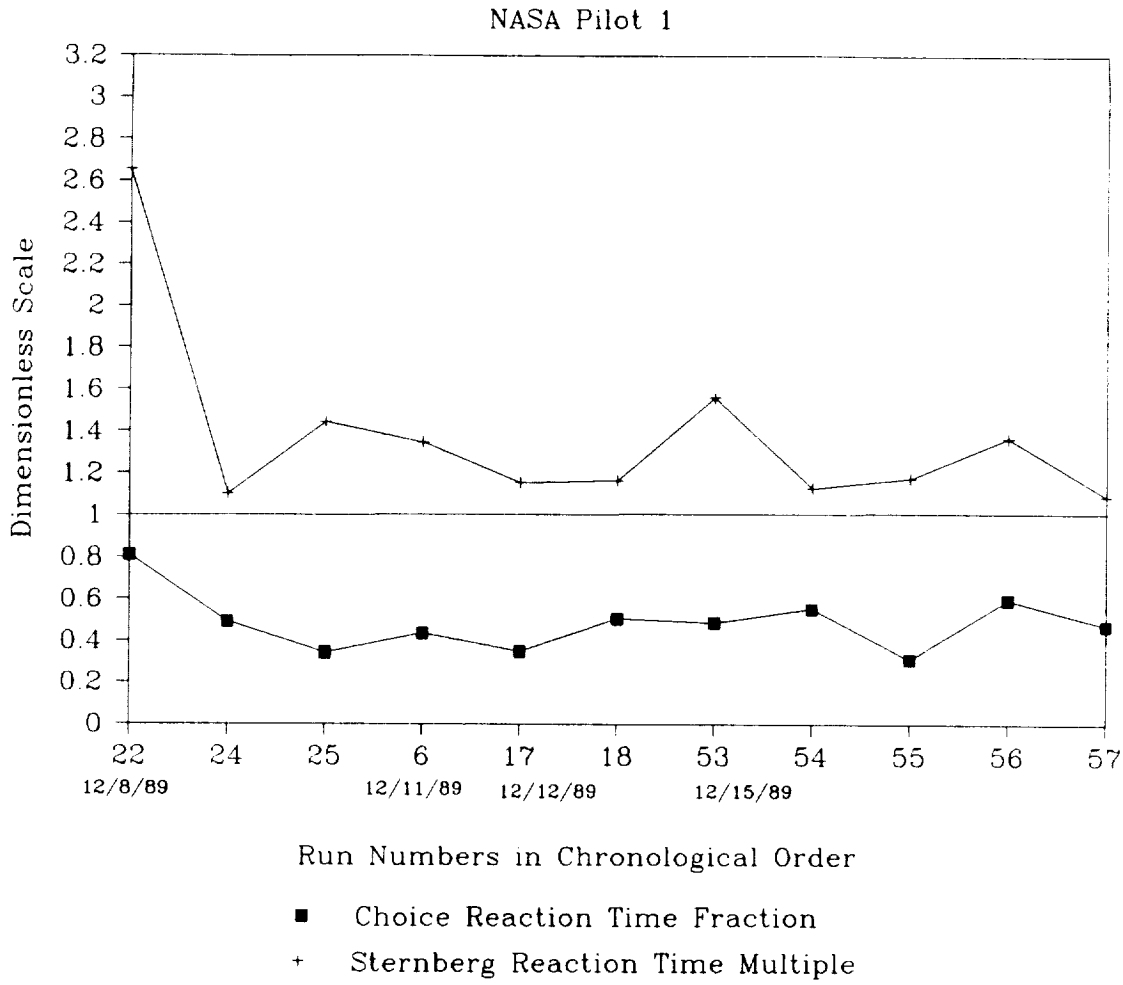

Figure I-1. Side Task Results for NASA ARC Pilot 1

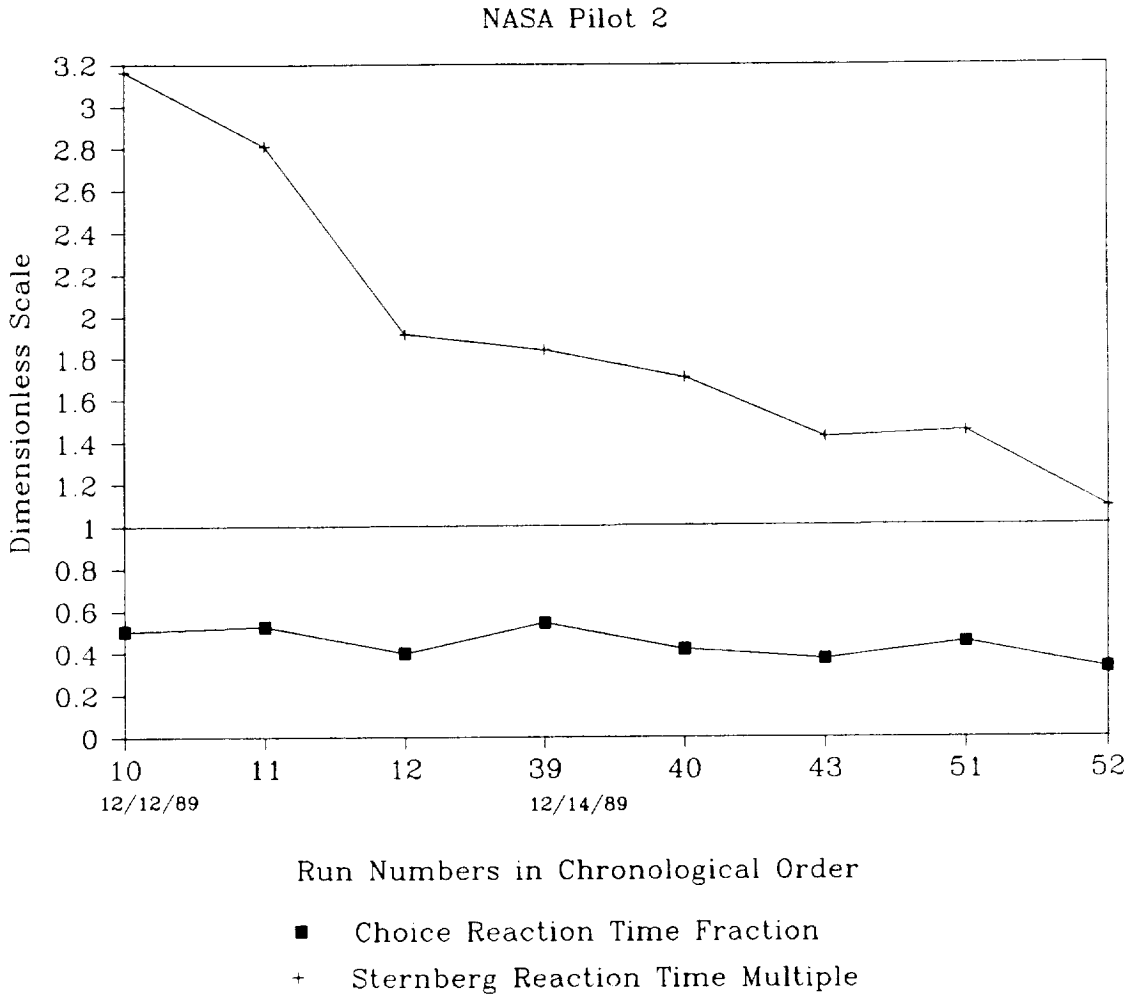

Figure I-2. Side Task Results for NASA ARC Pilot 2

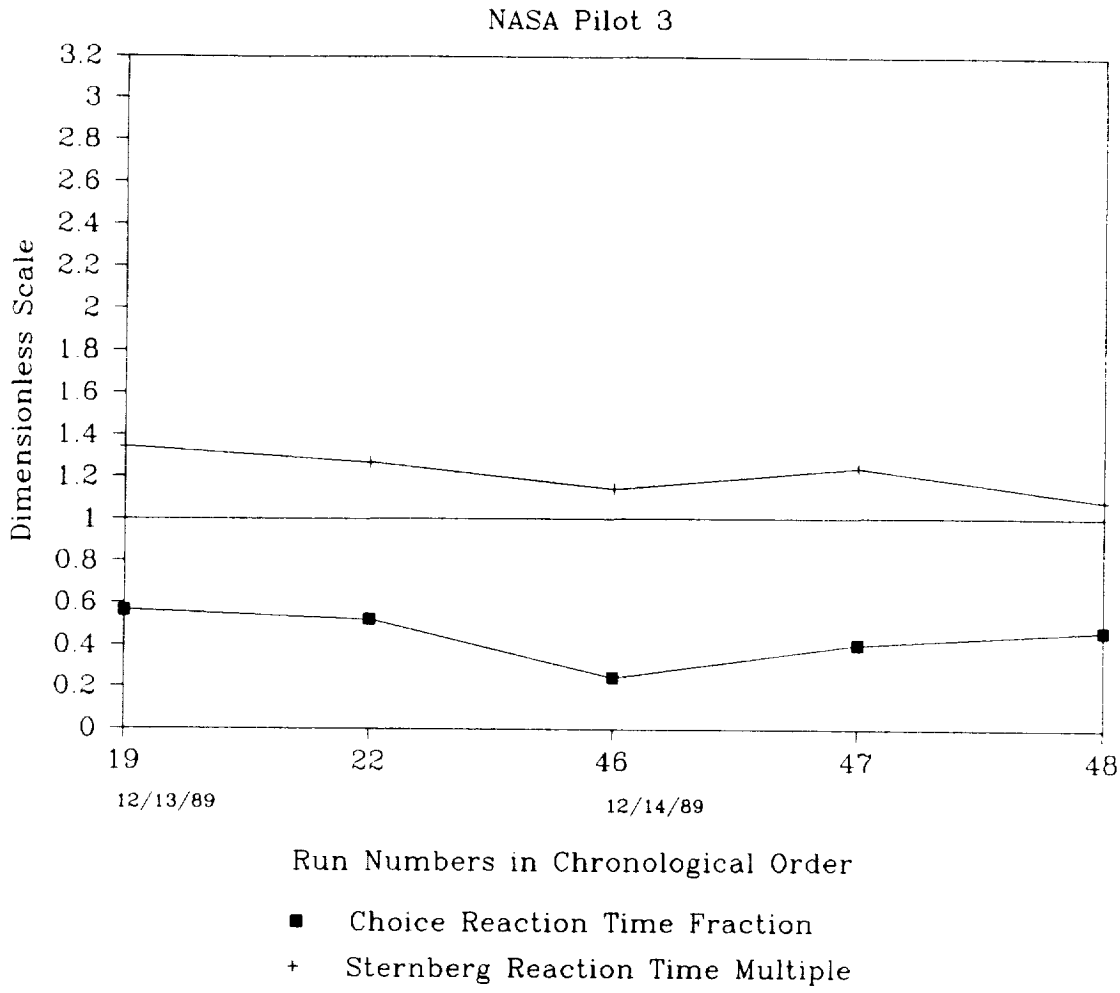

Figure I-3. Side Task Results for NASA ARC Pilot 3

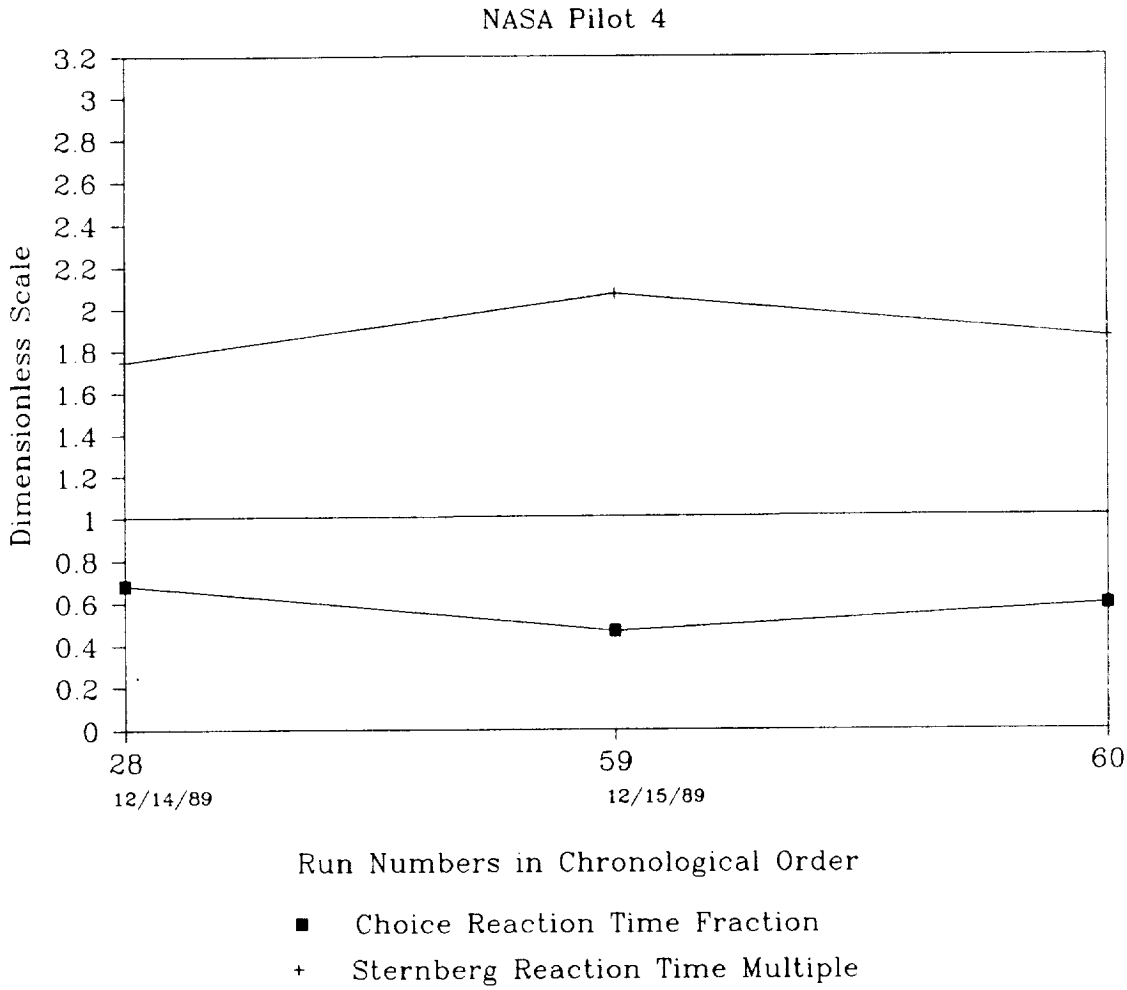

Figure I-4. Side Task Results for NASA ARC Pilot 4

TABLE H-1. MANUAL SIDE TASK RESULTS FROM AUTOMATICALLY GUIDED RUNS IN THE NASA ARC VMS

						STERNBERG MEAN TIME BETWEEN PRESENTATION OF STIMULI 48 SEC WITH A VALID SET OF 3 LETTERS OUT OF 26 LETTERS		SUBCRITICAL TRACKING TASK λ_{sc} = 0.5 RAD/SEC	
DATE	RUN NO.	PILOT	COURSE	RVR (FT)	MEAN FRACTIONAL CHOICE RT SCORE $\frac{RT}{RT_{max}}$ RT_{max} = 3 sec	MEAN STERNBERG TASK SCORE (SEC)	MULTIPLE STERNBERG TASK SCORE (DMLS)	TIME AT LIMIT / RUN TIME (SEC)	TASK ERROR (RMS) (DMLS)
12/8	22, (23)	1	2N	∞	0.81020	6.26523	2.655	YBNA	0.1587
	24	1	1N	∞	0.49098	2.59600	1.100	0	0.1000
	25	1	2S	∞	0.34467	3.40810	1.444	0	0.0808
12/11	6	1	?	?	0.43598	3.17794	1.347	0	0.0811
12/12	(9), 10 FB	2	1N	1000	0.50467	3.16350	3.1635	0	0.0386
	11	2	2N	500	0.52383	2.81038	2.810	0	0.0490
	12	2	1N	500	0.40040	1.91360	1.914	0	0.0256
	17	1	2S	500	0.34960	2.72550	1.155	YBNA	0.1188
	18	1	1N	200	0.50569	2.74972	1.165	YBNA	0.1465
12/13	19 FB	3	1N	500?	0.56373	2.68383	1.342	19.458 / 698	0.2179
	21	3	2S	500	Missing Pages 658, 659 Of Versatek Printout				
	22	3	1N	500	0.52378	2.53735	1.269	2.898 / 702	0.1489
12/14	28	4	2N	500?	0.68307	3.50229 (min)	1.75	not readable / 744	0.0225
	39	2	2S	1000	0.54224	1.84000	1.840	0	0.0816
	40 SUP OVR	2	1N	1000	0.41729	1.70711	1.707	0.966 / 296	0.0967
	43	2	2S	500	0.37168	1.42493	1.425	0	0.0627
	56 SUP OVR	3	2S	500	0.2484	2.29823	1.149	2.944 / 410	0.1510
	47	3	2N	500?	0.40587	2.49065	1.245	3.726 / 730	0.1623
	48	3	1N	500?	0.47143	2.18019 (min)	1.090	3.220 / 702	0.1130

FB = fixed base; YBNA = yes, but not available; SUP OVR = supervisory override

TABLE H-1 (CONCLUDED)

						STERNBERG MEAN TIME BETWEEN PRESENTATION OF STIMULI 48 SEC WITH A VALID SET OF 3 LETTERS OUT OF 26 LETTERS		SUBCRITICAL TRACKING TASK λ_{sc} = 0.5 RAD/SEC	
DATE	RUN NO.	PILOT	COURSE	RVR (FT)	MEAN FRACTIONAL CHOICE RT SCORE $\frac{RT}{RT_{max}}$ RT_{max} = 3 sec	MEAN STERNBERG TASK SCORE (SEC)	MULTIPLE STERNBERG TASK SCORE (DMLS)	$\frac{\text{TIME AT LIMIT}}{\text{RUN TIME}}$ (SEC)	TASK ERROR (RMS) (DMLS)
12/14	50	2	1N	500?	0.37797	1.51558	1.516	0	0.0439
	51	2	2N	500?	0.45222	1.4518	1.452	0	0.0278
	52	2	1N	500?	0.32660	1.09103 (min)	1.091	0	0.0260
12/15	53	1	2N	500	0.48748	3.68324	1.561	$\frac{7.958}{736}$	0.1828
	54 SUP OVR	1	1N	500	0.55338	2.66776	1.130	$\frac{14.122}{710}$	0.1959
	55	1	2N	1000	0.31418	2.77955	1.178	$\frac{3.680}{734}$	0.1789
	56	1	2S	500	0.59744	3.23328	1.370	$\frac{12.282}{728}$	0.2101
	57 SUP OVR	1	1N	500	0.47522	2.57485 (min)	1.091	$\frac{18.262}{711}$	0.2466
	59	4	2S	500	0.46669	4.15350	2.07	0	0.0348
	60 SUV OVR	4	1N	500	0.59227	3.72012	1.86	$\frac{5.474}{835}$	0.1208

FB = fixed base; YBNA = yes, but not available; SUP OVR = supervisory override

2. SUBCRITICAL TRACKING TASK

The subcritical tracking task (SCTT) root-mean-squared (RMS) tracking errors are presented chronologically for each pilot in Figs. I-5 through I-8. The dimensionless ordinate expresses a decimal fraction representing the ratio of the numerical RMS error to the maximum displayed value of the error. Table I-1 shows that during only miniscule fractions of the run times were the tracking errors limited at the maximum displayed value. There does, however, appear to be a correlation between runs with large RMS tracking errors on the SCTT and instances of intervention with supervisory manual overriding of automatic guidance as closer inspection will show.

The chronological trend in Fig. I-5 suggests skill development in the first three runs with unrestricted visibility of the computer-generated image (CGI). Thereafter, with varying levels of restricted RVR, relaxation of RMS error performance occurs, although not evidently correlated with course number. The local peak in RMS error in Run 54 and the largest RMS error in Run 57 were accompanied by pilot intervention with supervisory manual overriding of the automatic guidance (identified with the label "SUP OVR" in the figure).

In Fig. I-6, the largest RMS tracking error in Run 40 was also accompanied by pilot intervention with supervisory manual overriding of the automatic guidance. Thereafter occurs a progressive skill development in Runs 43 and 50 through 52. There is no evident correlation of RMS error with CGI visibility or course number among the results in Fig. I-6.

The chronological trend in Fig. I-7 suggests skill development with an hiatus. The instance of supervisory manual overriding of the automatic guidance in Run 46 marks the hiatus but not a local peak RMS error. There is no evident correlation of RMS error with CGI visibility or course number among the results in Fig. I-7.

The largest RMS error in Fig. I-8 in Run 60 was again accompanied by pilot intervention with supervisory manual overriding of the automatic guidance.

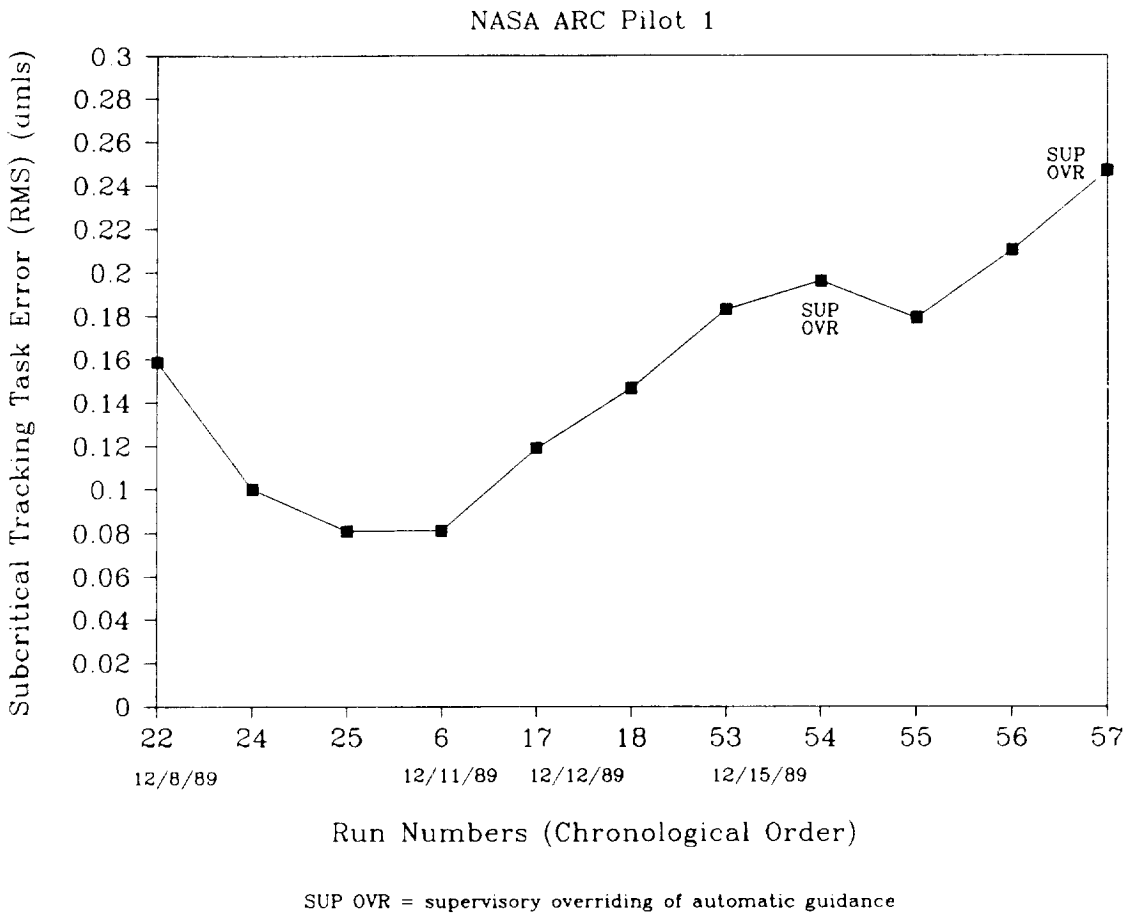

Figure I-5. Root-Mean-Square Subcritical Tracking Task Error for NASA ARC Pilot 1

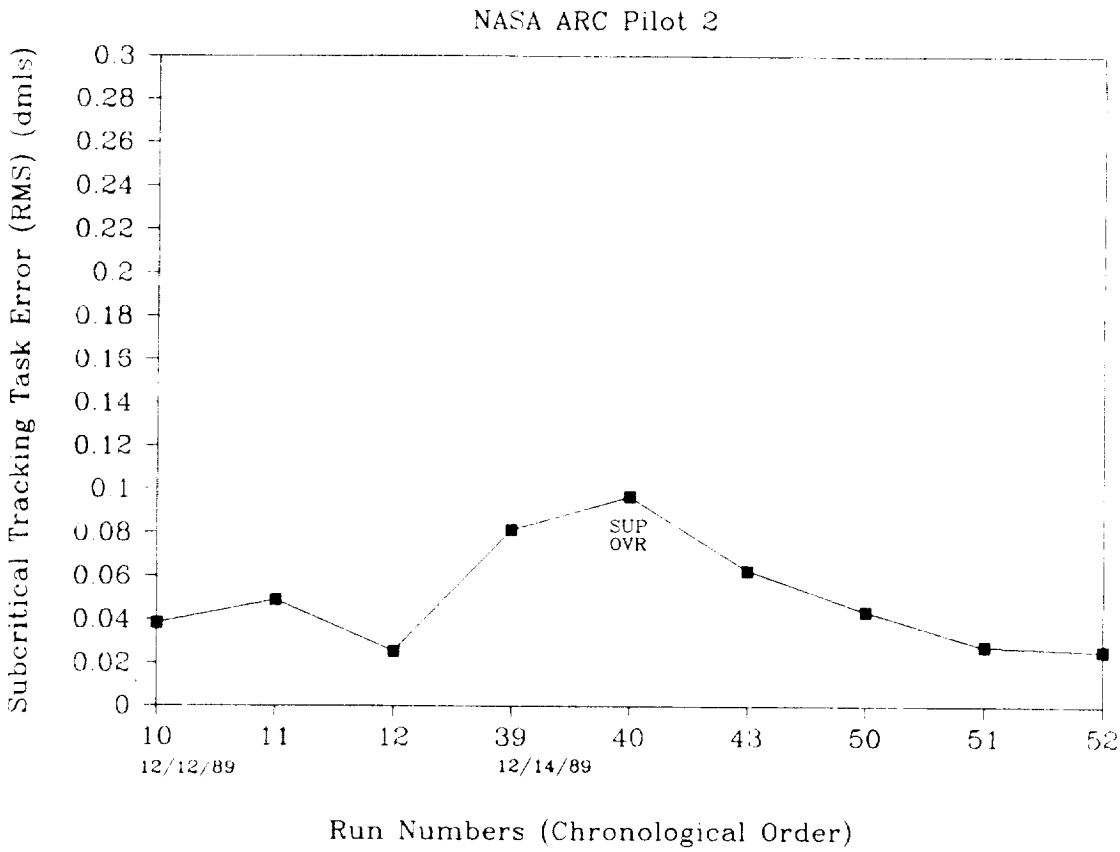

Figure I-6. Root-Mean-Square Subcritical Tracking Task Error for NASA ARC Pilot 2

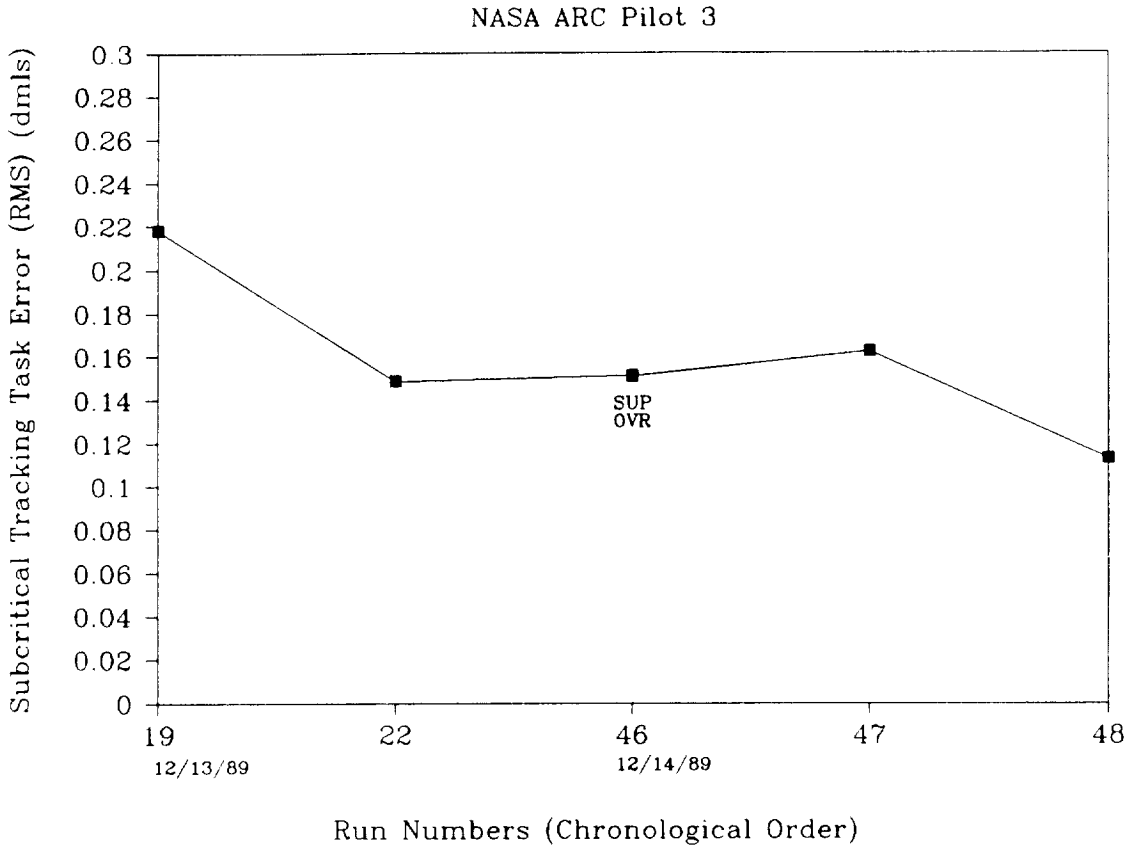

Figure I-7. Root-Mean-Square Subcritical Tracking Task Error for NASA ARC Pilot 3

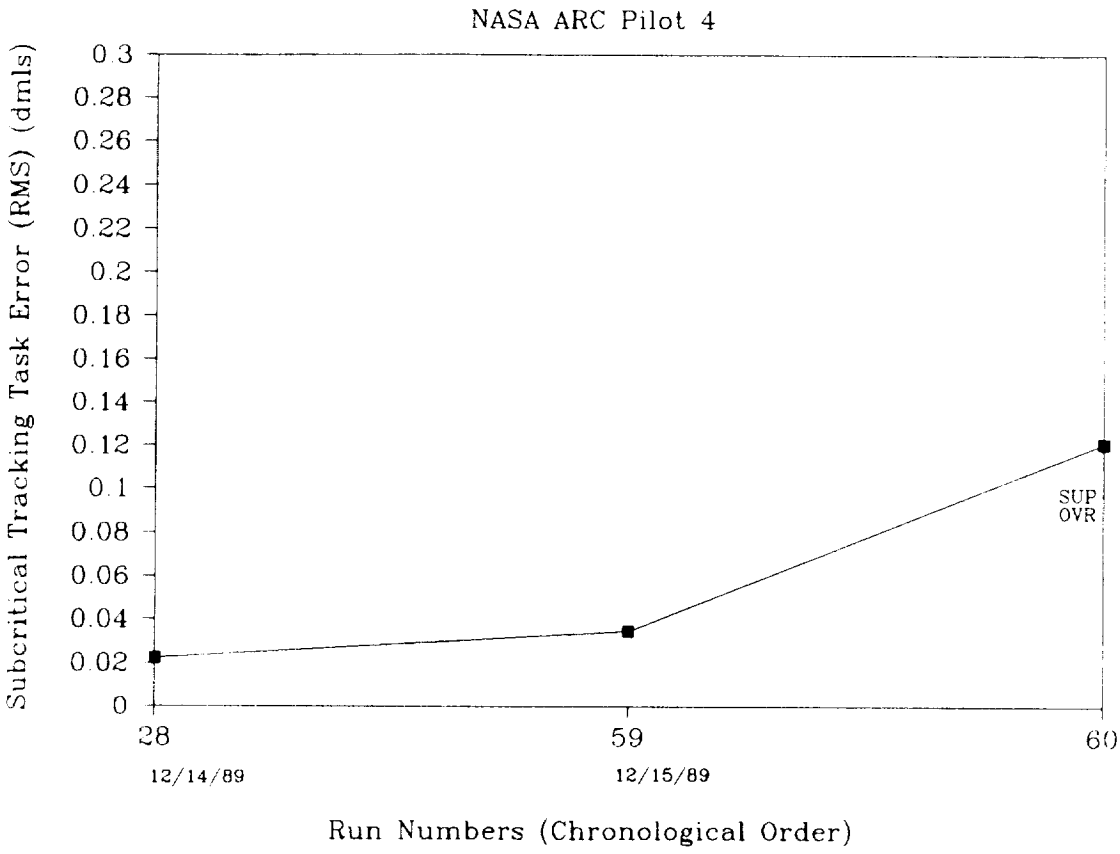

Figure I-8. Root-Mean-Square Subcritical Tracking Task Error for NASA ARC Pilot 4

NASA
National Aeronautics and Space Administration

Report Documentation Page

1. Report No.	2. Government Accession No.	3. Recipient's Catalog No.
NASA CR-177571		

4. Title and Subtitle

Fully Automatic Guidance and Control for Rotorcraft Nap-of-the-Earth Flight Following Planned Profiles. Volume I – Real-Time Piloted Simulation

5. Report Date

January 1991

6. Performing Organization Code

7. Author(s)

Warren F. Clement, Peter J. Gorder, and Wayne F. Jewell

8. Performing Organization Report No.

STI TR-1254-1

10. Work Unit No.

9. Performing Organization Name and Address

Systems Technology, Inc.
2672 Bayshore Parkway, Suite 505
Mountain View, CA 94043

11. Contract or Grant No.

NAS2-12640

13. Type of Report and Period Covered

Contractor Report

12. Sponsoring Agency Name and Address

National Aeronautics and Space Administration
Washington, DC 20546-0001

14. Sponsoring Agency Code

15. Supplementary Notes

Point of Contact: Harry Swenson, Ames Research Center, MS 210-9, Moffett Field, CA 94035-1000
(415) 604-5469 or FTS 464-5469

16. Abstract

Developing a single-pilot, all-weather nap-of-the-Earth (NOE) capability requires fully automatic NOE (ANOE) navigation and flight control. Innovative guidance and control concepts are investigated in a four-fold research effort that: (1) organizes the on-board computer-based storage and real-time updating of NOE terrain profiles and obstacles in course-oriented coordinates indexed to the mission flight plan; (2) defines a class of automatic anticipative pursuit guidance algorithms and necessary data preview requirements to follow the vertical, lateral, and longitudinal guidance commands dictated by the updated flight profiles; (3) automates a decision-making process for unexpected obstacle avoidance; and (4) provides several rapid response maneuvers. Acquired knowledge from the sensed environment is correlated with the forehand knowledge of the recorded environment (terrain, cultural features, threats, and targets), which is then used to determine an appropriate evasive maneuver if a non-conformity of the sensed and recorded environments is observed. This four-fold research effort has been evaluated in both fixed-base and moving-base real-time piloted simulations, thereby providing a practical demonstration for evaluating pilot acceptance of the automated concepts, supervisory override, manual operation, and re-engagement of the automatic system. Volume I describes the major components of the guidance and control laws as well as the results of the piloted simulations. Volume II describes the complete mathematical model of the fully automatic guidance system for rotorcraft NOE flight following planned flight profiles.

17. Key Words (Suggested by Author(s))	18. Distribution Statement
Automatic flight guidance and control Rotorcraft Nap of the Earth	Unclassified-Unlimited Subject Category - 08

19. Security Classif. (of this report)	20. Security Classif. (of this page)	21. No. of Pages	22. Price
Unclassified	Unclassified	154	A08

For sale by the National Technical Information Service, Springfield, Virginia 22161